Theory and simulation of polymer adsorption in flowing fluids

A DISSERTATION

SUBMITTED TO THE FACULTY OF THE GRADUATE SCHOOL

OF THE UNIVERSITY OF MINNESOTA

BY

Sarit Dutta

IN PARTIAL FULFILLMENT OF THE REQUIREMENTS

FOR THE DEGREE OF

DOCTOR OF PHILOSOPHY

Advisors: **Kevin D. Dorfman** & **Satish Kumar**

September, 2014

Acknowledgements

I would like to thank my advisors Kevin Dorfman and Satish Kumar for allowing me the opportunity to work in their groups and for mentoring me on how to progress in scientific research. I am grateful to all the members of the Dorfman group as well as the Kumar group over the past several years for providing a congenial environment for research at the university. I am particularly thankful to Jaesol Cho, who helped me to get started on my research during my first year at graduate school. Doug Tree and Abhiram Muralidhar have been a great source of knowledge in polymer physics as well as various aspects of computer simulations. Abhiram particularly deserves special thanks for periodically updating me with news from the "outside world". I would also like to thank Professors Xiang Cheng, Yiannis Kaznessis, and Vincent Noireaux for serving on my thesis defense committee.

I am grateful to the University of Minnesota Supercomputing Institute, where most of the simulation work was performed, for providing the necessary computational resources for this work. For my work, I have benefitted immensely from the discussions and solutions provided by the wonderful people at StackOverflow and TeX.Sx. Moreover, the fantastic collection of computer programs by John Burkardt have come to my rescue many times during the last five years.

I am grateful for the financial support from the David and Lucile Packard Fellowship

awarded to Kevin Dorfman, the National Institute of Health (Grant No. R01-HG005216), the National Science Foundation (Grant No. CBET-0642794 and Grant No. CBET-1132083), and the University of Minnesota (Doctoral Dissertation Fellowship). In addition, I would also like to acknowledge the financial support made available by the Department of Chemical Engineering and Materials Science during my first year in the form of the Rutherford Aris Memorial Fellowship and the College of Science and Engineering in the form of teaching assistantships and instructor positions.

Abstract

Adsorption and desorption of polymers in the presence of flowing fluids lies at the heart of many technological applications such as thin film deposition via layer-by-layer fabrication, development of surface coatings and responsive interfaces, stabilization of colloidal suspensions, and rheology modifiers. Adsorption under flow also constitutes a key step in many physiological mechanisms, e.g., formation of a platelet plug during hemostasis. Moreover, flow induced adsorption/desorption offers a rich source of problems from the point of view of fundamental polymer physics. However, despite its importance little is understood about the behavior of adsorbed polymers under flow, in contrast to the well-developed field of adsorption from a quiescent solution. Some experimental observations regarding the effect of flow on adsorption/desorption exist in the literature, but they are mutually conflicting and the underlying physics involved is yet to be explained.

In this work, we provide new insight into the mechanism of adsorption/desorption under shear flow near a single planar wall using kinetic theory and Brownian dynamics (BD) simulations. We show that in the presence of shear flow accounting for hydrodynamic interactions (HI) between the polymer molecules and the wall is crucial to observe the experimentally obtained trends of the amount of adsorbed polymer with respect to shear rate and molecular weight. The amount adsorbed is governed by a balance between HI-induced repulsion and polymer-wall attraction. At a fixed molecular weight increasing shear rate increases HI, causing a reduction in the amount adsorbed. Moreover, if the shear rate is fixed the amount adsorbed decreases with an increase in molecular weight. These trends are in qualitative agreement with prior experimental observations of Lee and Fuller [*J. Colloid Interface Sci.* 103 (1985) 569]. In the case of desorption, the trend for the amount adsorbed with respect to molecular weight depends on the polymer-wall interaction energy. We show that when adsorption is weak, desorption increases with an increase in molecular weight, but for strong adsorption the trend is reversed. We provide an explanation for this reversal in terms of the change in polymer conformations with increase in the interaction energy, thereby resolving the apparently conflicting experimental observations of Lee and Fuller and Soga and Granick [*Langmuir* 14, 4266 (1998)].

Contents

List of Tables

List of Figures

Chapter 1

Introduction

Summary

An overview of adsorption of polymers from a quiescent solution as well as from a flowing solution is presented. Some applications pertaining to polymer adsorption are discussed and several outstanding questions regarding the effects of flow on adsorption are briefly touched upon. The current research goal is introduced and an outline to the material presented in succeeding chapters is provided.

1.1 Adsorption of polymers

Adsorption refers to the enhanced accumulation of a chemical species near a solid or a liquid surface compared to the bulk. It is a surface phenomenon, depending upon the chemical nature of the species (adsorbate) and the surface (adsorbent), as well as external conditions like temperature, pressure, and bulk concentration. Adsorption can be observed for a wide variety of substance/surface combinations, a common example

being that of gas molecules to a solid surface (e.g. CO_2 on activated carbon). If the increase in interfacial concentration is due to physical forces between the adsorbate molecules and the adsorbent, e.g. van der Waals forces or electrostatic interactions, the process is called physisorption, and if creation of covalent bonds are involved, then it is called chemisorption.

An important class of problems in adsorption arises when the adsorbate is a polymeric material and the adsorbent is a solid surface. The behavior of polymer molecules near solid surfaces offers a rich set of problems in fundamental polymer physics, with deep connections to probability theory and critical phenomena in magnetic systems (Eisenriegler, 1993; Fleer et al., 1993). Moreover, adsorption of polymers is central to many industrial processes, particularly those involving manufacture of materials with tailor-made surface properties. An important example is the development of polymeric multilayer coatings via the layer-by-layer deposition process (see Figure 1.1 for a schematic of the method). Such coatings are commonly used to modify surface properties in a controlled manner, e.g. to create water repelling surfaces, biocompatible coatings on medical implants, and microelectronic devices. The functionality and stability of coatings depend essentially on the dynamics of the long chain-like polymer molecules at the solid surface. In addition, polymer adsorption is important for stabilization of colloidal suspensions (Sato and Ruch, 1980; Russel et al., 1991), nanoscale surface patterning (Cox et al., 1999), modification of tribological properties (Migler et al., 1993; Brown, 1994), and separation of biopolymers (Wolfe et al., 2002). Numerous novel applications of polymer adsorption are also discussed in the review article by Granick et al. (2003).

Polymer adsorption typically occurs from a solvent containing dissolved polymer in contact with an adsorbing surface. In contrast to adsorption of small molecules, polymer adsorption is a much more complicated phenomenon because of the entropic effects due to the long chain-like structure of the polymer molecules. For a polymer molecule to be

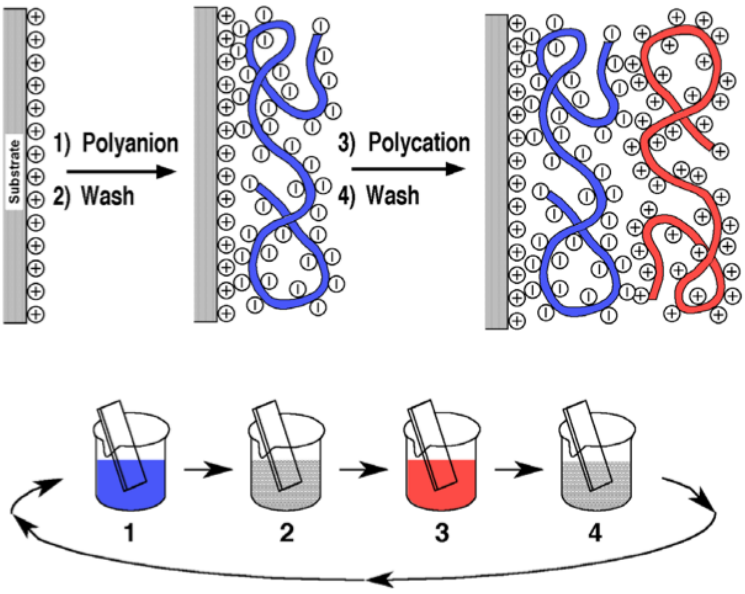

Figure 1.1. Schematic of the layer-by-layer deposition process. Step 1 involves adsorption of a polyanion onto a charged substrate followed by washing off the excess material (Step 2). Step 3 is the adsorption of a polycation over the polyanion layer followed by washing (Step 4). The sequence of steps 1 – 4 can be repeated several times to build mutilayered coatings. (From Decher (1997))

adsorbed, the entropic loss due to the confinement to a surface needs to be compensated by the energetic gain from association with the surface. The thickness of the adsorbed layer formed by small molecules is typically of the order of their size, whereas adsorbed polymer layers can be many orders of magnitude thicker than their bulk molecular size.

In spite of the inherent difficulties, significant progress has been made in understanding adsorption from quiescent solutions. The development can be categorized under two broad areas: (i) the equilibrium chain structure, and (ii) the kinetics of adsorption.

The simplest problem involving chain structure is that of an isolated chain near an adsorbing surface. The equilibrium conformation of an isolated adsorbed chain is usually described in terms of three kinds of subchains – (i) *trains*, which have all their segments in contact with the surface, (ii) *tails*, which are non-adsorbed chain ends, and (iii) *loops*, which are sections of the chain between two trains (see Figure 1.2 for a schematic). For a chain consisting of N segments the train fraction (also known as the bound fraction), defined as m/N where m is the number of segments directly in contact with the surface, provides an important measure for characterizing the equilibrium chain structure. The average train, loop, and tail fractions depend on the segment-surface interaction energy as well as the number of segments in the chain. The equilibrium chain structure is determined by a balance between the chain-surface attraction and the entropic repulsion.

Neglecting interchain interactions, the thickness of the adsorbed layer in the mean-field regime can by calculated via a scaling approach by minimizing the chain free energy (de Gennes, 1987). However, this prediction for the thickness turns out to be valid only for a strongly adsorbed chain or when the segment-surface potential is long-ranged (Netz and Andelman, 2001). Beyond the single chain, the equilibrium structure of an adsorbed layer can be determined using the Scheutjens-Fleer (SF) self-consistent field theory (Fleer et al., 1993). Although originally proposed for polymers on a lattice (Scheutjens and

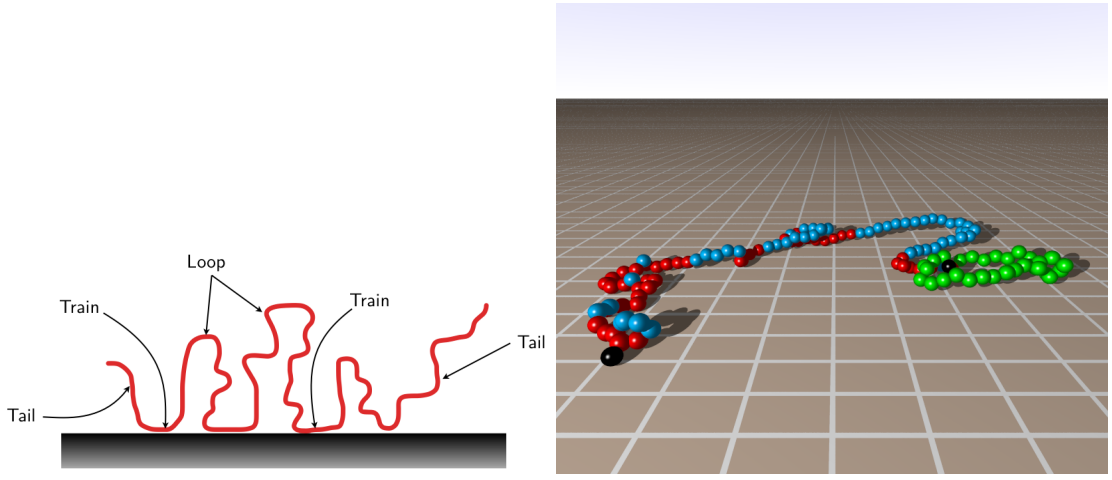

Figure 1.2. **(a)** Cartoon of an adsorbed chain showing the loop, tail, and train sections. **(b)** A computer rendering of an adsorbed chain in three dimensions using a bead-spring model. The red beads indicate segments forming trains, the blue beads indicate loops and the green beads represent segements in the tails. The black beads mark the segments at the chain ends.

Fleer, 1979; Scheutjens and Fleer, 1980), a continuum version of the theory has been developed as well (Mavrantzas et al., 2005). It is a remarkably successful theory that can predict the distributions of the loops, tails, and trains in the adsorbed layer and has shown excellent agreement with experimental results. However, the SF theory does not admit an analytical solution, rather it generates a system of coupled equations that need to be solved numerically.

The kinetics of polymer adsorption are usually treated in the same way as mass transport problems in chemical engineering. Here we briefly mention the general picture of adsorption kinetics that have emerged from numerous experimental studies. A short summary of the most important experimental results is given by Cohen Stuart and de Keizer (2001) and Fleer et al. (1993) provide a more detailed discussion. Some newer hypotheses regarding equilibration of adsorbed layers can be found in the review article by O'Shaughnessy and Vavylonis (2005). Adsorption consists of three stages:

(i) Transport of the polymer molecules from the bulk to the surface, (ii) attachment of the molecules to the surface, and (iii) spreading and subsequent change in conformation on the surface. Compared to small molecules, the diffusion coefficient of polymer molecules is about two orders of magnitude lower due to their size. Hence the rate of transport to the surface is much slower as well. During the initial stages of adsorption to a bare surface, the rate of attachment is rapid and the overall rate of adsorption is governed by the rate of advection of the molecules to the surface. However, as the surface comes close to saturation, the rate of attachment slows down because of the diminishing free area available on the surface. It has been proposed that the molecules arriving at the surface in the early stages of adsorption have a larger section of the surface under coverage, while the late arriving molecules need to deform to find pockets of unoccupied space on the surface. This leads to the formation to two subpopulations of chains – the early arriving ones form a tight layer in the immediate vicinity of the surface and the late arriving chains form a fluffy diffuse layer extending far into the solution. After adsorption, the polymer molecules change conformations as they undergo a very slow relaxation process. Little is known about the nature of the surface relaxation mechanism and owing to its very slow nature, experimental studies are difficult to carry out.

1.2 Adsorption from flowing solutions

Compared to adsorption from a stagnant solution, a more technologically relevant scenario is when polymer molecules are adsorbed from a solution flowing past a solid surface. Such situations arise in many applications like thin film deposition via layer-by-layer fabrication (Decher, 1997), development of surface coatings (Robb, 2007), responsive interfaces (Cohen Stuart et al., 2010), stabilization of colloidal suspensions (Garcia et al., 2006), and rheology modifiers (Schulz and Glass, 1991). Many of these applications

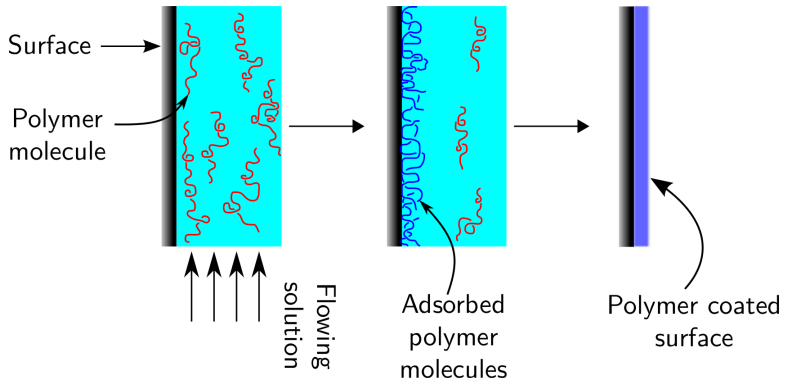

Figure 1.3. Schematic of the development of a surface coating by adsorption of polymers from a flowing solution.

can be performed in the absence of flow as well, but flow based processes are advantageous because they are more amenable to continuous operations. Figure 1.3 shows a process similar to the layer-by-layer deposition technique discussed earlier, but now the solution flows past the surface instead. Moreover, recent advances have been made in microfluidic technology based on adsorption behavior of certain polymers, e.g., selective adsorption in microchannels as a method for separation of DNA (Wolfe et al., 2002).

Apart from technology, adsorption under flow is important in understanding many physiological phenomena. One example is the mechanism of hemostasis (stopping of bleeding from a wound) in the human body. When blood vessels rupture, a glycoprotein called von Willebrand factor (vWF) helps in trapping the platelets in blood to allow the formation of a clot. Within a healthy blood vessel the vWF molecule stays in a globular form, but when the vessel ruptures they unfold and adsorb onto the vessel wall, creating a mesh like structure that allows platelets to adhere to it forming a plug. Current research (Schneider et al., 2007; Sing, 2012) has revealed that the unfolding and subsequent adsorption of vWF is triggered by the increased shear rate of blood near the ruptured vessel wall (see Figure 1.4), although a complete understanding of the

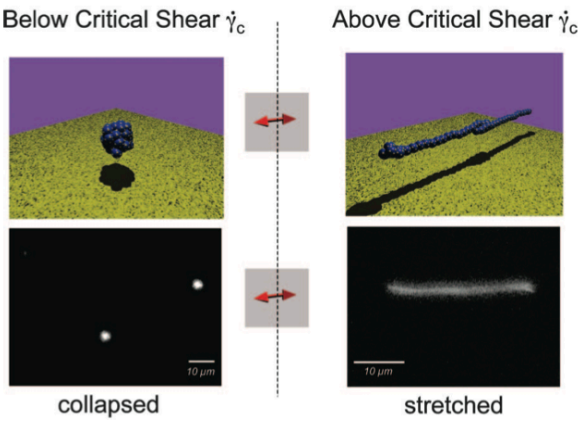

Figure 1.4. Schematic (top) and flourescence image (bottom) of the vWF molecule in a collpased and stretched state. Above a critical shear rate (typically several thousand s^{-1}) the molecule unfolds to adopt a stretched conformation. (From Schneider et al. (2007))

adsorption mechanism has not yet been achieved.

From a theoretical standpoint, accounting for flow-induced effects on adsorption is a hard problem involving the fluid mechanics of the solvent coupled to transport processes and the statistical mechanics of the polymer chains. In the presence of flow, polymer molecules interact with the flow field via hydrodynamic interaction (HI), engendering a qualitatively different mechanism of adsorption. The system is far away from equilibrium, and hence the equilibrium theories developed for adsorption in the absence of flow break down, necessitating newer tools for analysis. Kinetic theories may be developed, but they often lead to non-trivial systems of equations having no analytical solution because of the coupled many-body interactions involved. As one may expect, very little is known about the mechanism of adsorption in the presence of flow. There are several experimental studies that highlight the effect of flow on adsorption (Gramain and Myard, 1981; Cohen and Metzner, 1982; Lee and Fuller, 1984; Lee and Fuller, 1985a; Cohen, 1988; McGlinn et al., 1988; Chin and Hoagland, 1991; Chang and Chung, 1991; Soga and Granick, 1998),

but a comprehensive explanation of their observations still eludes us. Some of the important experiments are discussed in Sec. 2.1.

1.3 Desorption into flowing fluids

Desorption is the opposite phenomenon of adsorption, i.e., reduction in the concentration of a preadsorbed species near the interface compared to the bulk. Adsorbed polymer molecules under quiescent conditions typically do not exhibit significant desorption, though for polydisperse samples in contact with their solution replacement of shorter chains by longer ones can occur (Fleer et al., 1993). Even in contact with a pure solvent, only relatively short chains (e.g. 9.2K polystyrene) show slow desorption to a small extent (Dijt et al., 1994).

However, if adsorbed polymer layers are subjected to strong flow fields significant desorption of polymer chains may occur (Gramain and Myard, 1981; Cohen and Metzner, 1982; Lee and Fuller, 1985a; Cohen, 1988; Besio et al., 1988; Bagassi et al., 1989; Chin and Hoagland, 1991; Chang and Chung, 1991; Chatterjee et al., 2014). Almost complete desorption has also been reported for polymer brushes, which can be considered as end-adsorbed polymer chains, when exposed to strong shear flow (Baker et al., 2000; Anastassopoulos et al., 2006; Anastassopoulos et al., 2013). Figure 1.5 shows a cartoon of desorption in unimodal (all chains in the brush are of the same molecular weight) and bimodal (brush consisting of chains of two different molecular weights) physisorbed brushes under shear flow. Experiments have shown that for a unimodal brush desorption occurs only beyond a certain critical shear rate, whereas for a bimodal brush two critical shear rates exist, the first marking the desorption of longer chains and the second that of shorter chains.

Desorption is often highly undesirable in many applications. For example, Figure 1.6

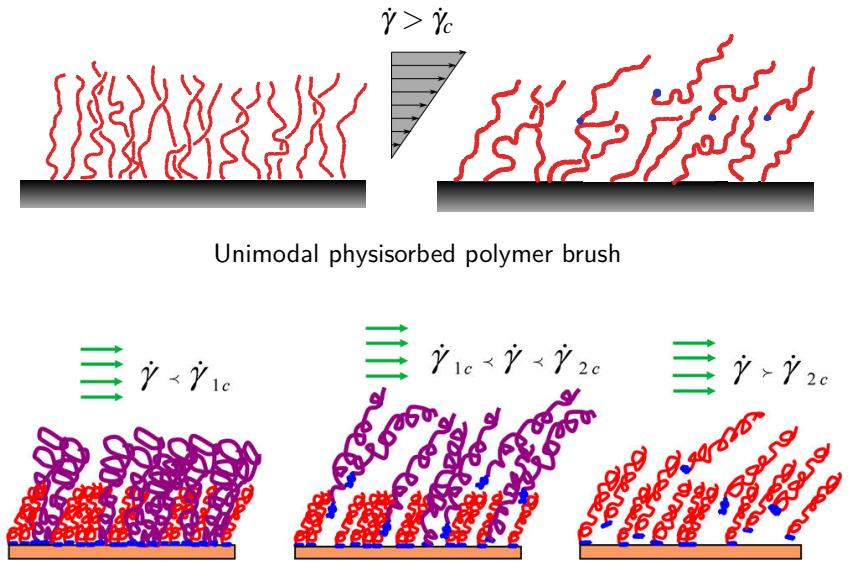

Figure 1.5. Cartoon showing desorption in unimodal (top) and bimodal (bottom) brushes. $\dot{\gamma}_c$ indicates the critical shear rate above which desorption occurs. For bimodal brushes there are two critical shear rates, $\dot{\gamma}_{1c}$ and $\dot{\gamma}_{2c}$ corresponding to the two different molecular weights. The lower critical shear rate sets the threshold for the desorption of the higher molecular weight chains and vice versa. The bottom sketch is taken from Anastassopoulos et al. (2013).

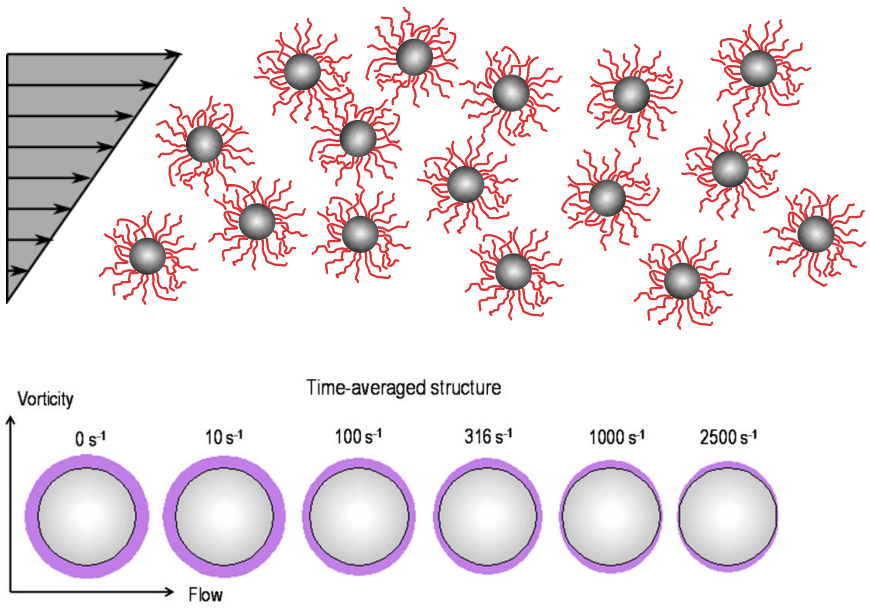

Figure 1.6. (Top) Cartoon of a suspension of polymer-grafted latex spheres subject to shear flow. (Bottom) Time-averaged thickness of the grafted polymer layer on a single latex sphere in the ambient flow-vorticity plane. Note the asymmetric distribution of the polymer layer thickness at high shear rates in contrast to the symmetric distribution at lower shear rates. The single latex figure is reproduced from Chatterjee et al. (2014).

shows a cartoon of a suspension of polymer-grafted latex spheres, a common formulation used in rheology modifiers. When such suspensions are subjected to strong shear flow considerable desorption of the grafted polymer chains occur, causing unintended modification of rheology (Chatterjee et al., 2014). Little is understood about the mechanism of desorption under flow, though it is believed that hydrodynamic drag plays a major role in the detachment of individual polymer chains from the surface (Cohen Stuart and de Keizer, 2001).

1.4 Research outline

The current research investigates the effect of simple shear flow on adsorption and desorption of homopolymers near a planar surface using kinetic theory and Brownian dynamics (BD) simulations. We focus specifically on physisorbed polymers when the adsorption energy is small or comparable to the thermal energy. Moreover, our studies neglect interchain interactions as a simplifying assumption. The effect of flow is incorporated by accounting for HI with the surface, similar to that done in the theory of shear-induced migration of polymers (Ma and Graham, 2005).

In Chapter 2 we review some of the important experimental studies on the effect of flow on adsorption and desorption of polymers. Particular emphasis is given to the classic studies by Lee and Fuller (1985a) and also to the desorption experiments of Soga and Granick (1998). Throughout our investigations, we will compare our results to those of Lee and Fuller (1985a) and attempt to develop an explanation for their experimental observations. The relevant theoretical and simulation studies are also mentioned in this chapter.

We begin our investigation by developing a kinetic theory based on a bead-spring dumbbell model of the polymer in Chapter 3. We incorporate HI via Blake's solution of the velocity field due to a point force near a wall (Blake, 1971). We present results for the amount of polymer adsorbed and the film thickness at steady-state in the presence of shear flow as a function of flow strength and the parameters of the polymer-wall attraction potential. We find that dumbbell-wall HI reduces the amount adsorbed on increasing flow strength. We also develop a scaling law relating the critical shear rate for desorption and the parameters of the adsorption potential for the strong attraction limit.

In Chapter 4 we look at the transient problem for dumbbells using kinetic theory.

Our kinetic theory leads to an advection-diffusion equation in terms of the dumbbell concentration, which we solve numerically using a pseudospectral collocation method. In addition to flow strength, here we investigate the effect of molecular weight on adsorption as well. For a dumbbell, the molecular weight is taken into account by varying the finite extensibility of the spring connecting the two beads. For adsorption onto a bare wall, we show that the amount adsorbed reduces with an increase in flow strength when the molecular weight is held constant, and with increase in molecular weight when the flow strength is held constant. For desorption of a preadsorbed layer, shear rate and molecular weight has an opposite effect. We compare our results to the experiments of Lee and Fuller (1985a) and point out the qualitative agreement between them.

Next we focus solely on the desorption problem in Chapter 5. Moving beyond the dumbbell model, here we perform BD simulations of bead-spring chains. We present results that explicitly show the effects of flow strength, molecular weight, and adsorption energy on desorption. Shear flow is shown to assist desorption due to increased chain-wall HI similar to the predictions from dumbbell kinetic theory. The main result here is that for weak adsorption energy desorption increases with an increase in molecular weight, but the trend is reversed when adsorption energy is strong. This observation is shown to be a consequence of the chain conformations and the resulting HI with the wall. We also discuss how our results reconcile the conflicting experimental observations of Lee and Fuller (1985a) and Soga and Granick (1998) on desorption. Finally in Chapter 6 we conclude by summarizing our findings and discussing some future directions of research.

Chapter 2

Literature review

2.1 Experimental studies

2.1.1 Experiments involving hydrodynamic film thickness

Early experimental investigations of adsorption from flowing solutions primarily focused on measuring the thickness of the adsorbed layer. Most of these studies were reviewed in detail by Kawaguchi and Takahashi (1992), so here we mention only a few of the important results. Gramain and Myard (1981) studied the adsorption of partially hydrolyzed polyacrylamide (HPAM) and polystyrene (PS) onto porous media and found that at constant molecular weight, film thickness increases with an increase in shear rate. Moreover, upon increasing molecular weight, dilatant behavior was observed only at high shear rates; the critical shear rate required reducing with increase of molecular weight. The film thickness in these experiments was in fact an effective hydrodynamic thickness (EHT), inferred from flow rate and pressure drop measurements under the assumption that the adsorbed layer reduces the pore diameter.

The above observations were in contrast to those by Cohen and Metzner (1982),

who, using the same polymers but in stainless steel capillaries instead of porous media, found the EHT to decrease with increase of shear rate. Further work by Cohen (1988) highlighted the effect of solvent quality on adsorption. For a good solvent, he observed the expected decrease of EHT with increase of shear rate. But for a θ-solvent, the EHT initially increased till the shear rate reached a critical value, beyond which an opposite trend was observed. However, experimenting with adsorbing surfaces of varying degrees of roughness, Bagassi et al. (1989) showed that for very smooth surfaces under shear flow, dilatational behavior do not exist. They hypothesized that previous observations of shear thickening resulted from elongational flow induced coil-stretch transition of the adsorbed polymer chains due to surface rugosity or irregularities in pore structure.

2.1.2 Experiments of Lee and Fuller

In a comprehensive set of experiments, Lee and Fuller (Lee and Fuller, 1984; Lee and Fuller, 1985a) demonstrated the effect of hydrodynamic forces on adsorption of polystyrene (PS) from cyclohexane onto chrome surfaces under shear flow. Using ellipsometric measurements, they showed that for preadsorbed films subjected to flow for short durations of time (1–2 minutes), the film thickness remained constant (within limits of experimental detection) with increasing shear rate for low-molecular-weight samples. Only for very high-molecular-weight samples ($\approx 20 \times 10^6$) and at very high shear rates ($\geq 2000\,\mathrm{s}^{-1}$) did the film thickness decrease with an increase in shear rate. When the flow was made to persist over longer periods of time (200–900 minutes), the adsorbed amount at any point in time was found to decrease with an increase in shear rate at a given molecular weight, and with an increase in molecular weight at a given shear rate. Figure 2.1 (a) shows the increase in relative adsorbance A/A_0 with respect to time for PS of molecular weight 20×10^6 g/mol at different shear rates. The relative adsorbance, defined as the ratio of the adsorbance under flow (A) to that at a quiescent state (A_0),

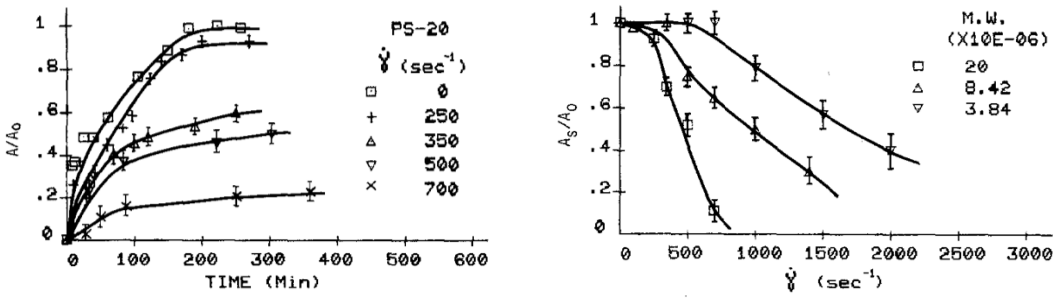

(a) **(b)**

Figure 2.1. (**a**) Adsorption curves for PS of molecular weight 20×10^6 g/mol at various shear rates. (**b**) Amount adsorbed at steady-state for PS of various molecular weights as a function of shear rate. [Ref. Lee and Fuller (1985a)]

is a measure of the amount of polymer adsorbed onto the surface. The steady-state adsorbance also showed the same overall trend, although at low shear rates a plateau value was observed, which gradually disappeared with increasing molecular weight (see Figure 2.1 (b), where A_s represents that amount adsorbed at the steady-state).

In the case of desorption of a preadsorbed film, the reduction in film thickness with time was observed only at very high shear rates, though the amount adsorbed exhibited a gradual decrease to a steady-state value at all shear rates. Moreover, it was shown that at high enough shear rates, complete desorption of a preadsorbed polymer layer is possible. For a given molecular weight sample, their experiments showed that increasing shear rate leads to enhanced desorption. Moreover, at low shear rate desorption occured at constant film thickness. This thickness is an averaged quantity determined by assuming the total adsorbed amount to be concentrated in a homogeneous film over the entire adsorbent surface (Stromberg et al., 1965). Figure 2.2 (a) shows the decrease in relative adsorbance A/A_0 with respect to time for PS of molecular weight 20×10^6 g/mol at different shear rates. Note that at lower shear rates, the amount adsorbed levels off to a finite value, but at higher shear rates complete desorption is achieved. In addition, at

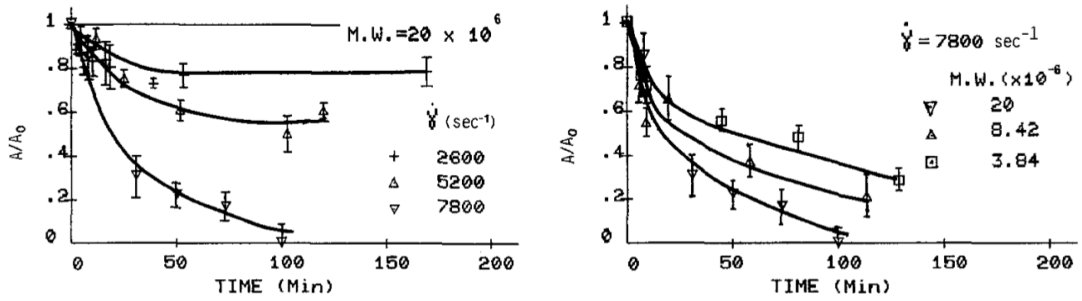

Figure 2.2. (**a**) Desorption curves for PS of molecular weight 20×10^6 g/mol at various shear rates. (**b**) Desorption curves for PS of various molecular weights at a shear rate of 7800 s^{-1}. [Ref. Lee and Fuller (1985a)]

shear rates large enough to cause complete desorption, higher molecular weight samples desorbed faster than lower molecular weight samples (see Figure 2.2 (b)).

2.1.3 Experiments of Soga and Granick

In contrast to Lee and Fuller (1985a)'s observations, Soga and Granick (1998) found minimal effect of shear flow on desorption of polymethyl methacrylate (PMMA) preadsorbed onto a germanium oxide (GeO_2) surface, even at shear rates much higher than those considered by Lee and Fuller (1985a). Since PMMA binds to GeO_2 via the carbonyl group, they measured the bound and free carbonyl groups at the interface using infrared spectroscopy. Figure 2.3 shows the amount of free and bound carbonyl groups at the surface. Note that there is a small reduction in the total carbonyl peak at the interface (denoted by ●) on increasing the shear rate. Comparing these results to that of Lee and Fuller (1985a), we note that the adsorption energy of PMMA to GeO_2 is approximately four times that of PS Soga and Granick (1998), but the highest shear rate considered in this case was also approximately four times greater; so it is surprising that the amount of PMMA desorbed was so low.

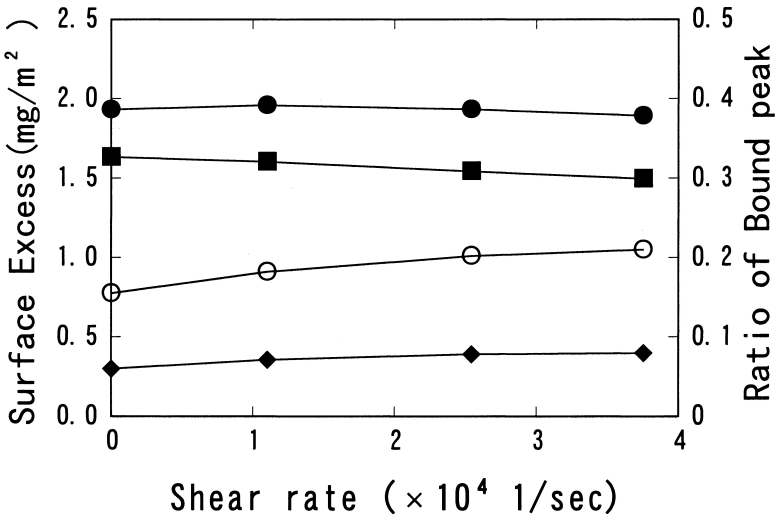

Figure 2.3. Surface excess and bound fraction plotted against shear rate: Free carbonyl peaks (■); bound carbonyl peaks (◆); the sum of free and bound carbonyl peaks (●); the ratio of the bound to the sum of free and bound peaks (○). [Ref. Soga and Granick (1998)]

2.1.4 Other studies

Experiments by Chin and Hoagland (1991) on adsorption of PS from cyclohexane onto chrome showed results qualitatively similar to those of Lee and Fuller (except that instead of a low-shear-rate plateau, they observed a continuous decrease in the adsorption level with shear rate). For a PS/decalin system, however, they found adsorption to be independent of shear rate even for high-molecular-weight samples. This indicates that the nature of the solvent plays a significant role in adsorption. However, unlike Lee and Fuller's observations, where a steady-state value in the adsorbed amount was eventually reached, McGlinn et al. (1988) found that the adsorbed amount for polymethylmethacrylate in carbon tetrachloride at low shear rates ($\approx 3\,\mathrm{s}^{-1}$) continued to increase with time without any sign of leveling off. The authors attributed their observations to entanglements and possible multilayer adsorption mechanisms.

At shear rates much lower ($0 - 120\ \mathrm{s}^{-1}$) than those considered in the experiments

discussed above, Chin and Hoagland (1991) found shear flow to have no effect on the desorption of PS in decalin from a chrome surface. Chang and Chung (1991) studied the desorption of polyethylene oxide (PEO) and polyvinyl alcohol (PVA) from PS latex spheres. For a preadsorbed layer of PEO, they observed the film thickness to decrease rapidly with time and level off to a steady-state value, irrespective of shear rate and molecular weight. For PVA, a reduction in the film thickness with time was observed only at very high shear rates and for low molecular weights. Because of the strong hydrophobic interaction of the residual acetate groups in PVA with the PS latex surface, the authors reasoned that PVA molecules will have a higher resistance to shear-induced desorption (Chang and Chung, 1991).

Experiments on suspensions of latex spheres with surface-grafted polymer molecules (polyethylene oxide urethanes) exposed to shear flow showed significant reduction of the adsorbed film thickness in the ambient flow as well as the ambient vorticity direction Chatterjee et al. (2014). This indicates possible desorption of grafted chains under shear. Similar to Lee and Fuller (1985a)'s results, the reduction in film thickness was monotonic with increase in shear rate. In contrast, at constant shear rate the film thickness initially decreased with an increase in molecular weight of the grafted polymers, followed by a later increase at higher molecular weight. Table 2.1 summarizes the anomalous trends observed in several experimental studies discussed above.

2.2 Theory and simulation

Several attempts have been made to develop a theoretical understanding of polymer adsorption in flow. The overall idea in these efforts is to account for the polymer-surface interaction via a potential and couple it with a polymer model. In an early study, Aubert (1983) developed a kinetic theory for adsorption from a quiescent fluid, using

Polymer/solvent/surface	(Ad/De)sorption	Effects	Reference
PS/C_6H_6/chrome	Adsorption	Amt. adsorbed decreases with an increase in shear rate as well as mol. wt.	Lee and Fuller (1985a)
PS/C_6H_6/chrome	Adsorption	Amt. adsorbed decreases with an increase in shear rate as well as mol. wt.	Chin and Hoagland (1991)
PS/decalin/chrome	Adsorption	No effect of shear rate/mol. wt.	Chin and Hoagland (1991)
PS/C_6H_6/chrome	Desorption	Desorption increases with an increase in shear rate as well as mol. wt.	Lee and Fuller (1985a)
PS/decalin/chrome	Desorption	No effect of shear rate	Chin and Hoagland (1991)
PEO/water/PS-latex	Desorption	No effect of shear rate/mol. wt.	Chang and Chung (1991)
PVA/water/PS-latex	Desorption	EHT decreases only for low mol. wt. samples at high shear rate	Chang and Chung (1991)
PMMA/CCl_4/GeO_2	Desorption	No effect of shear rate	Soga and Granick (1998)

Table 2.1: Summary of anomalous experimental results for polymer adsorption under shear flow.

a linear dumbbell model without hydrodynamic interaction (HI) for the polymer, and a square-well potential. Atkinson et al. (1984) used bead-spring chains without HI to model polymer fragments attached to a surface in steady shear flow. For Hookean springs, the analytically calculated film thickness showed no dependence on shear rate. For nonlinear springs with finite extensibility, Monte Carlo simulations showed a drop in film thickness, particularly beyond a critical shear rate. Also, it was shown that presence of an elongational component can lead to an increase in film thickness, as reported by Gramain and Myard (1981).

The effect of flow was considered by Grisafi and Durning (1989b) using linear dumbbells interacting with the surface through a 12-6 Lennard-Jones (LJ) potential. However, to obtain a closed-form solution, they considered the attraction-dominated limit. Their calculations predicted a shear-rate-independent film thickness, which corresponds to the observations of Lee and Fuller (1984) at low molecular weights. This study was further developed by considering multibead free-draining chains with Hookean springs interacting via a Sutherland potential (Grisafi and Durning, 1989a). However, similar to the linear dumbbell-based model, this model predicts no change in the film thickness from its equilibrium value in the presence of flow.

Earlier theoretical work, also due to Lee and Fuller (Lee and Fuller, 1985b), indicated that hydrodynamic interaction (HI) between the polymer segments and the adsorbing surface may be an important factor. In that work, an adsorbed loop was modeled by a single bead connected to two points on a planar surface by two nonlinear springs. The loop could be reduced to a dangling end if the distance between the two points on the surface was allowed to go to zero. The thickness of the adsorbed layer at steady state was calculated from the moments of the diffusion equation governing the motion of the bead. If HI with the wall was taken into account, i.e., the bead diffusion coefficient was allowed to depend on the distance from the wall, significant reduction in the layer

thickness was observed. But if the diffusion coefficient was assumed to be constant, the reduction in the layer thickness was relatively less.

A number of computational studies (de Pablo et al., 1992; Chopra and Larson, 2002; Panwar and Kumar, 2005; Hoda and Kumar, 2007c; Hoda and Kumar, 2008; Sendner and Netz, 2008; Serr et al., 2010) have also attempted to develop an understanding of the experimental results discussed above. In most of these studies, the primary emphasis was on understanding steady-state adsorption, though transient behavior was specifically investigated by de Pablo et al. (1992) and Chopra and Larson (2002). For rod-like polymer molecules, stochastic simulations (in the absence of HI) by de Pablo et al. (1992) showed an increase in the depletion layer thickness at high shear rates and a transient decrease at low to intermediate shear rates. These observations are qualitatively different from those of Lee and Fuller (1985a), possibly due to the differences between the behavior of flexible and rigid polymers under shear flow near a wall (Saintillan et al., 2006). The simulations of Chopra and Larson (2002) also neglect HI.

Incorporating HI and using the more realistic finitely extensible nonlinear elastic (FENE) dumbbbell, Hoda and Kumar (2007d) developed a kinetic theory for studying adsorption of polyelectrolytes in shear flow, with surface interactions described via a screened Coulombic potential. Their theory also accounts for the migration of polyelectrolytes in shear flow, which has a considerable effect on the steady-state concentration profile, and hence the quantity adsorbed. In subsequent works (Hoda and Kumar, 2007c; Hoda and Kumar, 2008), they used Brownian dynamics (BD) simulations to systematically study the effects of solvent quality and patterned surfaces on polyelectrolyte adsorption in great detail. It was found that in addition to flow strength, adsorption depends on the strength of electrostatic screening. Sendner and Netz (2008) studied stiff polymers and obtained scaling results for the repulsive force causing shear-induced depletion. Serr et al. (2010) also studied the effect of surface friction due to a corru-

gated interaction potential on polyelectrolyte adsorption and found it to weaken surface attraction.

Chapter 3

Kinetic theory: Steady state

Summary

Adsorption of homopolymers from a dilute solution to a planar wall in the presence of shear flow is studied using a bead-spring dumbbell model. The bead-bead and bead-wall interactions are described by generalized Lennard-Jones potentials. A kinetic theory incorporating bead-wall hydrodynamic interaction is developed in order to obtain an analytical expression for the steady-state dumbbell concentration profile. The concentration profile exhibits an exclusion zone in the immediate vicinity of the wall, is followed by a peak, and finally approaches the bulk concentration far away from the wall. Using the analytical expression, the amount adsorbed and the equivalent film thickness are studied as a function of flow strength and the parameters characterizing the bead-wall interaction potential. Shear flow causes migration of the dumbbells due to bead-wall hydrodynamic interaction, which leads to desorption. On increasing the flow strength, the quantity adsorbed and the film thickness decrease until complete desorption occurs. The dependence of the flow strength required for desorption on the model parameters is also studied and a scaling law is derived for the strong-interaction limit. Brownian dynamics simulations are performed to verify the predictions from the kinetic theory. Although the theory makes a number of simplifying assumptions, it captures many of the key features

seen in the simulations.

This chapter was published as S. Dutta, K. D. Dorfman, and S. Kumar, "Adsorption of single polymer molecules in shear flow near a planar wall", J. Chem. Phys. **138**, 034905 (2013).

3.1 Introduction

As discussed in Chapter 1, adsorption of homopolymers from a flowing fluid onto a solid surface is of considerable interest due to both its technological significance and fundamental importance. Although a number of experimental studies exist, a comprehensive explanation of their results is lacking, and the mechanisms of adsorption in flow remain far from understood. Here we provide insight into the adsorption process by developing a kinetic theory for polymer molecules, modeled as bead-spring dumbbells, which interact with a surface through a generalized Lennard-Jones (LJ) potential in the presence of shear flow. In particular, we investigate the following two issues: (i) how the amount of adsorbed polymer depends on the interaction potential and flow strength, and (ii) how the flow strength at which polymers desorb depends on the interaction potential.

It should be noted that all the theories discussed earlier (see Sec. 2.2) have been developed under the assumption that the polymer molecules do not interact with each other. This is a good assumption for dilute solutions in the bulk, but may break down in the region close to the wall. Here, polymer molecules interact with each other, possibly forming entanglements. Nevetheless, it is still worthwhile to develop kinetic theores based on the diluteness assumption for two reasons. First, analytical progress can be made, and this can yield considerable physical insight relative to purely numerical approaches. Second, such theories allow for a thorough examination of an important limiting case,

which can provide a solid foundation for the development of theories that relax the diluteness assumption. With this view in mind, we developed a dumbbell-based kinetic theory for neutral homopolymers interacting with a surface through a general power-law potential. Our principal motivation is to account for adsorption due to non-electrostatic forces, e.g. hydrogen bonds (Phillips et al., 2007; Horinek et al., 2008) and van der Waals forces (van Oss et al., 1986; Roth et al., 1996), which are usually modeled using LJ-type potentials. Before proceeding, we briefly explain the mechanism of polymer migration in shear flow. As will be seen later, this mechanism is central to the adsorption problem considered here.

Modeling a polymer molecule as a bead-spring dumbbell, shear-induced migration can be explained as a consequence of HI between the beads and a nearby wall (Ma and Graham, 2005). We briefly summarize the mechanism here with the help of Figure 3.1. In the presence of shear flow parallel to the wall, the dumbbells will be stretched and are more likely to orient themselves as shown in Figure 3.1 (a). Considering the non-hydrodynamic force on each bead to be localized at a point, and invoking the assumption of zero Reynolds number, the Stokes equations can be solved to obtain the velocity field near a single wall due to each point force. Figure 3.1 (b) shows the velocity field in the xz-plane due to each of the beads. The z-velocity at bead 2 due to bead 1 points away from the wall and, without inertia, the force is proportional to the velocity. This causes bead 2 to move away from the wall. A similar reasoning applies to bead 1 also, resulting in a net migration of the dumbbell in the wall-normal direction.

Our paper is organized as follows: In Sec. 4.2 we develop the kinetic theory, followed by a description of our BD simulation algorithm in Sec. 5.2. We present results for steady-state concentration profile, amount adsorbed, and desorption behavior in Sec. 3.4, and finally, we conclude by summarizing our key findings in Sec. 3.5.

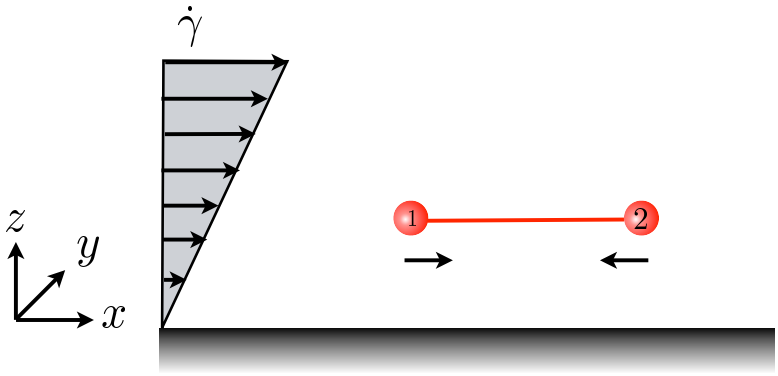

(a)

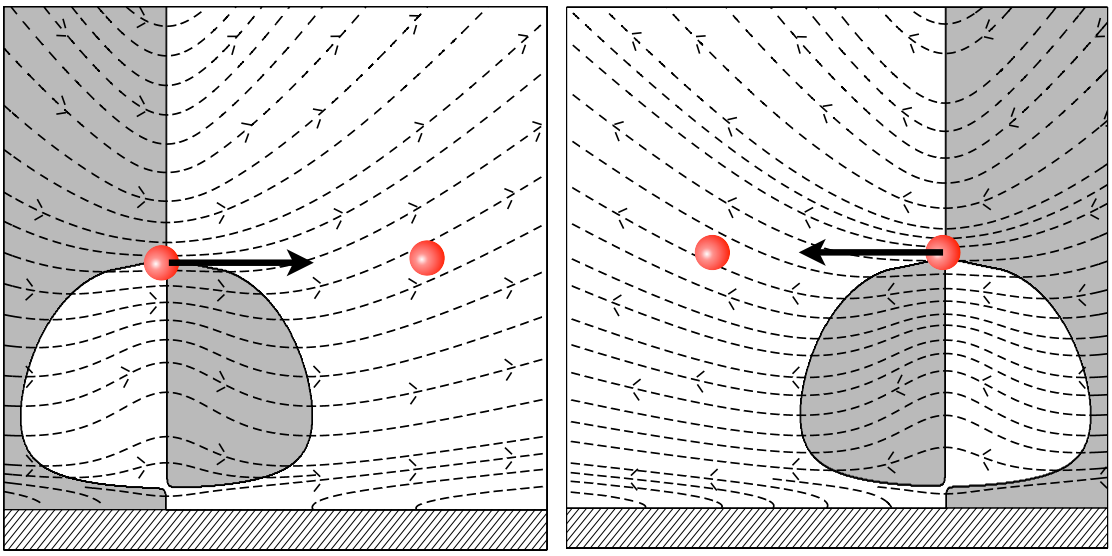

(b)

Figure 3.1. (a) Schematic of a dumbbell in shear flow near a wall. The arrows pointing in opposite directions indicate forces on the beads. **(b)** The velocity field in the xz-plane induced by each bead of the dumbbell acting as a point force parallel to the wall. The regions where the velocity has a component toward the wall are shaded in gray.

3.2 Kinetic theory for dumbbells

We consider a dilute polymer solution of uniform concentration at rest in a semi-infinite domain bounded from below by a solid wall at $z = 0$. At time $t = 0$, the solution is subjected to a shear flow with shear rate $\dot{\gamma}$ parallel to the x-axis. We wish to determine the steady-state concentration profile in the solution.

We model a polymer molecule by two beads, each of radius ξ, connected via a massless spring. If the centers of the two beads are at $\mathbf{r}_1$ and $\mathbf{r}_2$, the center of mass of the dumbbell is $\mathbf{r}_c = (\mathbf{r}_1 + \mathbf{r}_2)/2$ and the connector vector is $\mathbf{Q} = \mathbf{r}_2 - \mathbf{r}_1$. The translational velocity of the dumbbell center $\dot{\mathbf{r}}_c$ can be obtained from the equations of motion of the beads. Neglecting inertia, the equation of motion for bead i can be obtained by balancing the forces acting on it:

$$\mathbf{F}_i^B + \mathbf{F}_i^S + \mathbf{F}_i^{BB} + \mathbf{F}_i^{BW} + \mathbf{F}_i^H = \mathbf{0}, \qquad i = 1, 2 \tag{3.1}$$

where $\mathbf{F}_i^B$ is the Brownian force resulting from thermal fluctuations, $\mathbf{F}_i^S$ is the spring force, $\mathbf{F}_i^{BB}$ is the force due to bead-bead interaction, $\mathbf{F}_i^{BW}$ is the force due to bead-wall interaction, and $\mathbf{F}_i^H$ is the hydrodynamic drag force due to the solvent. Assuming a Maxwellian distribution for bead momenta, the Brownian force is (Bird et al., 1987)

$$\mathbf{F}_i^B = -kT \frac{\partial}{\partial \mathbf{r}_i} \ln \psi, \tag{3.2}$$

where $\psi = \psi(\mathbf{r}_c, \mathbf{Q}, t)$ is the configurational distribution function of the dumbbell.

The expression for spring force is given by the finitely extensible nonlinear elastic spring law with the Peterlin approximation (FENE-P) (Peterlin, 1966; Bird et al., 1980):

$$\mathbf{F}_i^S = \frac{H}{1 - \langle Q^2/Q_0^2 \rangle} (\mathbf{r}_j - \mathbf{r}_i), \qquad i, j = 1, 2 \tag{3.3}$$

where H is the spring constant, $Q = |\mathbf{Q}|$, Q_0 is the maximum spring length, and the angle brackets denote an average over all connector vectors. The spring extensibility parameter is $b_k = HQ_0^2/kT = 3N_k$, where N_k is the number of Kuhn segments per spring.

The force due to bead-bead interaction is chosen to be of the form derived from a generalized Lennard-Jones potential:

$$\mathbf{F}_i^{BB} = \frac{\varepsilon_b kT}{\sigma_b}\left[a\left(\frac{\sigma_b}{Q}\right)^{a+1} - b\left(\frac{\sigma_b}{Q}\right)^{b+1}\right]\frac{\mathbf{r}_i - \mathbf{r}_j}{|\mathbf{r}_i - \mathbf{r}_j|}, \tag{3.4}$$

where ε_b determines the strength of the interaction (in units of kT), σ_b is the interbead distance at which the interaction potential vanishes, and a and b are the repulsive and attractive exponents ($a > b$) respectively. This force can be considered as an excluded volume interaction with appropriate values of a and b. Alternatively, it can be reduced to a purely attractive force by dropping the repulsive term and vice-versa. The bead-wall interaction is similarly chosen as above, but with a different set of parameters:

$$\mathbf{F}_i^{BW} = \frac{\varepsilon_s kT}{\sigma_s}\left[c\left(\frac{\sigma_s}{z}\right)^{c+1} - d\left(\frac{\sigma_s}{z}\right)^{d+1}\right]\hat{\boldsymbol{z}}, \tag{3.5}$$

where ε, σ_s, c, and d play similar roles, and $\hat{\boldsymbol{z}}$ is the unit vector along the z-axis.

Under creeping-flow conditions, the hydrodynamic drag force is given by

$$\mathbf{F}_i^H = -\zeta\left(\dot{\mathbf{r}}_i - \mathbf{v}_i\right), \tag{3.6}$$

where $\mathbf{v}_i$ is the solvent velocity at $\mathbf{r}_i$, $\zeta = 6\pi\eta\xi$ is the bead friction coefficient, and η is the solvent viscosity. The solvent velocity is $\mathbf{v}_i = \mathbf{v}_i^0 + \mathbf{v}_i^{pf}$, where $\mathbf{v}_i^0$ is the velocity at $\mathbf{r}_i$ in the absence of other beads, and $\mathbf{v}_i^{pf}$ is the perturbation at $\mathbf{r}_i$ due to the motion of other beads. Following the works of Ma and Graham (2005) and Hoda and Kumar

(2007d), we obtain $\mathbf{v}_i^0$ by Taylor expanding the solvent velocity about the dumbbell center of mass $\mathbf{r}_c$ and retaining terms only up to second order. The perturbation $\mathbf{v}_i^{pf}$ can be obtained by solving the Stokes equations considering the hydrodynamic drag force due to other beads $\mathbf{F}_j^H$ as point forces acting on the solvent,

$$\mathbf{v}_i^{pf} = -\sum_j \mathbf{\Omega}_{ij} \cdot \mathbf{F}_j^H, \tag{3.7}$$

where $\mathbf{\Omega}_{ij}$ is the HI tensor between beads i and j and $\mathbf{F}_j^H$ is the hydrodynamic drag force on bead j.

For a dumbbell, there are only two beads, so the summation above reduces to a single term. In the case of a single wall, the HI tensor was calculated by (Blake, 1971) using the method of images to be

$$\mathbf{\Omega}_{ij} = \frac{1}{8\pi\eta}\left[\mathbf{S}\left(\mathbf{r}_i - \mathbf{r}_j\right) - \mathbf{S}\left(\mathbf{r}_i - \mathbf{r}_j^{im}\right) + 2z_j^2\mathbf{P}^D\left(\mathbf{r}_i - \mathbf{r}_j^{im}\right) - 2z_j\mathbf{S}^D\left(\mathbf{r}_i - \mathbf{r}_j^{im}\right)\right], \tag{3.8}$$

where z_j is the z-component of $\mathbf{r}_j$, $\mathbf{r}_j^{im} = [x_j, y_j, -z_j]$ is the image of $\mathbf{r}_j$ about the wall, and the tensors $\mathbf{S}$, $\mathbf{P}^D$, and $\mathbf{S}^D$ are the free-space Stokeslet, the potential dipole, and the Stokeslet doublet respectively, defined as follows:

$$S_{ij}\left(\mathbf{x}\right) = \frac{\delta_{ij}}{|\mathbf{x}|} + \frac{x_i x_j}{|\mathbf{x}|^3}, \tag{3.9}$$

$$P_{ij}^D\left(\mathbf{x}\right) = \left(1 - 2\delta_{j3}\right)\left(\frac{\delta_{ij}}{|\mathbf{x}|^3} - 3\frac{x_i x_j}{|\mathbf{x}|^5}\right), \tag{3.10}$$

$$S_{ij}^D\left(\mathbf{x}\right) = x_3 P_{ij}^D\left(\mathbf{x}\right) + \left(1 - 2\delta_{j3}\right)\left(\frac{\delta_{j3}x_i - \delta_{i3}x_j}{|\mathbf{x}|^3}\right), \tag{3.11}$$

where δ_{ij} is the Kronecker delta. Using the above equations, transforming variables from bead positions to center of mass position and the connector vector, and using the

relations $\mathbf{F}^{BB} = \mathbf{F}_1^{BB} = -\mathbf{F}_2^{BB}$ and $\mathbf{F}^{S} = \mathbf{F}_1^{S} = -\mathbf{F}_2^{S}$ for a dumbbell, we obtain

$$\begin{aligned}\dot{\mathbf{r}_c} = \mathbf{v} + \frac{1}{8}\mathbf{QQ} : \nabla\nabla\mathbf{v} + \frac{1}{2}\overline{\boldsymbol{\Upsilon}} \cdot \left[\mathbf{F}^{S} + \mathbf{F}^{BB} - \frac{1}{2}\left(\mathbf{F}_2^{BW} - \mathbf{F}_1^{BW}\right)\right] + \frac{1}{2}kT\overline{\boldsymbol{\Upsilon}} \cdot \frac{\partial}{\partial \mathbf{Q}} \ln\psi \\ - \mathbf{D}_K \cdot \left[\frac{\partial}{\partial \mathbf{r}_c} \ln\psi - \frac{1}{kT}\left(\mathbf{F}_1^{BW} + \mathbf{F}_2^{BW}\right)\right],\end{aligned} \tag{3.12}$$

where $\mathbf{v}$ is the solvent velocity at $\mathbf{r}_c$,

$$\overline{\boldsymbol{\Upsilon}} = \left(\boldsymbol{\Upsilon}_{11} - \boldsymbol{\Upsilon}_{22}\right) + \left(\boldsymbol{\Upsilon}_{21} - \boldsymbol{\Upsilon}_{12}\right), \tag{3.13}$$

and

$$\boldsymbol{\Upsilon}_{ij} = \boldsymbol{\Omega}_{ij} - \frac{\delta_{ij}}{8\pi\eta}\mathbf{S}\left(\mathbf{r}_i - \mathbf{r}_j\right). \tag{3.14}$$

The Kirkwood diffusivity is

$$\mathbf{D}_K = \frac{1}{4}\left(\mathbf{D}_{11} + \mathbf{D}_{12} + \mathbf{D}_{21} + \mathbf{D}_{22}\right), \tag{3.15}$$

where

$$\mathbf{D}_{ij} = kT\left(\frac{\delta_{ij}}{6\pi\eta a}\mathbf{I} + \boldsymbol{\Upsilon}_{ij}\right). \tag{3.16}$$

The conservation equation for the configurational distribution function ψ is (Bird et al., 1987)

$$\frac{\partial\psi}{\partial t} = -\frac{\partial}{\partial \mathbf{r}_c} \cdot \left(\dot{\mathbf{r}_c}\psi\right) - \frac{\partial}{\partial \mathbf{Q}} \cdot \left(\dot{\mathbf{Q}}\psi\right). \tag{3.17}$$

We assume ψ can be factorized as $\psi\left(\mathbf{r}_c, \mathbf{Q}, t\right) = n\left(\mathbf{r}_c, t\right)\hat{\psi}\left(\mathbf{r}_c, \mathbf{Q}, t\right)$, where $n\left(\mathbf{r}_c, t\right) = \int \psi\left(\mathbf{r}_c, \mathbf{Q}, t\right) \mathrm{d}\mathbf{Q}$ is the distribution of the dumbbell center of mass and $\hat{\psi}\left(\mathbf{r}_c, \mathbf{Q}, t\right)$ can be considered as a conditional distribution of $\mathbf{Q}$ on $\mathbf{r}_c$. Integrating Equation (3.17) with

respect to $\mathbf{Q}$, we obtain

$$\frac{\partial n}{\partial t} = -\frac{\partial}{\partial \mathbf{r}_c} \cdot (n\langle \dot{\mathbf{r}}_c \rangle) = -\frac{\partial}{\partial \mathbf{r}_c} \cdot \mathbf{j}_c, \tag{3.18}$$

where $\mathbf{j}_c$ is the flux of the dumbbell center of mass. Here and in all subsequent occurrences, for any quantity x we define,

$$\langle x \rangle = \int x\hat{\psi}\, \mathrm{d}\mathbf{Q}. \tag{3.19}$$

Multiplying Equation (3.12) with ψ and integrating over $\mathbf{Q}$ we have

$$\begin{aligned} \mathbf{j}_c = n\mathbf{v} + \frac{n}{8}\langle \mathbf{QQ} \rangle : \nabla\nabla\mathbf{v} + \frac{n}{2}\left\langle \overline{\boldsymbol{\Upsilon}} \cdot \left[\mathbf{F}_1^S + \mathbf{F}_1^{BB} - \frac{1}{2}\left(\mathbf{F}_2^{BW} - \mathbf{F}_1^{BW} \right) + kT\frac{\partial \ln \hat{\psi}}{\partial \mathbf{Q}} \right] \right\rangle \\ - \langle \mathbf{D_K} \rangle \cdot \frac{\partial n}{\partial \mathbf{r}_c} - n\left\langle \mathbf{D_K} \cdot \frac{\partial \ln \hat{\psi}}{\partial \mathbf{r}_c} \right\rangle + \frac{n}{kT}\left\langle \mathbf{D_K} \cdot \left(\mathbf{F}_1^{BW} + \mathbf{F}_2^{BW} \right) \right\rangle, \end{aligned} \tag{3.20}$$

Using the Kramers expression for the stress tensor

$$\frac{\boldsymbol{\tau}^p}{nkT} = -\frac{1}{kT}\left\langle \mathbf{Q}\left\{ \mathbf{F}_1^S + \mathbf{F}_1^{BB} - \frac{1}{2}\left(\mathbf{F}_2^{BW} - \mathbf{F}_1^{BW} \right) \right\} \right\rangle + \mathbf{I}, \tag{3.21}$$

we rewrite Equation (3.20) as

$$\begin{aligned} \mathbf{j}_c = n\mathbf{v} + \frac{n}{8}\langle \mathbf{QQ} \rangle : \nabla\nabla\mathbf{v} - \mathbf{M} : \boldsymbol{\tau}^p - \langle \mathbf{D_K} \rangle \cdot \frac{\partial n}{\partial \mathbf{r}_c} - n\left\langle \mathbf{D_K} \cdot \frac{\partial \ln \hat{\psi}}{\partial \mathbf{r}_c} \right\rangle \\ + \frac{n}{kT}\left\langle \mathbf{D_K} \cdot \left(\mathbf{F}_1^{BW} + \mathbf{F}_2^{BW} \right) \right\rangle, \end{aligned} \tag{3.22}$$

where $\mathbf{M}$ is a third-order tensor defined as $\mathbf{M} = 3\widetilde{\mathbf{M}}/64\pi\eta z^2$. The components of $\widetilde{\mathbf{M}}$ are

(Hoda and Kumar, 2007d)

$$\widetilde{M}_{333} = -\frac{2}{1-\langle Q_z^2\rangle/4z^2}, \tag{3.23}$$

$$\widetilde{M}_{311} = \widetilde{M}_{322} = \frac{1-\langle Q_z^2\rangle/4z^2}{\left[1+\left(\langle Q_x^2\rangle+\langle Q_y^2\rangle\right)/4z^2\right]^{5/2}}, \tag{3.24}$$

$$\widetilde{M}_{131} = \widetilde{M}_{232} = -\frac{1-\langle Q_z^2\rangle/4z^2}{\left[1+\left(\langle Q_x^2\rangle+\langle Q_y^2\rangle\right)/4z^2\right]^{5/2}}, \tag{3.25}$$

$$\widetilde{M}_{113} = \widetilde{M}_{223} = -\frac{1}{1-\langle Q_z^2\rangle/4z^2}, \tag{3.26}$$

$$\widetilde{M}_{ijk} = 0, \qquad \text{other} \quad i,j,k, \tag{3.27}$$

and z is the z-component of $\mathbf{r}_c$. An equivalent expression for the stress tensor is the Giesekus form

$$\frac{\boldsymbol{\tau}^p}{nkT} = \frac{\zeta}{4kT}\langle\mathbf{QQ}\rangle_{(1)} + \frac{1}{4kT}\left\langle\mathbf{Q}\left(\mathbf{F}_2^{BW}-\mathbf{F}_1^{BW}\right)-\left(\mathbf{F}_2^{BW}-\mathbf{F}_1^{BW}\right)\mathbf{Q}\right\rangle, \tag{3.28}$$

where the subscript (1) denotes the upper convected derivative (Bird et al., 1980). We further simplify the bead-wall forces by Taylor expanding about the dumbbell center of mass (Hoda and Kumar, 2007d) and neglecting terms beyond first order.

Comparing the Kramers and Giesekus expressions (Equation (3.21) and Equa-

tion (3.28)), we obtain three nonlinear equations:

$$\frac{2\mathrm{Wi}^2 b_k^2 C_3}{\frac{b_k}{1-C_4} - \frac{\alpha}{C_4^{1+\frac{a}{2}}} + \frac{\beta}{C_4^{1+\frac{b}{2}}} + \frac{1}{4}\left\{\frac{\gamma}{Z^{c+2}} - \frac{\delta}{Z^{d+2}}\right\}} - C_1\left[\frac{b_k}{1-C_4} - \frac{\alpha}{C_4^{1+\frac{a}{2}}} + \frac{\beta}{C_4^{1+\frac{b}{2}}}\right] + 1 = 0, \tag{3.29}$$

$$C_2\left[\frac{b_k}{1-C_4} - \frac{\alpha}{C_4^{1+\frac{a}{2}}} + \frac{\beta}{C_4^{1+\frac{b}{2}}}\right] - 1 = 0, \tag{3.30}$$

$$C_3\left[\frac{b_k}{1-C_4} - \frac{\alpha}{C_4^{1+\frac{a}{2}}} + \frac{\beta}{C_4^{1+\frac{b}{2}}} + \frac{1}{2}\left\{\frac{\gamma}{Z^{c+2}} - \frac{\delta}{Z^{d+2}}\right\}\right] - 1 = 0. \tag{3.31}$$

Here, the Weissenberg number $\mathrm{Wi} = \lambda_H \dot{\gamma}$ is a measure of the flow strength, $\lambda_H = \zeta/4H$ is the Rouse relaxation time for a dumbbell, and Z is the z-component of the dumbbell center of mass non-dimensionalized by $\sqrt{kT/H}$. The other variables appearing in the equations are defined as follows:

$$\begin{aligned}
C_1 &= \left\langle \frac{Q_x^2}{Q_0^2} \right\rangle, & C_2 &= \left\langle \frac{Q_y^2}{Q_0^2} \right\rangle, \\
C_3 &= \left\langle \frac{Q_z^2}{Q_0^2} \right\rangle, & C_4 &= C_1 + C_2 + C_3, \\
\alpha &= a\varepsilon_b \left(\frac{\sigma_b}{Q_0}\right)^a, & \beta &= b\varepsilon_b \left(\frac{\sigma_b}{Q_0}\right)^b, \\
\gamma &= b_k c\,(c+1)\,\varepsilon_s \sigma_s^{*c}, & \delta &= b_k d\,(d+1)\,\varepsilon_s \sigma_s^{*d},
\end{aligned} \tag{3.32}$$

where $\sigma_s^* = \sigma_s/\sqrt{kT/H}$.

After solving for C_1, C_2, and C_3, the stress tensor can be obtained from either the

Kramers or the Giesekus expressions:

$$\begin{aligned}
\frac{\tau_{xx}^p}{nkT} &= -\left[\frac{b_k}{1-C_4} - \frac{\alpha}{C_4^{1+\frac{a}{2}}} + \frac{\beta}{C_4^{1+\frac{b}{2}}}\right] C_1 + 1, \\
\frac{\tau_{xz}^p}{nkT} &= -\mathrm{Wi} b_k C_3 \left[1 + \frac{\frac{1}{4}\left\{\frac{\gamma}{Z^{c+2}} - \frac{\delta}{Z^{d+2}}\right\}}{\frac{b_k}{1-C_4} - \frac{\alpha}{C_4^{1+\frac{a}{2}}} + \frac{\beta}{C_4^{1+\frac{b}{2}}} + \frac{1}{4}\left\{\frac{\gamma}{Z^{c+2}} - \frac{\delta}{Z^{d+2}}\right\}}\right], \\
\frac{\tau_{zx}^p}{nkT} &= -\mathrm{Wi} b_k C_3 \left[1 - \frac{\frac{1}{4}\left\{\frac{\gamma}{Z^{c+2}} - \frac{\delta}{Z^{d+2}}\right\}}{\frac{b_k}{1-C_4} - \frac{\alpha}{C_4^{1+\frac{a}{2}}} + \frac{\beta}{C_4^{1+\frac{b}{2}}} + \frac{1}{4}\left\{\frac{\gamma}{Z^{c+2}} - \frac{\delta}{Z^{d+2}}\right\}}\right],
\end{aligned} \tag{3.33}$$

and all other components are zero. Note that the stress tensor here is not symmetric due to the presence of the bead-wall interaction, which results in unequal forces on the beads. This was also the case in the derivaton by Hoda and Kumar (2007d), although the authors did not explicitly point it out.

To proceed analytically, we replace $\mathbf{D}_K$ as well as its average $\langle \mathbf{D}_K \rangle$ by the free-draining value $D_K = kT/12\pi\eta\xi$, i.e., $\mathbf{D}_K = \langle \mathbf{D}_K \rangle = kT/12\pi\eta\xi$. This makes the fifth term in Equation (3.22) vanish. Also, for shear flow, $\mathbf{v} = [\dot{\gamma} z, 0, 0]$. Therefore for the z-direction at steady state, Equation (3.18) reduces to

$$\frac{d}{dz}\left[-D_K \frac{dn}{dz} - \frac{3\left[\widetilde{\mathbf{M}} : \boldsymbol{\tau}^p\right]_z}{64\pi\eta n}\left(\frac{n}{z^2}\right) + 2nD_K\varepsilon_s\left\{-\frac{c\sigma_s^{*c}}{z^{c+1}} + \frac{d\sigma_s^{*d}}{z^{d+1}}\right\}\right] = 0, \tag{3.34}$$

where the subscript z refers to the z-component. Nondimensionalizing length by $\sqrt{kT/H}$ and concentration by the bulk concentration n_{bulk}, we have

$$\frac{d}{dZ}\left[-\frac{d\theta}{dZ} + L_d\frac{\theta}{Z^2} + 2\left\{\frac{\gamma}{b\,(c+1)\,Z^{c+1}} - \frac{\delta}{b\,(d+1)\,Z^{d+1}}\right\}\theta\right] = 0, \tag{3.35}$$

where $\theta = n/n_{bulk}$, the depletion layer thickness

$$L_d = -\frac{9}{16}\sqrt{\pi}h^* \frac{\left[\widetilde{\mathbf{M}} : \boldsymbol{\tau}^p\right]_z}{nkT},$$

and the hydrodynamic interaction parameter $h^* = (\zeta/\eta)\sqrt{H/36\pi^3 kT}$. Solving Equation (3.35) with the boundary conditions

$$\begin{aligned} &Z \to \infty, \qquad \theta \to 1 \\ &Z \to 0, \qquad j_{c,z} = 0 \implies \frac{d\theta}{dZ} \to 0 \end{aligned}$$

gives the concentration profile at steady state:

$$\theta = \exp\left[-\int_Z^\infty \frac{L_d}{Z^2}\,\mathrm{d}Z + 2\varepsilon_s\left\{\left(\frac{\sigma_s^*}{Z}\right)^d - \left(\frac{\sigma_s^*}{Z}\right)^c\right\}\right]. \tag{3.36}$$

The first term within the square bracket above accounts for migration of the dumbbells away from the wall due to bead-wall HI, the second term accounts for migration toward the wall due to bead-wall attraction, and the last term represents the effect of bead-wall repulsion. The steady-state concentration profile is determined by the relative strengths of each of these terms. Note that $\theta < 1$ indicates reduced concentration relative to the bulk, whereas $\theta > 1$ indicates enhanced concentration relative to the bulk. A similar expression was derived by Hoda and Kumar (2007d) for polyelectrolytes, but their result did not contain any contribution due to bead-wall repulsion. Of course, this is purely a consequence of using an LJ-type potential here in contrast to a screened Coulombic potential with opposite charges on the beads and the wall, which is a purely attractive interaction. The presence of a strong repulsive term will lead to the formation of an exclusion zone in the immediate vicinity of the wall. This effect is important in order to account for any steric hindrance on the dumbbells. Using Equation (3.36), we will

analyze the effect of flow and the parameters of the potential on the concentration profile and the amount adsorbed in Sec. 3.4.

3.3 Brownian dynamics simulation

Our simulation algorithm is the same as that described in Appendix A of Hoda and Kumar (2007c). In the simulation, length is made dimensionless by $\sqrt{kT/H}$, time by ζ/H, force with $\sqrt{kTH}$, and diffusivity with kT/ζ. The dumbbell trajectories are calculated by numerically solving the stochastic differential equation:

$$\mathbf{r}^{new} = \mathbf{r}^{old} + \left[\mathbf{u} + \mathbf{D}\cdot\mathbf{F} + \frac{\partial}{\partial \mathbf{r}}\cdot\mathbf{D}\right] dt + \sqrt{2}\mathbf{B}\cdot d\mathbf{w}, \tag{3.37}$$

where $\mathbf{r}^{old}$ is the vector of bead positions at time t, $\mathbf{r}^{new}$ is the vector of bead positions at time $t + dt$, $\mathbf{u}$ is the unperturbed solvent velocity at the bead positions, $\mathbf{F}$ is the non-Brownian non-hydrodynamic force on the beads, $\mathbf{D}$ is the diffusivity tensor, dt is the time step, $\mathbf{B} = \sqrt{\mathbf{D}}$, and $d\mathbf{w}$ is a Gaussian process with zero mean and variance dt. The tensor $\mathbf{B}$ is determined by factorizing $\mathbf{D}$ as $\mathbf{D} = \mathbf{B}\cdot\mathbf{B}^{\mathrm{T}}$ using Cholesky decomposition.

The diffusivity tensor consists of 3×3 blocks denoted by the subscript ij,

$$\mathbf{D}_{ij} = \mathbf{\Omega}_{ij} + \delta_{ij}\mathbf{I}, \tag{3.38}$$

where

$$\mathbf{\Omega}_{ij} = (1 - \delta_{ij})\,\mathbf{\Omega}_{ij}^{RPY} + \mathbf{\Omega}_{ij}^{W}. \tag{3.39}$$

In the above equation, $\mathbf{\Omega}_{ij}^{RPY}$ is the Rotne-Prager-Yamakawa (RPY) tensor (Rotne and

Prager, 1969; Yamakawa, 1970)

$$\mathbf{\Omega}_{ij}^{RPY} = \begin{cases} \frac{3\xi}{4r_{ij}}\left[C_1\mathbf{I} + C_2\frac{\mathbf{r}_{ij}\mathbf{r}_{ij}}{r_{ij}^2}\right] & r_{ij} \geq 2\xi \\ C_1'\mathbf{I} + C_2'\frac{\mathbf{r}_{ij}\mathbf{r}_{ij}}{r_{ij}^2} & r_{ij} < 2\xi \end{cases} \tag{3.40}$$

$$\begin{aligned} C_1 &= 1 + \frac{2\xi^2}{3r_{ij}^2}, & C_2 &= 1 - \frac{2\xi^2}{3r_{ij}^2}, \\ C_1' &= 1 - \frac{9r_{ij}}{32\xi}, & C_2' &= \frac{r_{ij}}{32\xi}, \end{aligned} \tag{3.41}$$

where $\mathbf{r}_{ij} = |\mathbf{r}_i - \mathbf{r}_j|$ and $r_{ij} = |\mathbf{r}_{ij}|$. The wall mobility tensor is

$$\mathbf{\Omega}_{ij}^{W} = \mathbf{\Omega}_{PF,ij}^{W} - \frac{2\xi^2}{3}\mathbf{\Omega}_{c,ij}^{W}, \tag{3.42}$$

where $\mathbf{\Omega}_{PF,ij}^{W}$ is the mobility tensor obtained by Blake for a point force near a solid wall in Stokes flow and $(2\xi^2/3)\,\mathbf{\Omega}_{c,ij}^{W}$ is a correction term which accounts for finite bead size. The expressions for $\mathbf{\Omega}_{PF,ij}^{W}$ and $\mathbf{\Omega}_{c,ij}^{W}$ are given in Appendix B of Hoda and Kumar (2007c).

The divergence of diffusivity in Equation (5.4)

$$\left[\frac{\partial}{\partial\mathbf{r}}\cdot\mathbf{D}\right]_i = \left(\frac{1.125\xi}{z_i^2} - \frac{1.5\xi^3}{z_i^4}\right)\hat{\boldsymbol{z}} \tag{3.43}$$

will cause bead motion toward the wall for $z_i \geq 1.16a$ and away from the wall otherwise (Hoda and Kumar, 2007c). The bead-bead and bead-wall interaction forces are the same as in equations (4.4) and (4.5). For the spring force, instead of Equation (4.3), we use the finitely extensible nonlinear elastic (FENE) force law

$$\mathbf{F}_i^S = \frac{H}{1 - Q^2/Q_0^2}\left(\mathbf{r}_j - \mathbf{r}_i\right). \tag{3.44}$$

Note that Equation (4.3) is actually meant to be an approximation to the FENE force law (Bird et al., 1980).

Equation (5.4) was integrated with a dimensionless time step of 5×10^{-5}, except for higher Wi, where a smalller time step was used. Prior to imposing a shear flow, each dumbbell was allowed to relax for 2.5×10^5 time steps in free solution, and for another 2.5×10^5 time steps in the presence of the wall. We simulated each dumbbell for 10^5 Rouse relaxation times. The semi-infinite domain was treated by considering a large but finite-sized domain. We chose a dimensionless distance of 50 normal to the wall as our box length along z-axis. This distance was large enough so that the effect of the wall becomes negligible for all cases of bead-wall interaction considered in this work. If the center of mass of any dumbbell moved beyond this distance, it was reflected back into the domain. The bead positions were saved every 500 time steps. For each set of parameters, an ensemble of 32 trajectories was generated. To calculate the concentration profile, we generated histograms for the bead centers of mass along the z-axis from all trajectories, with a bin size of 0.1, and normalized by dividing by the maximum value.

3.4 Results and discussion

Having discussed the kinetic theory and the BD simulation method, we proceed to study the effects of various parameters on the steady-state concentration profile, the amount adsorbed, and the film thickness. As we are primarily interested in the effects of flow and bead-wall interaction, we fix the parameters of the bead-bead interaction and vary those of the bead-wall interaction. We note here that bead-bead interaction indeed does have an effect on the adsorption behavior, but this effect is small for the short-range interactions considered here. For all the results presented here, we choose $b_k = 56.25$, $\xi = 0.5\sqrt{kT/H}$, $\sigma_b = 1\sqrt{kT/H}$, $\varepsilon_b = 4$, $a = 12$, and $b = 6$. This makes the

maximum extensible spring length $Q_0 = 7.5\sqrt{kT/H}$ and each spring accounts for 18.75 Kuhn lengths. For each set of parameters, the set of nonlinear equations (3.31) was solved numerically using routines from the MINPACK library (Cowell, 1984) to obtain the depletion layer thickness L_d, and the integral in Equation (3.36) was evaluated numerically using routines from the QUADPACK (Piessens et al., 1983) library to obtain the concentration profile.

3.4.1 Steady state concentration profile

The steady-state concentration of dumbbells is dictated by a balance between bead-wall attraction, which pulls the dumbbells toward the wall, and the combined effect of bead-wall HI and bead-wall repulsion, which pushes the dumbbells away from the wall. The individual contribution from each of these sources can be isolated by rewriting the expression for the concentration profile (Equation (3.36)) as

$$\theta = \exp\left[-\int_Z^\infty \frac{L_d}{Z^2}\,\mathrm{d}Z + 2\varepsilon_s\left\{\left(\frac{\sigma_s^*}{Z}\right)^d - \left(\frac{\sigma_s^*}{Z}\right)^c\right\}\right] \tag{3.45}$$

$$= \theta_f \cdot \theta_a \cdot \theta_r, \tag{3.46}$$

where $\theta = n/n_{bulk}$ is the dimensionless number density of the dumbbells, which can be interpreted as a concentration profile, $\theta_f = \exp\left[-\int_Z^\infty L_d/Z^2\,\mathrm{d}Z\right]$ is the contribution from bead-wall HI, $\theta_a = \exp\left[2\varepsilon_s\left(\sigma_s^*/Z\right)^d\right]$ is the contribution from bead-wall attraction, and $\theta_r = \exp\left[-2\varepsilon_s\left(\sigma_s^*/Z\right)^c\right]$ is the contribution from bead-wall repulsion. This separation is possible because Equation (3.36) has the form of a product of exponentials. The quantities θ_a and θ_r are independent of Wi, and hence constant at all flow strengths. But θ_f, which depends on Wi through L_d, decreases with increasing Wi. Figure 3.2 shows plots of θ_f at increasing values of Wi, along with the resulting total concentration.

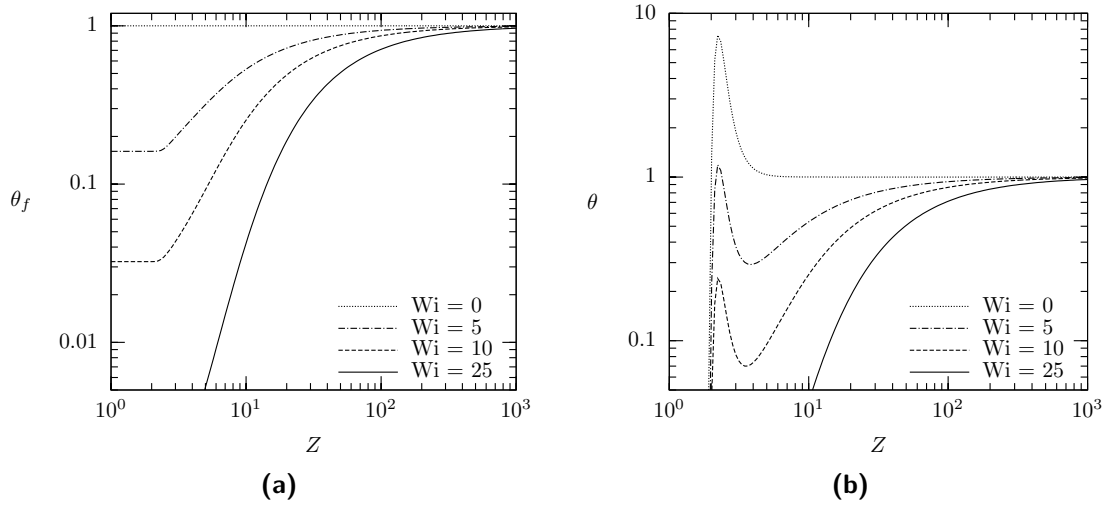

Figure 3.2. (a) Contribution of bead-wall HI to the concentration profile at different flow strengths. **(b)** The concentration profiles at different values of flow strength. The bead-wall interaction parameters are: $\varepsilon_s = 4$, $\sigma_s^* = 2$, $c = 12$, and $d = 6$.

At equilibrium, i.e. Wi = 0, there is no contribution from the flow, as indicated by the horizontal line for $\theta_f = 1$ in Figure 3.2 (a). Increasing the flow strength causes stretching of the dumbbells. The stress increases, which in turn increases L_d and reduces θ_f. As can be seen from Equation (3.46), decreasing θ_f also reduces θ. So, increasing flow strength causes enhanced migration of the dumbbells away from the wall. At the wall, the concentration $\theta_{wall} = 0$ for all cases due to the presence of bead-wall repulsion. This is in contrast to Hoda and Kumar (2007d)'s result for polyelectrolyte adsorption, which predicted a non-zero concentration at the wall due to the absence of any bead-wall repulsion. Far away from the wall, the concentration asymptotically approaches the bulk value $\theta = 1$, similar to what was observed in Hoda and Kumar (2007d). A peak is observed in the concentration profile (Figure 3.2 (b)) as a result of the balance between repulsion and attraction. Similar peaks were also observed by Grisafi and Durning (1989a) and Hoda and Kumar (2007d) and Hoda and Kumar (2008). At sufficiently high Wi, effectively all dumbbells move away from the wall, and the concentration peak

vanishes. This indicates that at higher shear rates, it is easier to desorb an already adsorbed dumbbell; similarly it will be harder to adsorb from a solution at high shear rates.

Next, we look at results from BD simulations and discuss how well the theory matches the simulation. Figure 3.3 (a) shows the concentration profiles from simulation and kinetic theory both in the presence and absence of flow. In this figure, the concentration profile is normalized by its maximum value. Qualitatively, there is good agreement between the theory and simulation. However, especially for lower Wi, they are not in quantitative agreement. The reason for this is the number of approximations made in the theory to facilitate analytical solution. The two most significant assumptions are the Taylor expansion of the bead-wall interaction about the dumbbell center of mass and the use of the FENE-P spring-force law. The effect of the first assumption can be easily seen from Figure 3.3 (b). Here we repeated the BD simulations using the Taylor expanded force instead of the exact form, and the agreement with the theory is considerably improved. However, the Taylor series expansion is not necessarily a bad approximation in many instances. In our case, the bead-wall potential is relatively steep. For a softer potential, this assumption will not cause significant deviation. For example, Figure 8 of Hoda and Kumar (2007c) shows good agreement between theory and simulation for the softer screened Coulombic interaction. The effect of using the FENE-P law instead of the FENE law manifests itself in the magnitude of the stress term. The stress of a FENE-P spring is larger than that of a FENE spring (Herrchen and Öttinger, 1997), hence the L_d term in Equation (3.36) is larger, leading to enhanced migration. This accounts for the higher concentration predicted from the simulation compared to that of the theory. However, for very high Wi, the L_d term becomes large enough to make the difference between the two spring-force laws negligible.

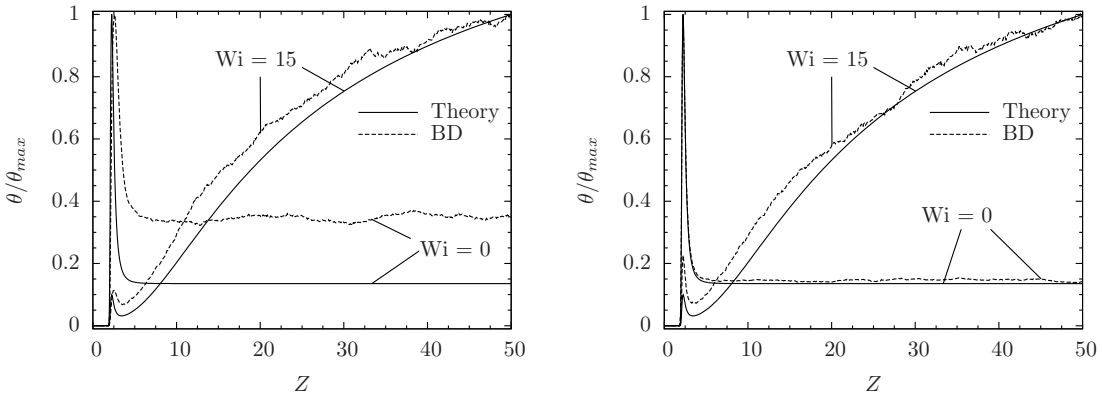

Figure 3.3. (a) Comparison between concentration profiles predicted from kinetic theory and BD at Wi = 0 and Wi = 15. The bead-wall interaction parameters are: $\varepsilon_s = 4$, $\sigma_s^* = 2$, c = 12, and d = 6. **(b)** Comparison with BD simulations performed with a Taylor expanded bead-wall force.

3.4.2 Adsorbed amount and film thickness

From the concentration profile it is possible to calculate the quantity of adsorbed polymer at the surface. Following Grisafi and Durning (1989a) and Aubert and Tirrell (1982), we define the surface adsorption as

$$\Gamma = \int_0^\infty (\theta - 1)\ \mathrm{d}Z. \tag{3.47}$$

Here, Γ measures the quantity of polymer at the interface relative to the bulk. A positive value of Γ indicates more polymer at the interface, which corresponds to adsorption. Similarly, negative values of Γ correspond to desorption.

When there is adsorption, i.e. $\Gamma > 0$, we define the adsorbed film thickness δ_h as the thickness of a homogeneous film of uniform density containing the total adsorbed quantity. Hence,

$$\int_0^\infty (\theta - 1)\ \mathrm{d}Z = (\theta_h - 1)\,\delta_h, \tag{3.48}$$

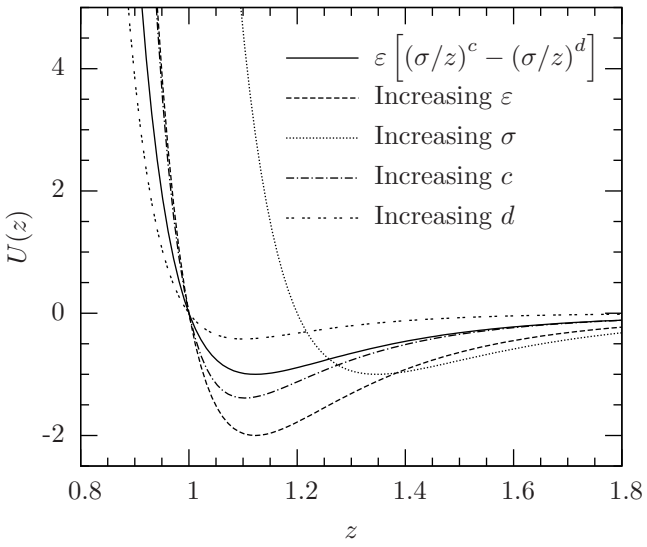

Figure 3.4. The LJ potential for different parameter values: The solid curve shows the 12-6 LJ potential with $\varepsilon = 4$ and $\sigma = 1$. The other curves show how the shape of the potential deviates from the 12-6 LJ curve on increasing ε (= 8), σ (= 1.2), c (= 16), and d (= 9).

where θ_h is the uniform density. Following Stromberg et al. (1965), the uniform density is

$$\theta_h = \frac{\int_0^\infty \theta\,(\theta - 1)\ \mathrm{d}Z}{\int_0^\infty (\theta - 1)\ \mathrm{d}Z}. \tag{3.49}$$

This can be thought of as a weighted average of θ over the entire adsorbent surface with $(\theta - 1)$ as the weighting function. From Equation (3.48) and Equation (3.49),

$$\delta_h = \frac{\left\{\int_0^\infty (\theta - 1)\ \mathrm{d}Z\right\}^2}{\int_0^\infty (\theta - 1)^2\ \mathrm{d}Z}. \tag{3.50}$$

Note that δ_h is a positive quantity defined only for $\Gamma > 0$. Higher values of δ_h indicate enhanced adsorption.

Before proceeding to explore the dependence of the quantity adsorbed and the film thickness on the parameters of the bead-wall interaction potential, its is useful to recall some qualitative features of the shape of the potential. Figure 3.4 shows the familiar

12-6 LJ potential (solid curve), along with the potentials that result on increasing the parameters. We note that increasing ε increases the depth of the potential well, and increasing σ shifts the potential in the positive z-direction as well as making it flatter. Increasing the repulsive exponent c results in a deeper well, and increasing the attractive exponent d does the reverse. As we will see shortly, these qualitative features of the LJ potential, along with Wi, control the amount of adsorbed polymer and the film thickness.

Figure 3.5 (a) shows the isoadsorbs as function of the bead-surface interaction ε_s and the interaction radius σ_s^* at no-flow conditions. The parameter ε_s controls the strength of interaction; hence, increasing ε increases Γ. Increasing σ_s^* shifts the potential well away from the wall as well as making it flatter. The former leads to a zone of low concentration near the wall, and the latter causes enhanced concentration over a larger distance away from the wall. The balance between these two effects produces a net increase in Γ with increase of σ_s^*. However, the effect of increased interaction strength is stronger than that of the interaction radius, as reflected in Figure 3.5 (a).

On increasing the flow strength, the concentration reduces near the surface due to migration caused by bead-wall HI, leading to desorption. Figure 3.5 (c) shows the isoadsorbs at Wi = 5. The region of parameter space where flow leads to desorption at Wi = 5 is shaded. In this case, increasing σ_s^* also leads to lower HI with the wall, thereby contributing to adsorption. Comparing the $\Gamma = 50$ isoadsorb in presence and absence of flow, it can be seen that a higher ε_s is required for the same amount of adsorption when flow is present. The clustering of the isoadsorbs under flow is a result of the nonlinear dependence of Γ on the flow strength, ε, and σ_s^*. On gradually increasing the flow, the shaded part will occupy a progressively larger area of the parameter space. The equivalent film thickness at Wi = 0 is shown in Figure 3.5 (b) and that at Wi = 5 is shown in Figure 3.5 (d). Comparing these two plots, it can be seen that flow tends to reduce the film thickness.

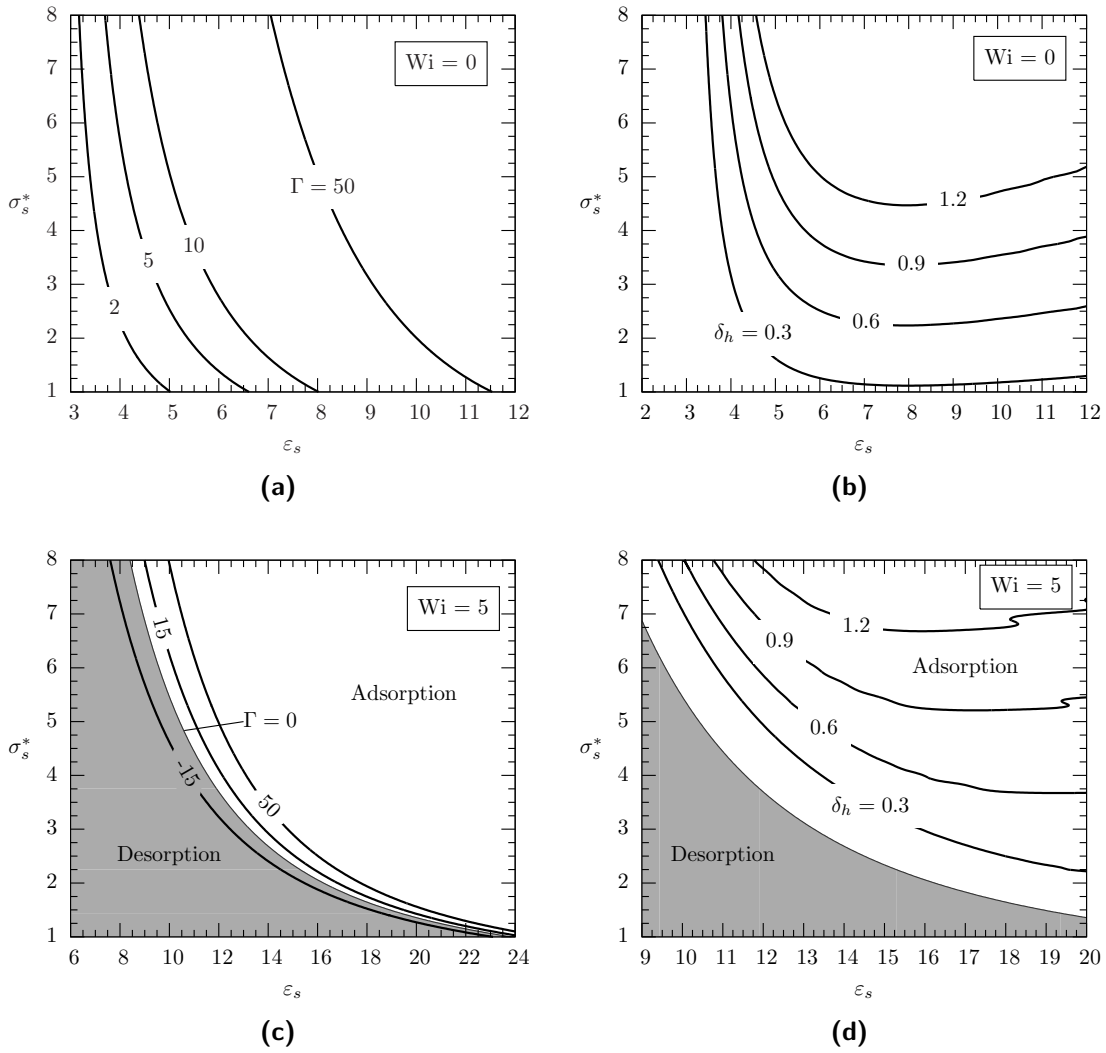

Figure 3.5. Isoadsorbs [(a), (c)] and film thickness [(b), (d)] as function of σ_s^* and ε_s at $\mathrm{Wi} = 0$ and $\mathrm{Wi} = 5$. The bead-wall interaction parameters are $c = 12$, and $d = 6$. The shaded region shows the part of parameter space corresponding to desorption, i.e., $\Gamma < 0$.

Figure 3.6 explores the influence of the repulsive exponent c and the attractive exponent d. Increasing c increases the depth of the potential well, and increasing d does the reverse. As a result, the amount adsorbed increases with c but decreases with d. With an increase of Wi, the same trend can be observed, but over a much smaller range of d. Similar to above, this clustering effect is a result of the nonlinear dependence of Γ on the flow strength and the exponents. The plots for film thickness at Wi = 0 and Wi = 5 are shown in Figure 3.6 (b) and Figure 3.6 (d), respectively. In the presence of flow, adsorption is reduced and hence the film thickness.

3.4.3 Desorption behavior

From the previous discussion, we saw that with increasing flow strength, the film thickness gradually decreases until desorption occurs. The onset of desorption corresponds to $\Gamma = 0$. We denote the associated value of Wi by $\mathrm{Wi}_{\mathrm{desorb}}$.

In Figure 3.7, we have plotted $\mathrm{Wi}_{\mathrm{desorb}}$ as calculated from the kinetic theory for different parameters. The flow strength required increases with an increase in ε_s (see Figure 3.7 (a)). As mentioned previously, the interaction with the surface is a measure of the affinity toward the surface compared to the solvent. If ε_s is low, the adsorbed layer will be thin, and hence the shear rate required to desorb will not vary much. However, when ε_s is large enough, the film thickness will increase with ε_s and hence $\mathrm{Wi}_{\mathrm{desorb}}$ increases as seen. Larger σ_s^* also increases the amount adsorbed by reducing HI, which implies a higher $\mathrm{Wi}_{\mathrm{desorb}}$. The repulsive exponent has minimal effect on $\mathrm{Wi}_{\mathrm{desorb}}$, mainly because of its short-range nature. However, on increasing the exponent d, the potential becomes flater (see Figure 3.4) leading to reduced attraction, and hence the Wi required for desorption also reduces.

Using the kinetic theory prediction for concentration profile, it is possible to come up with a scaling law for $\mathrm{Wi}_{\mathrm{desorb}}$. From Equation (3.36), neglecting bead-bead interaction

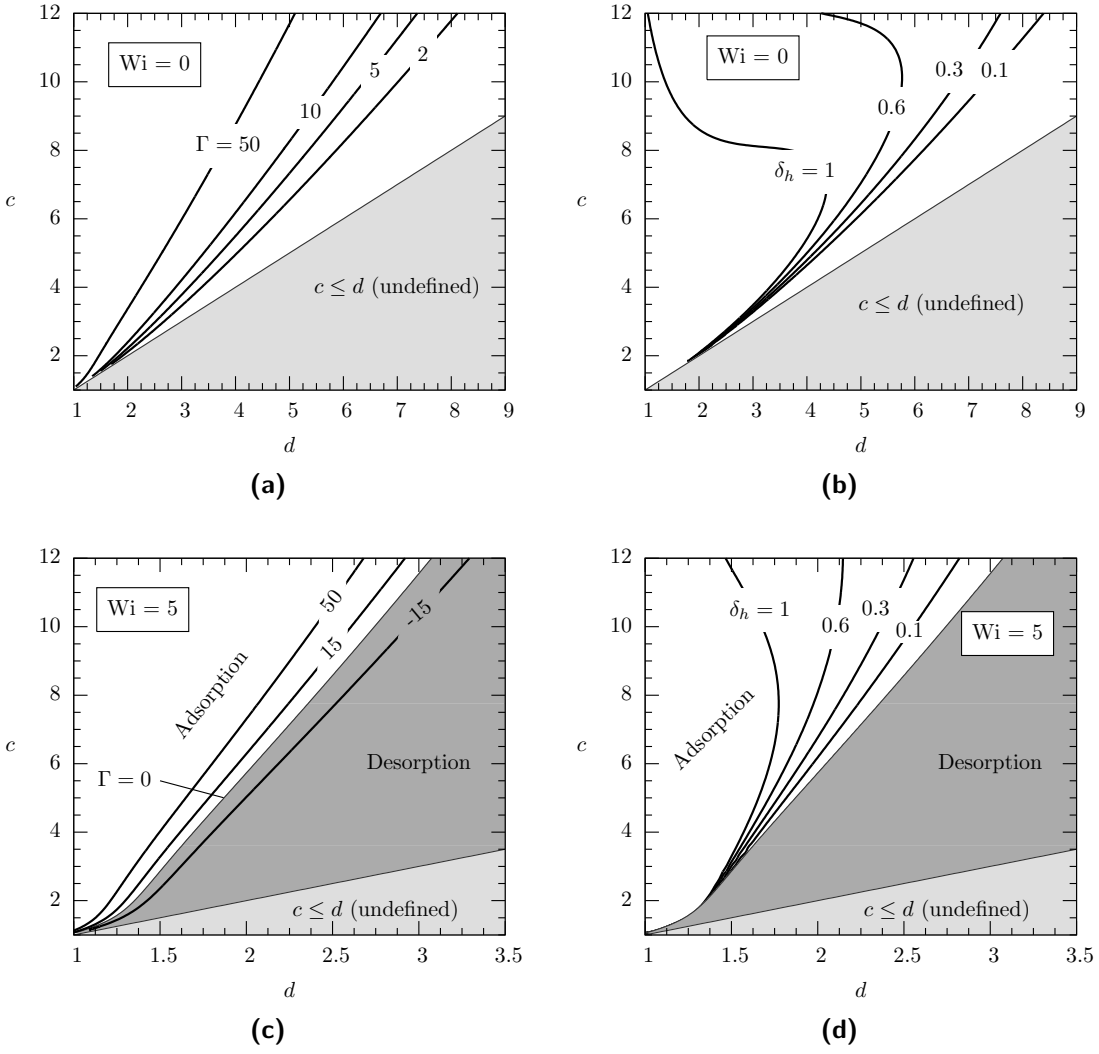

Figure 3.6. Isoadsorbs [(a), (c)] and film thickness [(b), (d)] as function of c and d at $\mathrm{Wi} = 0$ and $\mathrm{Wi} = 5$. The bead-wall interaction parameters are $\varepsilon_s = 8$ and $\sigma_s^* = 2$. The region with darker shading shows the parameter space corresponding to desorption, i.e. $\Gamma < 0$. The lighter shade indicates the unphysical zone corresponding to $c \leq d$.

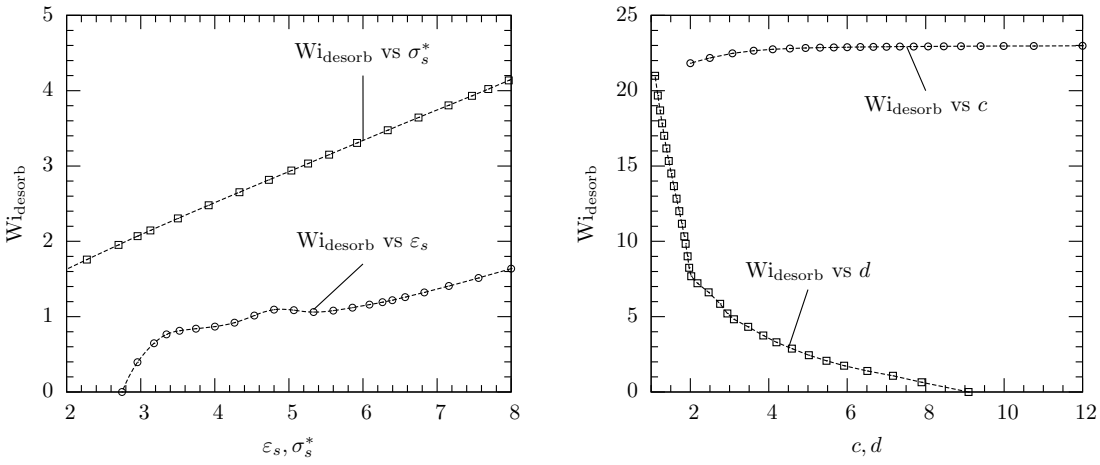

Figure 3.7. (a) $\mathrm{Wi}_{\mathrm{desorb}}$ as a function of σ_s^* at $\varepsilon_s = 8$, c = 12, d = 6 and ε_s at $\sigma_s^* = 2$, c = 12, d = 6 **(b)** $\mathrm{Wi}_{\mathrm{desorb}}$ as a function of c at $\varepsilon_s = 8$, $\sigma_s^* = 2$, d = 1 and d at $\varepsilon_s = 8$, $\sigma_s^* = 2$, c = 12. Dashed lines are only to guide the eye.

and assuming the beads to lie at the same height from the wall, we have

$$\begin{aligned}\theta &= \exp\left[-\frac{L_d^*}{Z} + 2\varepsilon_s\left\{\frac{1}{Z^{*d}} - \frac{1}{Z^{*c}}\right\}\right] \\ &= \exp\left[2\varepsilon_s\left\{-\frac{L_d^*}{2\varepsilon_s\sigma_s^* Z^*} + \left(\frac{1}{Z^{*d}} - \frac{1}{Z^{*c}}\right)\right\}\right]\end{aligned} \tag{3.51}$$

where $Z^* = Z/\sigma_s^*$ and L_d^* is the Z independent effective depletion layer thickness. At high Wi, $L_d^* \sim \mathrm{Wi}^{2/3}$ (Hoda and Kumar, 2007d). Hence,

$$\frac{L_d^*}{2\varepsilon_s\sigma_s^*} > K \qquad \Longrightarrow \qquad \mathrm{Wi}_{\mathrm{desorb}} \sim \varepsilon_s^{3/2}\sigma_s^{*3/2}, \tag{3.52}$$

where K is some constant.

Unfortunately, the expression for $\mathrm{Wi}_{\mathrm{desorb}}$ cannot be directly applied to BD simulation results because the simulations are performed in a finite domain. So, we use an analogous definition also based on the concentration profile. We quantify desorption by that value

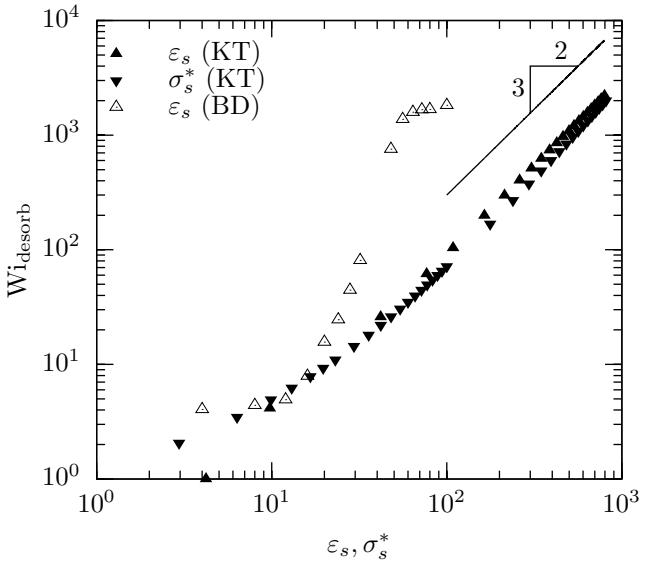

Figure 3.8. $\mathrm{Wi}_{\mathrm{desorb}}$ as a function of ε_s and σ_s^* from kinetic theory and BD simulation. The solid line shows the scaling result predicted from theory.

of Wi for which the area under the normalized concentration profile has reduced to half of its value at no-flow conditions. This can be thought of as the flow strength which has depleted half the amount of the polymers present at equilibrium. For a semi-infinite domain, where the concentration does not decay with distance, this area will diverge. So, we choose an upper limit for the integral as the distance when the bead-wall interaction has decayed sufficiently compared to its maximum value. For 12-6 LJ potential, we choose this distance to be $2.5\sigma_s^*$, where the potential has attains 1/60 of its minimum value. We note that other similar definitions can also be used, (e.g. see Hoda and Kumar (2007c)), for testing the high Wi limit.

Figure 3.8 shows $\mathrm{Wi}_{\mathrm{desorb}}$ as a function of ε_s from both kinetic theory and BD simulation. For high ε_s, the results from the theory follow the scaling law above. We note that the scaling law was derived in the high Wi limit, so it is not expected to be valid for low Wi and hence low ε_s.

The simulation results are not expected to match the theory for low values of ε_s. We attempted to verify the scaling law from the theory for high values of Wi using the simulation results. But on increasing ε_s, the dumbbells become more strongly trapped and hence it takes a longer time to reach steady state in the simulation. For high values the dumbbells in fact do not leave the trap at all within reasonable simulation time, until Wi becomes so strong as to push them out altogether. This is reflected in the approach to the plateau region in the plot.

3.5 Conclusion

We have developed an expression for the steady-state concentration profile of bead-spring dumbbells in shear flow near a solid wall with a general power-law interaction potential using the kinetic theory framework of Hoda and Kumar (2007c). This kind of potential is intended to model forces which are non-electrostatic in nature like van der Waals force or forces due to hydrogen bonds. We studied the adsorption behavior of the dumbbells as a function of flow strength and different parameters governing the interaction.

Under no-flow conditions, a balance between bead-wall attraction and repulsion leads to a peak in the concentration profile near the wall, corresponding to adsorption. When a shear flow is imposed, this peak gradually diminishes with an increase of flow strength. This is due to migration caused by bead-wall HI, and it leads to a monotonically increasing profile away from the wall, which corresponds to desorption. The location of the peak corresponds to a minimum between the attractive and repulsive forces. For stronger bead-wall interaction or longer range of interaction, a higher flow strength is required for desorption. We also developed a scaling law relating the flow strength required for desorption to the strength and range of interaction. The predictions from the kinetic theory were compared with BD simulations and found to be in qualitative agreement

over all parameter ranges and in quantitative agreement over certain parameter ranges. For the cases where they differ, we discussed the reasons behind the deviations. Overall, the theory is able to capture the key features of the adsorption process.

The model we presented is the most minimal required to highlight the role of various interactions and their relative importance. Qualitatively, the kinetic theory is able to account for enhanced desorption with increasing shear rate observed experimentally. As this is a dumbbell-based theory, we are not able to study the effect of molecular weight as done in the experiments. Also, we considered only steady-state behavior. Hence, our results are not expected to match experimental results without taking into account additional effects. These include using multiple beads instead of dumbbells, and even multiple chains, as the interaction between chains always exists in experiments. However, in making the model more realistic, we lose analytical tractibility and it will not be possible to derive explicit expressions like we did in this work. In our future work, we intend to consider the time-dependent version of the dumbbell model, as well as more extensive BD simulations, which we expect will build on the understanding of the adsorption process under flow obtained here.

Chapter 4

Kinetic theory: Transient solution

Summary

Adsorption of polymers from dilute solution subject to shear flow near a planar wall is studied using kinetic theory. A dumbbell model consisting of two beads connected by a nonlinear spring is used to describe the polymer molecules, and the beads interact with the wall via a short-range exponential potential. Bead-bead and bead-wall hydrodynamic interactions are also included in the theory. For an initially bare surface, it is found that the quantity of polymer adsorbed decreases with an increase in polymer molecular weight at a given shear rate and point in time. In addition, for a given molecular weight and point in time, the quantity adsorbed decreases with an increase in shear rate. When adsorbed polymer is initially present, similar trends are observed. Furthermore, complete desorption can be achieved at a sufficiently high shear rate. In all cases, the time required to approach a steady value of the adsorbed amount is many orders of magnitude larger than the dumbbell relaxation time. The above findings are in qualitative agreement with experimental measurements reported nearly three decades ago by Lee and Fuller [J. Colloid Interface Sci. **103**, 569 (1985)]. Our findings also suggest

that the physical mechanism underlying the long-standing observation that shear flow inhibits polymer adsorption and assists polymer desorption is hydrodynamic interaction between stretched polymer molecules and the adsorbing surface.

This chapter was published as S. Dutta, K. D. Dorfman, and S. Kumar, "Dynamics of polymer adsorption from dilute solution in shear flow near a planar wall", J. Chem. Phys. **139**, 174905 (2013).

4.1 Introduction

In Chapter 3, we had discussed the steady-state problem for the amount adsorbed using kinetic theory. Here we focus on the time evolution of the amount adsorbed under shear flow, though we discuss some steady-state results where appropriate. As before, we represent a polymer molecule as a bead-spring dumbbell, interacting with an adjacent planar wall via a short-range attractive potential. The purpose of the attractive potential is to account for short-range non-electrostatic forces encountered in weak physisorption of polymers (O'Shaughnessy and Vavylonis, 2005). A kinetic theory is used to calculate the time-dependent concentration profile in the wall-normal direction for two cases: (i) a polymer film which is already present, and (ii) an intially bare wall. These two cases correspond to the experiments for flow-assisted desorption and flow-inhibited adsorption by Lee and Fuller (1985a). The amount adsorbed and film thickness are then calculated from the concentration profile. The kinetic theory follows the framework developed by Ma and Graham (2005) (for elucidating shear-induced migration of neutral dumbbells) and Hoda and Kumar (2007d) (for polyelectrolyte adsorption in shear flow). Our theory is developed in the dilute limit, i.e., interactions among different polymer molecules

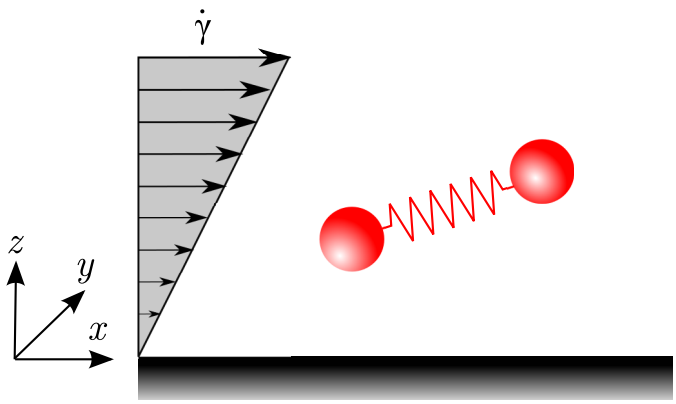

Figure 4.1. Schematic of a dumbbell in shear flow near a planar wall.

are not considered. Though exceedingly simple, our dumbbell kinetic theory is able to qualitatively reproduce the experimental trends observed by Lee and Fuller (1984) and Lee and Fuller (1985a), as will be shown in Sec. 4.4.

4.2 Kinetic theory

We consider a dilute polymer solution at rest bounded by a single planar wall at $z = 0$, and extending to infinity along the $x-$ and $y-$axes (Figure 5.1). At time $t = 0$, the solution is subjected to a simple shear flow parallel to the $x-$axis. The velocity field due to shear flow is $\mathbf{v} = [\dot{\gamma}z, 0, 0]$, where $\dot{\gamma}$ is the shear rate. We are interested in calculating the time evolution of the polymer concentration along the wall-normal direction.

We use a bead-spring dumbbell to model a polymer molecule. A dumbbell consists of two beads, each of radius ξ, connected by a massless spring. The bead positions are given by $\mathbf{r}_1$ and $\mathbf{r}_2$. The connector vector is $\mathbf{Q} = \mathbf{r}_2 - \mathbf{r}_1$ and the center-of-mass position is $\mathbf{r}_c = (\mathbf{r}_2 + \mathbf{r}_1)/2$.

Neglecting inertia, a force balance on each bead gives

$$\mathbf{F}_i^B + \mathbf{F}_i^S + \mathbf{F}_i^{BB} + \mathbf{F}_i^{BW} + \mathbf{F}_i^H = \mathbf{0}, \qquad i = 1, 2 \tag{4.1}$$

where $\mathbf{F}_i^B$ is the Brownian force resulting from thermal fluctuations, $\mathbf{F}_i^S$ is the spring force, $\mathbf{F}_i^{BB}$ is the force due to bead-bead interaction, $\mathbf{F}_i^{BW}$ is the force due to bead-wall interaction, and $\mathbf{F}_i^H$ is the hydrodynamic drag force due to the solvent. Assuming equilibration in momentum space, the Brownian force is (Bird et al., 1987)

$$\mathbf{F}_i^B = -kT\frac{\partial}{\partial \mathbf{r}_i}\ln\psi, \tag{4.2}$$

where $\psi = \psi(\mathbf{r}_c, \mathbf{Q}, t)$ is the configurational distribution function of the dumbbell.

The expression for the spring force is given by the finitely extensible nonlinear elastic spring law with the Peterlin approximation (FENE-P) (Peterlin, 1966; Bird et al., 1980):

$$\mathbf{F}_i^S = \frac{H}{1-\langle Q^2/Q_0^2\rangle}(\mathbf{r}_j - \mathbf{r}_i), \qquad i,j = 1,\,2 \tag{4.3}$$

where H is the spring constant, $Q = |\mathbf{Q}|$, and Q_0 is the maximum extensible spring length. Here and elsewhere, angle brackets denote an average over all possible conformations. The spring extensibility parameter is $b_k = HQ_0^2/kT$. We add a caveat that the isotropic spring force law above is not accurate in the presence of a wall and additional corrections need be taken into account (Woo et al., 2004). However, these corrections will have no bearing on the qualitative nature of the conclusions which will be drawn from this model.

The force due to bead-bead interaction is chosen to be of the form derived from a Lennard-Jones potential:

$$\mathbf{F}_i^{BB} = \frac{\varepsilon_b kT}{\sigma_b}\left[12\left(\frac{\sigma_b}{Q}\right)^{13} - 6\left(\frac{\sigma_b}{Q}\right)^{7}\right]\frac{\mathbf{r}_i - \mathbf{r}_j}{|\mathbf{r}_i - \mathbf{r}_j|}, \tag{4.4}$$

where ε_b determines the strength of the interaction (in units of kT) and σ_b is the interbead distance at which the interaction potential vanishes. We assume that there is a short-range attractive interaction between the polymer molecule and the wall, which

we describe with an exponential potential that generates a force of the form

$$\mathbf{F}_i^{BW} = -\varepsilon_s \kappa kT \exp\left(-\kappa z_i\right) \hat{\mathbf{z}}, \tag{4.5}$$

where ε_s and κ control the strength and range of the interaction, respectively.

The hydrodynamic drag force is given by

$$\mathbf{F}_i^H = -\zeta \left(\dot{\mathbf{r}}_i - \mathbf{v}_i\right), \tag{4.6}$$

where $\mathbf{v}_i$ is the solvent velocity at $\mathbf{r}_i$, the bead friction coefficient is $\zeta = 6\pi\eta\xi$, and η is the solvent viscosity. The solvent velocity can be written as $\mathbf{v}_i = \mathbf{v}_i^0 + \mathbf{v}_i^{pf}$, where $\mathbf{v}_i^0$ is the unperturbed velocity and $\mathbf{v}_i^{pf}$ is the contribution due to the perturbation of the velocity field by the motion of all other beads j. Assuming a vanishingly small Reynolds number, the perturbed velocity is given by

$$\mathbf{v}_i^{pf} = -\sum_j \mathbf{\Omega}_{ij} \cdot \mathbf{F}_j^H, \tag{4.7}$$

where $\mathbf{\Omega}_{ij}$ is the HI tensor between the beads i and j.

We obtain $\mathbf{v}_i^0$ by Taylor-expanding the solvent velocity about the dumbbell center-of-mass and retaining terms only up to second order. The bead-wall forces are Taylor-expanded about the dumbbell center-of-mass as well, and terms beyond first order are neglected. This is important in order to introduce a dependence on the connector vector, which will later be averaged out. The Taylor-expansion is a necessary approximation in order to make analytical progress; similar approaches have been employed before in the literature as well (Ma and Graham, 2005; Hoda and Kumar, 2007d). Substituting the force expressions in Equation (4.1), and averaging over all possible conformations, the

center-of-mass flux in the z-direction is given by (Dutta et al., 2013):

$$j_c = -\frac{1-\langle Q_z^2\rangle/4z^2}{\left[1+\left(\langle Q_x^2\rangle+\langle Q_y^2\rangle\right)/4z^2\right]^{5/2}}\left(\frac{3\tau_{xx}^p}{64\pi\eta z^2}\right)-D_K\frac{\partial n}{\partial z}+\frac{nD_K}{kT}\left(F_{1,z}^{BW}+F_{2,z}^{BW}\right), \quad (4.8)$$

where z is the z-component of the dumbbell center of mass, τ_{xx}^p is the xx-component of the polymer stress tensor, $D_K = kT/2\zeta$ is the free-draining Kirkwood diffusivity, and n is the polymer number density. Substituting the values of D_K, $F_{1,z}^{BW}$, $F_{2,z}^{BW}$, and after some rearrangement, we have

$$j_c = nkT\left(\frac{L_d}{2\zeta z^2}\right)\sqrt{\frac{kT}{H}}-\left(\frac{kT}{2\zeta}\right)\frac{\partial n}{\partial z}-nkT\left(\frac{\varepsilon_s\kappa}{\zeta}\right)\mathrm{e}^{-\kappa z}, \quad (4.9)$$

where

$$L_d = -\frac{9}{16}\sqrt{\pi}h^*\frac{1-\langle Q_z^2\rangle/4z^2}{\left[1+\left(\langle Q_x^2\rangle+\langle Q_y^2\rangle\right)/4z^2\right]^{5/2}}\left(\frac{\tau_{xx}^p}{nkT}\right) \quad (4.10)$$

is the depletion layer thickness (Hoda and Kumar, 2007d) and $h^* = (\zeta/\eta)\sqrt{H/36\pi^3 kT}$ is the HI parameter (Bird et al., 1987).

The conservation equation for the dumbbell center of mass is

$$\frac{\partial n}{\partial t} = -\frac{\partial}{\partial z}j_c. \quad (4.11)$$

From Equation (4.9) and Equation (4.11), we have

$$\frac{\partial n}{\partial t} = \left(\frac{kT}{2\zeta}\right)\frac{\partial^2 n}{\partial z^2}+kT\frac{\partial}{\partial z}\left[\left(-\frac{L_d}{2\zeta z^2}\sqrt{\frac{kT}{H}}+\frac{\varepsilon_s\kappa}{\zeta}\mathrm{e}^{-\kappa z}\right)n\right]. \quad (4.12)$$

We non-dimensionalize length with $\sqrt{kT/H}$, time with the Rouse relaxation time for a dumbbell $\lambda_H = \zeta/4H$, energy by kT, and concentration by the bulk concentration n_{bulk}. The flow strength is measured in terms of the Weissenberg number (Wi), defined

as $\mathrm{Wi} = \lambda_H \dot{\gamma}$. In the following, all starred quantities are the dimensionless variants of their unstarred forms. Then, Equation (4.12) can be written as an advection-diffusion equation

$$\frac{\partial \theta}{\partial t^*} = \frac{1}{8}\frac{\partial^2 \theta}{\partial z^{*2}} + \frac{\partial}{\partial z^*}\left[\left(-\frac{1}{8}\frac{L_d}{z^{*2}} + \frac{\varepsilon_s \kappa^*}{4}\exp\left(-\kappa^* z^*\right)\right)\theta\right], \tag{4.13}$$

where the dimensionless concentration $\theta = n/n_{bulk}$. Noting that L_d vanishes at $z^* = 0$, the boundary conditions are given by

$$\begin{aligned} &z^* \to \infty, \qquad \theta \to 1 \\ &z^* = 0, \qquad j_{c,z} = 0 \implies \frac{\partial \theta}{\partial z^*} + 2\varepsilon_s \kappa^* \theta = 0. \end{aligned} \tag{4.14}$$

The solutions of Equation (4.13) at different flow strengths give the time-dependent concentration profiles and will be the main focus of this work. Putting the time-derivative to zero, the steady-state solution is

$$\theta_s = \exp\left[-\int_{z^*}^{\infty} \frac{L_d}{q^2}\,\mathrm{d}q + 2\varepsilon_s \exp\left(-\kappa^* z^*\right)\right]. \tag{4.15}$$

To obtain L_d (see Equation (4.10) and Equation (4.13)), we need to evaluate the polymer stress. The stress tensor can be written in the Kramers form

$$\frac{\boldsymbol{\tau}^p}{nkT} = -\frac{1}{kT}\left\langle \mathbf{Q}\left\{\mathbf{F}_1^S + \mathbf{F}_1^{BB} - \frac{1}{2}\left(\mathbf{F}_2^{BW} - \mathbf{F}_1^{BW}\right)\right\}\right\rangle + \mathbf{I}, \tag{4.16}$$

or in the Giesekus form

$$\frac{\boldsymbol{\tau}^p}{nkT} = \frac{\zeta}{4kT}\langle \mathbf{QQ}\rangle_{(1)} + \frac{1}{4kT}\left\langle \mathbf{Q}\left(\mathbf{F}_2^{BW} - \mathbf{F}_1^{BW}\right) - \left(\mathbf{F}_2^{BW} - \mathbf{F}_1^{BW}\right)\mathbf{Q}\right\rangle, \tag{4.17}$$

where the subscript (1) denotes the upper convected derivative (Bird et al., 1980). Comparing the Kramers and the Giesekus forms, we obtain the following set of six

coupled ordinary differential equations (ODEs):

$$\begin{aligned}
\frac{\mathrm{d}C_1}{\mathrm{d}t^*} &= -\frac{C_1}{b_k}g + 2\mathrm{Wi}C_5 + \frac{1}{b_k},\\
\frac{\mathrm{d}C_2}{\mathrm{d}t^*} &= -\frac{C_2}{b_k}g + \frac{1}{b_k},\\
\frac{\mathrm{d}C_3}{\mathrm{d}t^*} &= -\frac{C_3}{b_k}\left[g + \frac{b_k\varepsilon_s\kappa^{*2}\mathrm{e}^{-\kappa^* z^*}}{2}\right] + \frac{1}{b_k},\\
\frac{\mathrm{d}C_4}{\mathrm{d}t^*} &= -\frac{C_4}{b_k}g + \mathrm{Wi}C_6,\\
\frac{\mathrm{d}C_5}{\mathrm{d}t^*} &= -\frac{C_5}{b_k}\left[g + \frac{b_k\varepsilon_s\kappa^{*2}\mathrm{e}^{-\kappa^* z^*}}{4}\right] + \mathrm{Wi}C_3,\\
\frac{\mathrm{d}C_6}{\mathrm{d}t^*} &= -\frac{C_6}{b_k}\left[g + \frac{b_k\varepsilon_s\kappa^{*2}\mathrm{e}^{-\kappa^* z^*}}{4}\right],
\end{aligned} \tag{4.18}$$

where

$$g = \frac{b_k}{1-C} - \frac{12\varepsilon_s}{C}\left(\frac{\sigma_b}{Q_0\sqrt{C}}\right)^{12} + \frac{6\varepsilon_s}{C}\left(\frac{\sigma_b}{Q_0\sqrt{C}}\right)^{6},$$

$C_1 = \langle Q_x^2/Q_0^2\rangle$, $C_2 = \langle Q_y^2/Q_0^2\rangle$, $C_3 = \langle Q_z^2/Q_0^2\rangle$, $C_4 = \langle Q_xQ_y/Q_0^2\rangle$, $C_5 = \langle Q_xQ_z/Q_0^2\rangle$, $C_6 = \langle Q_yQ_z/Q_0^2\rangle$, and $C = C_1 + C_2 + C_3$. Initially the soution is at rest. Hence, the initial conditions can be obtained by putting the time derivative and Wi to zero and solving the resulting set of nonlinear equations for different values of z^*. After solving the ODEs, τ_{xx}^p can be calculated from the Kramers expression as follows:

$$\frac{\tau_{xx}^p}{nkT} = -gC_1 + 1, \tag{4.19}$$

which allows calculation of L_d via Equation (4.10).

We can now solve Equation (4.13) to obtain the concentration profile. From the concentration profile we calculate the quantity of adsorbed polymer at the surface. Following Aubert and Tirrell (1982) and Grisafi and Durning (1989a) we define the

surface adsorption as

$$\Gamma(t^*) = \lim_{l\to\infty} \int_0^l \{\theta(z^*, t^*) - 1\}\, \mathrm{d}z^*. \tag{4.20}$$

Here, Γ measures the quantity of polymer at the interface relative to the bulk. A positive value of Γ indicates more polymer at the interface, which corresponds to adsorption. Similarly, negative values of Γ correspond to desorption.

When there is adsorption, i.e. $\Gamma > 0$, the adsorbed film thickness δ is defined as the thickness of a homogeneous film of uniform density containing the total adsorbed quantity (Stromberg et al., 1965; Grisafi and Durning, 1989a),

$$\delta(t^*) = \lim_{l\to\infty} \frac{\left[\int_0^l \{\theta(z^*, t^*) - 1\}\, \mathrm{d}z^*\right]^2}{\int_0^l \{\theta(z^*, t^*) - 1\}^2\, \mathrm{d}z^*}. \tag{4.21}$$

Note that δ is a positive quantity defined only for $\Gamma > 0$. Higher values of δ indicate enhanced film thickness.

4.3 Numerical methods

We determined Γ and δ for both steady and unsteady states by first calculating the concentration profile. The unsteady-state concentration profile was obtained by solving Equation (4.13) along with the boundary conditions Equation (4.14). The steady-state concentration θ_s at a particular value of z^* was obtained by evaluating the right-hand side of Equation (4.15). The integral inside the exponential in Equation (4.15) was evaluated by first mapping the semi-infinite domain to $[-1, 1]$ and then using Chebyshev-Gauss-Lobatto (CGL) quadrature (Press et al., 1992). The calculation procedure for the L_d values is discussed later.

To obtain the time-dependent concentration profile, we solved Equation (4.13) using a pseudospectral collocation method. Spectral methods have been widely used in the literature for the past three decades to solve ordinary and partial differential equations.* Standard references for spectral methods include, among many others, the texts by Peyret (2002), Canuto et al. (2006), and Hesthaven et al. (2007). Programming aspects of spectral methods are discussed in detail by Boyd (2001) and Kopriva (2009). In the following paragraphs, we briefly outline the method and discuss its implementation for the problem at hand.

In any spectral method, we attempt to find an approximation to the actual solution (of the PDE) in the form of a linear combination of a finite number of orthogonal basis functions. For Equation (4.13), we write the approximate solution $\tilde{\theta}\left(z^*, t^*\right)$ to $\theta\left(z^*, t^*\right)$ as

$$\theta\left(z^*, t^*\right) \approx \tilde{\theta}\left(z^*, t^*\right) = \sum_{j=0}^{N} \hat{\theta}_j\left(t^*\right) \Phi_j\left(z^*\right), \tag{4.22}$$

where $\hat{\theta}_j\left(t^*\right)$ are called the spectral coefficients and Φ_j are the basis functions. For time-dependent problems, as is the case in Equation (4.13), the spectral coefficients are functions of time. The basis functions may not be chosen arbitrarily; their choice is dictated by the nature of the solution, the boundary conditions, as well as the domain of definition of the solution. Here, we have used the Chebyshev polynomials of the first kind as basis functions. The nth degree Chebyshev polynomial of the first kind $T_n(x)$ is defined for $x \in [-1, 1]$ as

$$T_n\left(x\right) = \cos\left(n \cos^{-1} x\right), \qquad n = 0, 1, 2, \ldots. \tag{4.23}$$

Writing $x = \cos z$ and using elementary trigonometric identities, these polynomials can

*See `www.personal.umich.edu/~jpboyd/Chebbibintro.html` for a list of over 2000 articles.

also be recursively defined as

$$T_0(x) = 1, \qquad T_1(x) = x, \tag{4.24}$$

$$T_{n+1}(x) = 2xT_n(x) - T_{n-1}(x), \qquad n \geq 1. \tag{4.25}$$

These polynomials are orthogonal in $[-1, 1]$ with respect to a weight function $w(x) = 1/\sqrt{1-x^2}$. Chebyshev polynomials are widely used for non-periodic problems due to the existence of simple expressions in closed form for the derivative matrices as well as for all Gauss quadrature points and the corresponding weights. Moreover, Chebyshev expansions are closely related to Fourier series, which allows the usage of fast transform methods in evaluating the spectral coefficients (We have not used any fast transforms as our problem size is not large enough to result in any significant computational gain.).

For a function $u(x)$ defined on $[-1, 1]$, having a truncated Chebyshev expansion $\tilde{u}(x) = \sum_{j=0}^{N} \hat{u}_j T_j(x)$, it can be shown (Hesthaven et al., 2007) that $\tilde{u}(x)$ interpolates $u(x)$ at the $N+1$ Gauss quadrature points X_j associated with the Chebyshev polynomial, i.e., $u(X_j) = \tilde{u}(X_j)$, $j = 0, \ldots, N$. These points are known as collocation points (or nodes). We have used the points based on Gauss-Lobatto quadrature (i.e., the collocation points include the end points ± 1), as including the end points helps in implementing boundary conditions. The Chebyshev-Gauss-Lobatto (CGL) nodes are given by

$$X_j = -\cos\left(\frac{\pi j}{N}\right), \qquad j = 0, \ldots, N. \tag{4.26}$$

Note that if the nodes are computed by Equation (4.26), less accurate values are obtained (Weideman and Reddy, 2000; Baltensperger and Trummer, 2002) for j close to N, i.e., for X_j near 1. So we calculated the nodes using $X_j = -\sin[\pi(N-2j)/(2N)]$, $j = 0, \ldots, N$. Also, the CGL nodes are symmetric about $x = 0$. To ensure the symmetry in floating

point arithmetic, we calculated the nodes $X_j < 0$ and reflected them to obtain the nodes $X_j > 0$.

Using the discrete orthogonality property of the Chebyshev polynomials, the $N+1$ spectral coefficients $\hat{u}_j$ can be obtained (Peyret, 2002) from the values of the function at the CGL points $u(X_j)$:

$$\hat{u}_j = \frac{2}{\bar{c}_j N} \sum_{k=0}^{N} \frac{u(X_k)}{\bar{c}_k} \cos \frac{\pi j k}{N}, \tag{4.27}$$

where

$$\bar{c}_j = \begin{cases} 2, & j = 0, N \\ 1, & j = 1, \ldots, N-1. \end{cases} \tag{4.28}$$

This transformation is called the Discrete Chebyshev Transform (DCT) and involves a simple matrix-vector multiplication. The inverse transform (also a matrix-vector multiplication) given by (Peyret, 2002)

$$u(X_j) = \sum_{k=0}^{N} \hat{u}_k \cos \frac{\pi j k}{N}, \qquad j = 0, \ldots, N \tag{4.29}$$

can be used to determine the function values at the nodes from the spectral coefficients. Thus, we can represent the function $u(x)$ in terms of the spectral coefficients (called transform space) or in terms of its values at the collocation points (called physical space). In pseudospectral collocation, we determine the function values $u(X_j)$ in the physical space and calculate the coefficients using DCT if required (e.g. for error analysis). To obtain values of the function at points other than the CGL nodes, polynomial interpolation can be used. The collocation method is simpler to program than other variants of spectral methods, and is also particularly convenient for nonlinear problems.

To obtain the function values, we discretize the spatial dimensions into a grid consisting of the collocation points and enforce the governing differential equation at

each of the interior points of the domain and the boundary conditions at the boundary points. The spatial derivatives of the function at each node can be expressed as a linear combination of the function values at all the nodes. This allows us to evaluate the derivatives as matrix-vector products:

$$\left[\frac{\partial^p u\left(X_0\right)}{\partial x^p}, \ldots, \frac{\partial^p u\left(X_N\right)}{\partial x^p}\right]^T = \mathbf{D}^{(p)} \cdot \left[u\left(X_0\right), \ldots, u\left(X_N\right)\right]^T \tag{4.30}$$

where $\mathbf{D}^{(p)}$ is the pth derivative matrix. For a Chebyshev approximated function, explicit analytical formulas exist for calculating the derivative matrices (Peyret, 2002). However, a direct application of these formulas lead to severe round-off errors, especially for large values of N. Following the technique recommended by Peyret (2002), we calculated the off-diagonal elements of the first derivative matrix $\mathbf{D}^{(1)}$ using the explicit formulas. For the diagonal elements, we took the negative of the row sum of the off-diagonal elements along each row. The negative sum trick guarantees that the all row sums equate to zero, which ensures that the derivative of a constant function vanishes at the collocation points (Baltensperger and Trummer, 2002).

$$D_{jk}^{(1)} = \begin{cases} \dfrac{\bar{c}_j}{\bar{c}_k} \dfrac{(-1)^{j+k}}{(X_j - X_k)}, & j \neq k, \\ -\displaystyle\sum_{\substack{l=0 \\ l \neq j}}^{N} D_{jl}^{(1)}, & j = k. \end{cases} \tag{4.31}$$

The second derivative matrix $\mathbf{D}^{(2)}$ was calculated in two steps. First, we calculated a provisional second derivative matrix $\tilde{\mathbf{D}}^{(2)}$ by squaring $\mathbf{D}^{(1)}$ (calculated previously), and

then applied the negative sum trick to obtain the actual matrix:

$$D_{jk}^{(2)} = \begin{cases} \tilde{D}_{jk}^{(2)}, & j \neq k, \\ -\sum_{\substack{l=0 \\ l \neq j}}^{N} D_{jl}^{(2)}, & j = k. \end{cases} \tag{4.32}$$

This converts a PDE into a system of ODEs (with appropriate boundary conditions), or, for a boundary value problem, to a system of algebraic equations which can be solved by standard numerical methods.

So far our discussion of the pseudospectral method has been quite general. Now we turn to several aspects which are specific to our solution of Equation (4.13). Instead of applying a single global approximation to $\theta\left(z^*, t^*\right)$ over $z^* \in [0, \infty)$, we decompose the spatial domain into two subdomains $z^* \in [0, \ell] \cup [\ell, \infty)$, each possessing its own set of collocation points and approximating polynomial. We choose ℓ to be that value of z^* for which the concentration in the absence of flow decays to $\approx 10\%$ of the bulk concentration. We will represent $\theta^{(1)}\left(z^*, t^*\right)$ as the approximating polynomial in subdomain 1 and $\theta^{(2)}\left(z^*, t^*\right)$ as the approximating polynomial in subdomain 2. For convenience, we used the same number of collocation points for both subdomains. The two solutions are matched by imposing continuity of the function as well as the first derivative at the touching point $X_N^{(1)}$ $(= X_0^{(2)})$ of the subdomains (Pfeiffer et al., 2003). Note that the N^{th} collocation node of subdomain 1 and the 0th collocation node of subdomain 2 represent the same physical point. Domain decomposition allows us to use relatively lower degree polynomials in each subdomain compared to a single very high degree polynomial over the entire domain. High degree polynomials increase computational cost, and round-off errors become particularly prominent. In contrast, using lower degree polynomials for each subdomain also results in higher resolution near the wall. Moreover, the Jacobian matrix of the resulting system of ODEs becomes sparse with blocks of non-zero entries

corresponding to each subdomain.

As mentioned before, the Chebyshev polynomials are defined over the domain $[-1, 1]$. But $\theta(z^*, t^*)$ in Equation (4.13) is defined over $z^* \in [0, \infty)$. To apply Chebyshev approximation for $\theta(z^*, t^*)$, we need to map the domain $[0, \infty) \rightarrow [-1, 1]$. For subdomain 1, we used a simple linear mapping, and for subdomain 2 we used an algebraic mapping.

$$X = \begin{cases} \dfrac{2z^* - \ell}{\ell}, & z^* \in [0, \ell] \\ \dfrac{z^* - \ell - L_{map}}{z^* - \ell + L_{map}}, & z^* \in [\ell, \infty)\,. \end{cases} \tag{4.33}$$

The inverse mapping is given by

$$z^* = \begin{cases} \dfrac{\ell}{2}(X + 1)\,, & z^* \in [0, \ell] \\ \ell + L_{map}\left(\dfrac{1 + X}{1 - X}\right), & z^* \in [\ell, \infty)\,. \end{cases} \tag{4.34}$$

The quantity L_{map} above is called the mapping parameter and controls the degree of stretching of the grid. There is no apriori way of determining L_{map}; a certain amount of experimentation is inevitable. In all our calculations, we have used $L_{map} = 6$. For semi-infinte domains, other forms of mapping (e.g., exponential, logarithmic, etc.) also exist. Here we follow the guidelines suggested by Boyd for the choice of mapping for semi-infinite domains (see Chapters 16 and 17 of Boyd (2001) and the references therein, particularly Boyd (1982) and Boyd (1987)). According to Boyd, algebraic mapping with Chebyshev polynomials proves superior to other mappings for functions which exhibit algebraic decay or asymptote to a constant. Our function $\theta(z^*, t^*) \sim 1/z^*$ as $z^* \rightarrow \infty$ and asymptotes to 1. It is precisely because of the algebraic decay that Laguerre polynomials (or functions), which are defined over $(0, \infty]$, do not perform well in this situation. Boyd also showed that although an optimum value of the mapping parameter exists, the accuracy of the solution is quite insensitive to the choice of L_{map} as long as it

is of the same order of magnitude as the optimum value. Upon mapping to $[-1, 1]$, the spatial derivatives are transformed as follows:

$$\frac{\partial\theta\left(z^*,t^*\right)}{\partial z^*} = \left(\frac{\partial X}{\partial z^*}\right)\frac{\partial\theta\left(X,t^*\right)}{\partial X}, \tag{4.35}$$

$$\frac{\partial^2\theta\left(z^*,t^*\right)}{\partial z^{*2}} = \left(\frac{\partial X}{\partial z^*}\right)^2\frac{\partial^2\theta\left(X,t^*\right)}{\partial X^2} + \left(\frac{\partial^2 X}{\partial z^{*2}}\right)\frac{\partial\theta\left(X,t^*\right)}{\partial X}. \tag{4.36}$$

After mapping and spatial discretization of the subdomains, we obtain the following set of equations:

$$\begin{aligned}\frac{\mathrm{d}\theta_j^{(\mu)}}{\mathrm{d}t^*} = \frac{1}{8}\sum_{k=0}^{N}\left[\left(X_j^{'2}D_{jk}^{(2)} + X_j^{''}D_{jk}^{(1)}\right)\theta_k^{(\mu)}\right] \\ + X_j^{'}\sum_{k=0}^{N}\left[D_{jk}^{(1)}\left(-\frac{L_{dj}}{8z_j^{*2}} + \frac{\varepsilon_s\kappa^*}{4}\mathrm{e}^{-\kappa^* z_j^*}\right)\theta_k^{(\mu)}\right], \quad j = 1,\ldots,N-1, \quad \mu = 1,2,\end{aligned} \tag{4.37}$$

$$X_0^{'}\sum_{k=0}^{N}D_{0k}^{(1)}\theta_k^{(1)} + 2\varepsilon_s\kappa\theta_0^{(1)} = 0, \tag{4.38}$$

$$\theta_N^{(2)} = 1, \tag{4.39}$$

$$\theta_N^{(1)} = \theta_0^{(2)}, \tag{4.40}$$

$$X_N^{'}\sum_{k=0}^{N}D_{Nk}^{(1)}\theta_k^{(1)} = X_0^{'}\sum_{k=0}^{N}D_{0k}^{(1)}\theta_k^{(2)}, \tag{4.41}$$

where $X^{'} = \partial X/\partial z^*$ and $X^{''} = \partial^2 X/\partial z^{*2}$. Equation (4.37) results from enforcing the PDE at the interior collocation points, Equation (4.38) and Equation (4.39) are the boundary conditions, Equation (4.40) and Equation (4.41) imposes continuity of θ and $\partial\theta/\partial z^*$ respectively at the interface of the two subdomains.

We solved the ODEs above using the software package `VODE_F90`,[†] which is a Fortran

[†]See `www.radford.edu/~thompson/vodef90web/index.html` for the source code of the package `VODE_F90`.

90 extension of the well-known FORTRAN 77 ODE solver `VODE` (Brown et al., 1989). It uses variable coefficient Adams-Moulton (non-stiff case) and Backward Differentiation Formula methods (stiff case) in Nordseick form, treating the Jacobian as full or sparse. The routines incorporate a high degree of algorithmic automation and feature a very flexible user interface that significantly aids in code development. The step size used is variable and adjusted automatically to ensure convergence of the Newton iteration.

It is well known that the spectral derivative matrices are notoriously ill-conditioned (the condition number of the pth derivative matrix is $\mathcal{O}\left(N^{2p}\right)$), leading to an equally ill-conditioned Jacobian matrix, which severely slows down convergence of the Newton iteration and also involves loss of precision. Hence, the system of ODEs above should not be integrated naively. Instead, we used the Finite Difference (FD) approximation to the Jacobian matrix as a left preconditioner for solving the system of linear equations arising from each Newton step. This method, first proposed by Orszag (1980), performs remarkably well in reducing the condition number close to 1, at least for 1-D problems. The FD derivative matrices should be calculated based on the collocation nodes and transformed back to physical space using Equation (4.36). The FD derivatives at the jth collocation point are given by

$$\left(\frac{\partial\theta}{\partial X}\right)_j = \frac{1}{\Delta_+\Delta_-^2 + \Delta_-\Delta_+}\left[-\Delta_+^2\theta_{j-1} - \left(\Delta_-^2 - \Delta_+^2\right)\theta_j + \Delta_-^2\theta_{j+1}\right] \tag{4.42}$$

$$\left(\frac{\partial^2\theta}{\partial X^2}\right)_i = \frac{2}{\Delta_+\Delta_-^2 + \Delta_-\Delta_+}\left[\Delta_+\theta_{j-1} - \left(\Delta_- + \Delta_+\right)\theta_j - \Delta_-\theta_{j+1}\right] \tag{4.43}$$

where $\Delta_+ = X_{j+1} - X_j$ and $\Delta_- = X_j - X_{j-1}$. The FD matrix is tridiagonal, which further adds to computational efficiency. Along with the preconditioner, exploiting the sparse structure of the Jacobian, we used the iterative solver GMRES to solve the system of linear equations. Note that `VODE_F90` natively has no capability for accepting an user-supplied preconditioner or for using GMRES; we had to slightly modify the solver

routines to accept our options.

In order to solve the set of equations above, we also need the values of L_d at the collocation points as a function of time. We obtained L_d at the nodes by solving the system of ODEs Equation (4.18) using `VODE_F90` followed by application of equations (4.19) and (4.10). The initial conditions were determined by setting the time derivates and Wi equal to zero and solving the resulting set of nonlinear equations. Under no-flow condition, the polymer stress tensor vanishes, which ensures that at $t^* = 0$, C_4, C_5, and C_6 are identically zero. Looking at Equation (4.18), we observe that if C_4 and C_6 are initially zero, they remain zero for all subsequent times, and hence there is no need to solve for $C_4(t^*)$ and $C_6(t^*)$. Note that L_d attains a steady value within a short time (see Figure 4.2), after which we can use its constant value. This constant value was used for calculating the steady state concentration. The fast relaxation of L_d allows us to save the values in a look-up table and use linear interpolation to determine intermediate values as required.

After calculating the concentration profile as discussed above, we obtain the quantity adsorbed Γ and the equivalent film thickness δ by applying Equation (4.20) and Equation (4.21), respectively. Since the values of concentration we obtained are at the CGL nodes (a consequence of the spectral discretization), the integrals can easily be performed using CGL quadrature. Also, as we are interested in the concentration close to the wall, we truncated the upper limit of the integrals to ℓ, i.e., we integrated only over subdomain 1. The degree of the approximating polynomial N in each domain required some experimentation. Beyond $N = 96$, we observed no significant change of the amount adsorbed, and the results presented utilize this value of N.

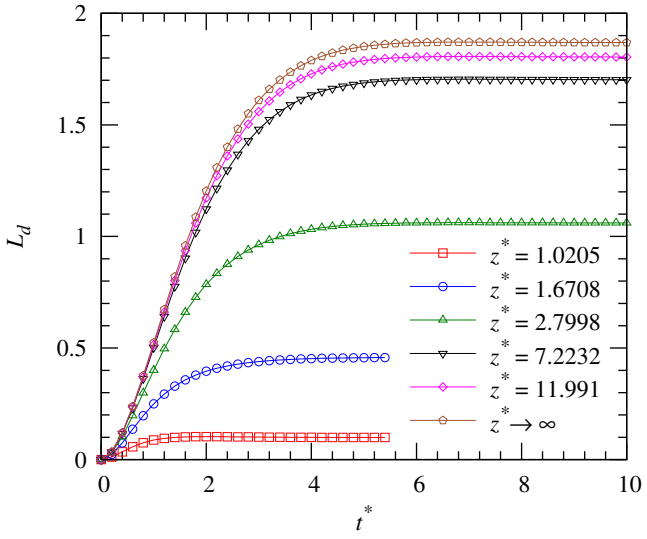

Figure 4.2. L_d as a function of t^* for various values of z^* at Wi = 2 and $b_k = 100$. Note that z^* are the collocation points.

4.4 Results and discussion

Since we want to focus on the effects of flow rate and molecular weight only, we fix the bead-bead interaction parameters to $\sigma_b = \varepsilon_b = 1$ and the bead-wall parameters to $\varepsilon_s = 1$ and $\kappa = 0.5$. Modifying these values will produce quantitative, but not qualitative, changes in the amount adsorbed. For a dumbbell model, the molecular weight $M \sim Q_0 = \sqrt{b_k kT/H}$. Hence, to study the effect of molecular weight, we vary the spring extensibility parameter b_k. The spring extensibility parameter $b_k \approx 3N_k$, where N_k is the number of Kuhn segments per spring. For PS, the molar mass per Kuhn segment is 720 g/mol (Rubinstein and Colby, 2003). Thus, the values of b_k investigated here represent PS chains of 6000-24000 g/mol. For comparison, we mention that the PS samples used in Lee and Fuller's experiments ranged from $3.84 \times 10^6 - 20 \times 10^6$ g/mol, which are much higher than the range probed here.

We calculate the amount adsorbed for two different initial conditions: (i) flow

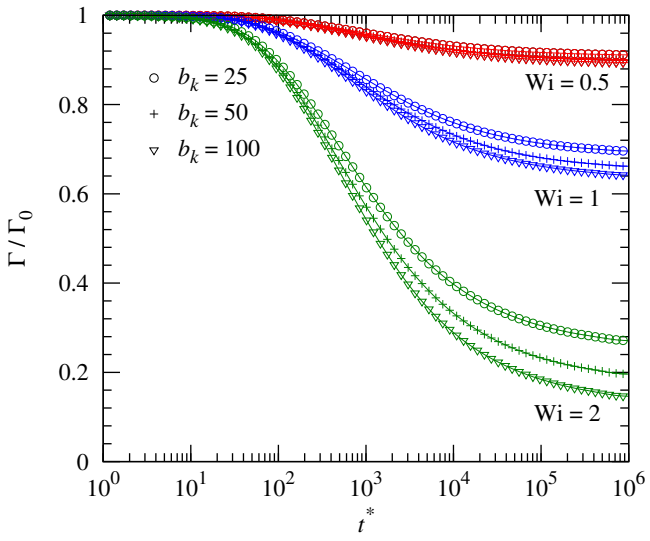

Figure 4.3. Normalized desorption curves for different values of Wi and b_k.

is initiated over a surface containing a preadsorbed polymer film, corresponding to desorption, and (ii) flow is initiated over a clean surface, corresponding to adsorption. Figures 5.9 and 4.4 show the time evolution of the normalized amount adsorbed at different shear rates and molecular weights for the above two cases respectively. The normalization factor is the amount that would have adsorbed from a quiescent solution. The amount adsorbed decreases with time for desorption and increases with time for adsorption. In both cases, an approach to a steady-state value in the long-time limit can be seen. Moreover, desorption is enhanced by an increase in shear rate as well as by an increase in molecular weight. Similarly, adsorption is inhibited. Comparing our results with Figures 3–5 (for desorption) and Figures 9–11 (for adsorption) of Lee and Fuller (1985a), we find that our dumbbell model effectively captures the qualitative trends observed in the experiments.

Figures 4.5 and 4.6 show the amount adsorbed and film thickness at steady-state for different shear rates and molecular weights. The amount adsorbed decreases with an

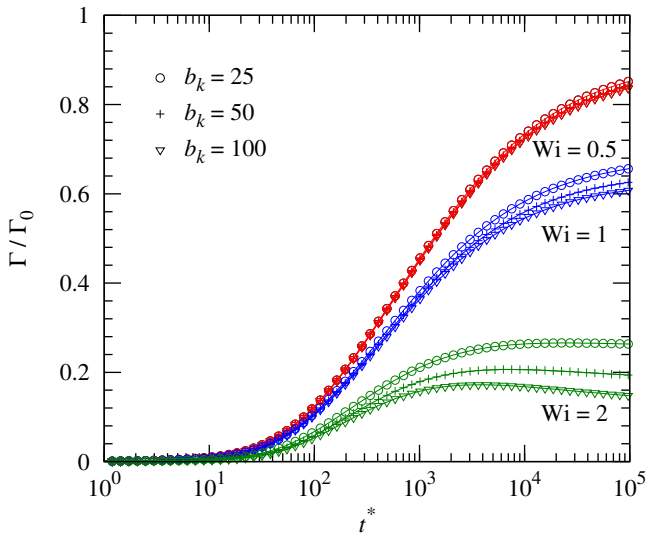

Figure 4.4. Normalized adsorption curves for different values of Wi and b_k.

increase in shear rate as well as with an increase in molecular weight. However, the film thickness remains almost constant for low shear rates, exhibiting a rapid drop at higher values. On increasing molecular weight, the film thickness decreases for all shear rates. At a sufficiently high shear rate, the amount adsorbed and film thickness can completely vanish. The steady-state results presented above are in good qualitative agreement with experimental observations (see Figures 6 and 12 of Lee and Fuller (1985a)).

To better understand our results, we examine the advection-diffusion equation (Equation (4.13)) governing the time evolution of the concentration profile. The first term on the right-hand side of Equation (4.13) represents diffusion, the first term inside the square brackets represents advection away from the wall due to dumbbell-wall HI, and the second term inside the square brackets represents advection toward the wall due to dumbbell-wall attraction. On moving away from the wall, the advection terms gradually diminish in magnitude, with the concentration approaching its bulk value. In case of desorption of a preadsorbed film, the amount adsorbed decreases with

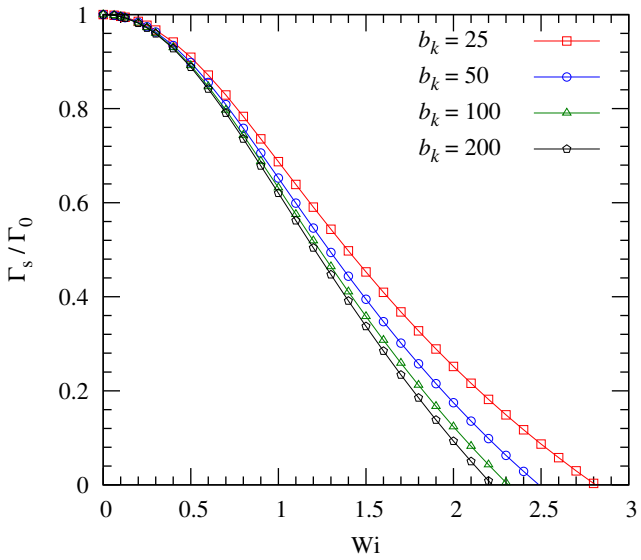

Figure 4.5. Normalized adsorbed amount at steady-state versus Wi for different values of b_k.

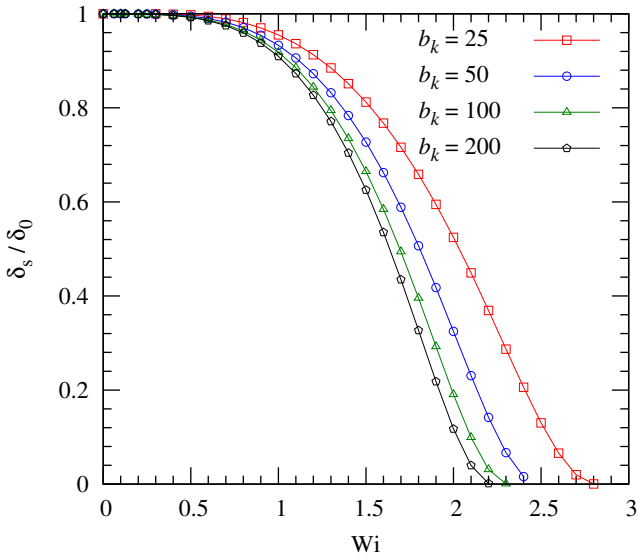

Figure 4.6. Normalized film thickness at steady-state versus Wi for different values of b_k.

time (Figure 5.9), indicating a gradual reduction of concentration near the wall. This reduction in concentration is caused by the migration of dumbbells away from the wall due to bead-wall HI. The migration mechanism is discussed in detail by Ma and Graham (2005) and Hoda and Kumar (2007d). In the absence of HI, the dumbbells will not be advected away from the wall. In the case of adsorption (Figure 4.4), initially we have a clean wall, so the dominant effect is that of dumbbell-wall attraction, leading to a progressive increase in concentration near the wall and hence the amount adsorbed until it is balanced by diffusion and advection away from the wall. Thus, it is the balance between dumbbell-wall attraction and HI-induced migration that dictates the development of the concentration profile for adsorption as well as desorption.

When the dumbbell-wall attraction does not change, HI is the sole determining factor for the amount adsorbed and film thickness. From Equation (4.10) and Equation (4.13) we see that HI-induced advection is proportional to the dumbbell stress, which depends on the extension of the dumbbell. On increasing the shear rate, the dumbbell stretches more, and the enhanced extension leads to stronger HI, which inhibits adsorption and assists desorption. At a particular shear rate, increasing the molecular weight (by increasing b_k) also leads to a larger extension, and hence increasing molecular weight has a similar type of effect on the adsorption and desorption curves. The effects of flow rate and molecular weight manifest themselves only through their ability to change how much the dumbbell stretches. In the absence of HI, the dumbbell model predicts that the amount adsorbed and film thickness will depend on neither the shear rate nor the molecular weight.

For both adsorption and desorption, it is interesting to note that the time required to attain a steady value is extremely long, even more than 10^5 times the longest relaxation time of the dumbbell (Figures 5.9-4.4). To understand the cause of such behavior, we have plotted the concentration profiles for desorption at different time instants in Figure 4.7.

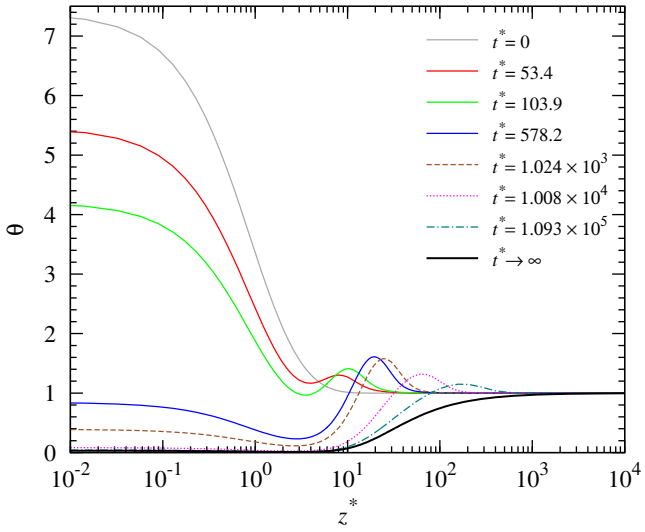

Figure 4.7. Concentration profiles at various times for Wi = 15 and $b_k = 100$. The value of Wi is intentionally chosen to be large in order to make the peaks noticeable.

Shortly after flow is initiated, bead-wall HI begins advecting the dumbbells away from the wall, resulting in a reduction of concentration in the immediate vicinity of the wall. As advection gradually weakens away from the wall, a peak appears because diffusion is not able to smooth out the concentration fast enough. This peak progressively broadens along with a slow drift, exhibiting a diffusion-dominated approach to steady-state. This results in the characteristic very long relaxation time. In the case of adsorption, the same mechanism is at work, but an upside-down peak is observed. Lee and Fuller (1985a)'s data for desorption of 8.42×10^6 molecular weight PS reaches a steady-state value after approximately 3.8×10^5 relaxation times ($\tau_{Rouse} = 7.7 \times 10^{-3}$ s), which is of the same order-of-magnitude as the kinetic theory prediction. Similar observations of long relaxation times were also made by Ma and Graham (2005) in the context of shear-induced migration of neutral polymers. It is interesting to note here the observations of McGlinn et al. (1988), who found that the amount adsorbed keeps increasing without

showing any indication of attaining a plateau value. We conjecture that one possible reason for this observation might be the extraordinarily long time required to reach the steady-state value.

Before concluding, we would like to discuss several observations of Lee and Fuller (1985a) that our dumbbell model is not able to capture. They found that the amount adsorbed at steady-state for different shear rates and molecular weights collapse onto a single power-law curve $\dot{\gamma}M^{0.7}$, where M is the molecular weight. Although it is possible to collapse the data in Figure 4.5 onto a single power-law curve, the exponent is much smaller (0.045) probably due to the simplicity of the dumbbell model. Lee and Fuller state that longer chains adsorb as well as desorb faster compared to low-molecular-weight chains, which also cannot be seen in Figures 5.9 and 4.4. Both of these observations pertain to molecular weight, which the dumbbell model accounts for by changing the spring extensibility parameter b_k. However, the change in b_k does not significantly change the advection term in Equation (4.13) to reflect the experimentally observed behavior. Ideally, one should also increase the adsorption strength with increase of b_k, which we have not incorporated. Even if this is taken into account, it will not have any significant impact on the advection term. The assumption that the effect of increase in molecular weight can be accounted for by increasing the length of the connector vector is clearly inadequate. The dumbbbell model simply does not have enough complexity to capture the effects due to molecular weight.

4.5 Conclusions

We have studied adsorption of homopolymers from a dilute solution subject to shear flow onto an adjacent planar wall using kinetic theory. The polymer molecules were modeled as bead-spring dumbbells interacting with the wall via a short-range exponential

potential. In the dilute limit, the kinetic theory leads to an advection-diffusion equation for the dumbbell concentration profile, which allowed us to calculate the amount adsorbed as well as the film thickness.

When flow is initiated over a clean wall, the amount adsorbed increases with time until it reaches a plateau value. The amount adsorbed decreases with both an increase in shear rate as well as an increase in molecular weight. On initiating the flow over a wall containing a preadsorbed polymer film, desorption was found to be facilitated by increasing shear rate as well as molecular weight, resulting in complete desorption at high enough shear rates. The time required to approach steady-state is many orders of magnitude longer than the dumbbell relaxation time, a consequence of the diffusion-dominated behavior away from the wall. These results are in qualitative agreement with the experimental observations of Lee and Fuller (1985a).

We have shown that the above results are a consequence of competition between the polymer-wall attractive force and the HI-induced polymer-wall repulsion. The repulsive interaction arises because the flow field generated by the force acting on each bead of the dumbbell acts away from the wall at the location of the other bead, resulting in a net migration of the dumbbell away from the wall. Increasing shear rate or molecular weight produces a larger force on each bead, enhancing migration of the dumbbells, which assists desorption and inhibits adsorption. In the absence of HI, the dumbbell model predicts that adsorption will be independent of shear rate and molecular weight, and desorption will not occur at all. Thus, our results indicate that polymer-wall HI is the dominant mechanism governing adsorption/desorption of dilute polymer solutions in shear flow.

Although our model is very minimalistic and includes several strong approximations, it is able to capture the essential features underlying adsorption in shear flow. However, the effects of including multiple beads (which may help in better describing effects

due to molecular weight), as well as the roles of solvent quality and polymer-surface intermolecular interactions still need additional study. Moreover, the dumbbell model cannot give any insight into the role of chain entanglements, which remains an open issue as well. We believe accounting for these factors might help explain some of the experimental results (see e.g., Chin and Hoagland, 1991; McGlinn et al., 1988; Chang and Chung, 1991) which exhibited deviations from the observations of Lee and Fuller.

Chapter 5

Brownian dynamics simulations of desorption under shear flow

Summary

We study desorption of isolated polymer molecules in the presence of shear flow using Brownian dynamics simulations. The polymer molecules are modeled as freely jointed bead-spring chains interacting with a planar wall via a short-range potential. The simulations include both intrachain and chain-wall hydrodynamic interaction (HI). Desorption is governed by an interplay between the chain-wall attraction and the wall-induced hydrodynamic repulsion. At constant molecular weight, desorption increases with an increase in shear rate and decreases with an increase in polymer-wall adsorption energy. When adsorption is weak, the chains form large loops and tails that generate stronger HI in the presence of the imposed flow field causing longer chains to desorb faster than shorter ones. In contrast, when adsorption is strong the chains adopt a flattened conformation, weakening HI and resulting in shorter chains with fewer sticking points desorbing faster than longer ones. The simulation results reconcile the apparently contradictory experimental studies by Lee and Fuller [J. Colloid Interface Sci. **103**, 569 (1985)] and Soga and Granick [Langmuir **14**, 4266 (1998)] concerning the effect of shear flow

on desorption of polymers.

5.1 Introduction

In this chapter we look at desorption of preadsorbed chains when subjected to shear flow. Although it may appear obvious that increasing shear rate will lead to more desorption because of an increase in drag on the chain, the real cause for desorption is a consequence of hydrodynamic interaction (HI) between the polymer chain and the wall (see Chapters 3 and 4). In the absence of HI with the wall, there is no mechanism forcing the chains to drift away from the wall other than diffusion. If an adsorbed chain does indeed unbind from the surface, it will readsorb and on average, there will be no change of the amount of polymer adsorbed. Of course, diffusion cannot be solely responsible for the drift as no desorption is observed in the absence of flow. Prior studies involving polyelectrolytes under shear flow have also identified polymer-wall HI as the primary cause for desorption (Hoda and Kumar, 2007d; Hoda and Kumar, 2007c; Hoda and Kumar, 2008). The HI involved here is the same as that causing polymer chains to drift away from a confining wall under shear flow, a phenomenon known as shear-induced migration (see Chapter 3 and Ma and Graham (2005)). Briefly, the mechanism involved is the following: In the presence of shear flow, the velocity gradient across a polymer chain causes a net stretching of the chain along the flow direction. The resulting entropic restoring force behaves as a pair of oppositely directed point forces acting on the solvent. Owing to the no-slip and the no-penetration conditions at the wall, the velocity field induced by these point forces possesses some component directed away from the wall, leading to a net migration of the chain.

However, most of the previous studies primarily focused on the steady state desorption under shear flow and the transient behavior was not explored. In addition, the effect of adsorption energy and molecular weight was not studied. Even in the case of shear rate, no attempt seems to have been made to reassess the experimental observations in the light of the insights gained from the simulations. One exception is our previous work discussed in Chapter 4, where we used a kinetic theory based on a dumbbell model of the polymer to study the time evolution of the amount adsorbed as a function of shear rate as well as molecular weight. Although the dumbbell model is useful in providing qualitative understanding of the desorption process as well as emphasizing the role of polymer-wall HI, it is too simple to capture the effects due to internal conformations of the chain. These conformations are important because they allow the formation of structures like loops, tails, and trains that significantly alter the hydrodynamic behavior of the chain.

In this chapter, we use Brownian dynamics (BD) simulations of polymer chains to explore the effects of shear rate, adsorption energy, and molecular weight on the transient behavior of desorption under shear flow. Our simulations are performed at the single-molecule level, i.e. we neglect all effects due to interchain interactions. Figure 5.1 shows a schematic of the system in our simulation. We show that increasing shear rate enhances desorption, while an increase in adsorption energy inhibits desorption. In addition, when adsorption is weak, i.e. close to the critical point of adsorption, higher molecular weight chains desorb easily compared to lower molecular weight chains, but the trend reverses in the case of strong adsorption.

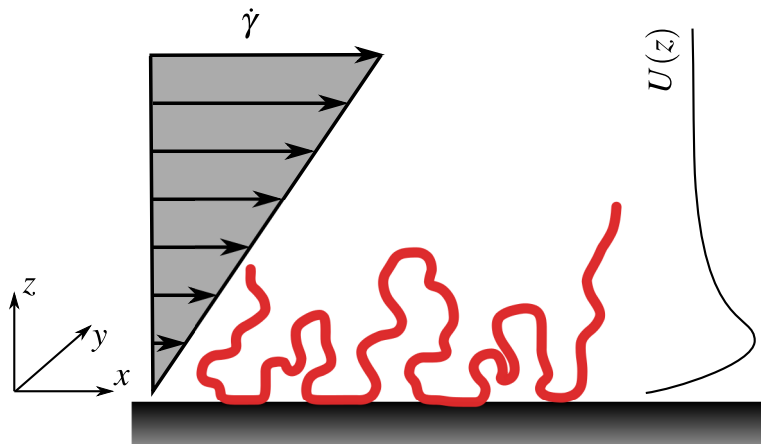

Figure 5.1. Schematic showing a single adsorbed chain under shear flow near a planar wall. The short-range adsorption potential is denoted by $U(z)$.

5.2 Simulation method

5.2.1 Polymer model

We represent a polymer molecule by a sequence of N beads connected by finitely extensible, nonlinear elastic (FENE) springs. The beads are assigned a hydrodynamic radius a and a drag coefficient ζ, representing the friction of a bead. From the Stokes-Einstein relation, the bead diffusivity is kT/ζ and the bead diffusion time is $\tau = \zeta a^2/kT$, where k is the Boltzmann constant and T is the temperature. We choose a as the unit of length, kT as the unit of energy, and τ as the unit of time. Thus the unit of force is kT/a and the unit of diffusivity is kT/ζ.

The spring force between two connected beads i and j is derived from the Kremer-Grest potential (Grest and Kremer, 1986),

$$U_{ij}^{sp} = \begin{cases} -\frac{1}{2} H R_{max}^2 \ln\left[1 - \dfrac{r_{ij}^2}{R_{max}^2}\right], & r_{ij} \leq R_{max} \\ 0, & r_{ij} > R_{max} \end{cases} \tag{5.1}$$

where $\mathbf{r}_i$ and $\mathbf{r}_j$ are the positions of bead i and bead j respectively, $r_{ij} = |\mathbf{r}_j - \mathbf{r}_i|$, $H = 30\varepsilon/\sigma^2$, the maximum spring extension $R_{max} = 1.5\sigma$, and σ and ε are the length and energy parameters. This form of the spring potential accounts for the finite length of the chain and in conjunction with the repulsive potential in Equation (5.2) prevents unphysical chain crossing (Grest and Kremer, 1986). The short-range repulsive potential is of the form

$$U_{ij}^{ev} = \begin{cases} 4\varepsilon \left[\left(\dfrac{\sigma}{r_{ij}} \right)^{12} - \left(\dfrac{\sigma}{r_{ij}} \right)^{6} + \dfrac{1}{4} \right], & r_{ij} < 2^{1/6}\sigma \\ 0, & r_{ij} \geq 2^{1/6}\sigma, \end{cases} \tag{5.2}$$

where $\sigma = 2a$ and $\varepsilon = 1kT$. Note that in contrast to a conventional bead-spring chain (Bird et al., 1987) where each spring represents several Kuhn lengths, each spring in the Kremer-Grest chain accounts for one Kuhn length.

The polymer chain is confined to the $z > 0$ half-space by a solid wall at $z = 0$. The beads interact with the surface via the 10-4-3 Steele potential (Steele, 1973; Siderius and Gelb, 2011)

$$U_i^w = \pi\sigma_w^2\varepsilon_w \left[\left(\frac{2}{5} \right) \left(\frac{\sigma_w}{z_i} \right)^{10} - \left(\frac{\sigma_w}{z_i} \right)^{4} - \frac{\sigma_w^4}{3\Delta \left(z_i + 0.61\Delta \right)^3} \right], \tag{5.3}$$

where $\Delta = 2\sqrt{2}a$ and $\sigma_w = 0.5\sigma$. This form of the potential is particularly suitable for modeling fluid-solid interaction (Siderius and Gelb, 2011) and has been used in the literature for modeling the bead-wall interaction for adsorbed polymers (Desai et al., 2006).

5.2.2 Equilibrium sampling

Although our primary goal in this work is to investigate desorption under flow, we will see later in Sec. 5.3.2 that an understanding of the conformations of an adsorbed chain in the absence of flow (i.e., at equilibrum) will prove valuable in interpreting the results for flow-induced desorption. Moreover, we will use conformations sampled at equilibrium to start our dynamic simulations. Hence we discuss the methods used for sampling the chain conformations in the absence of flow.

We performed the equilibrium sampling using the Metropolis Monte Carlo (MC) scheme. Sampling is carried out for two different purposes: (i) estimation of equilibrium properties (e.g., bound fraction, average loop length) of an adsorbed chain, and (ii) generation of initial conformations for dynamic simulations.

In the first case, the chain is tethered at one end to prevent it from drifting away from the wall, which is especially important for a non-adsorbing wall or when the adsorption energy is very weak. Tethering one of the chain ends is a commonly used technique in the literature (Milchev and Binder, 1996; Baschnagel et al., 2003; Descas et al., 2004) for sampling chain conformations in the presence of a wall and does not significantly affect equilibrium properties such as the bound fraction.

In the second case, the chain is not tethered because tethering can introduce chain-end bias if used as the starting configuration for dynamic simulations. For shorter chains, absence of a tether point often results in the chain drifting away from the wall during relaxation, though this is not an issue for longer chains. To circumvent this problem, we reject any MC move that can lead to complete desorption of the chain from the wall during relaxation. This sampling scheme generates chains only in an adsorbed condition.

A chain is considered adsorbed if any of its beads is bound to the surface. Since the beads are point particles interacting via a soft potential with the wall, precise contact

with the surface is ambiguous. Instead, we choose to classify a bead as bound if it is closer than the nominal bead diameter $2a$ from the wall. This distance is roughly equal to the width of the wall interaction potential.

An MC run begins with a chain positioned on a cubic lattice such that the distance between successive beads is 80% of the maximum spring length. Each MC cycle for an N-bead chain consists of N moves. Both tethered as well as non-tethered chains are first allowed to relax for 10^4 cycles, followed by a second relaxation phase of 10^5 cycles. For tethered chains, relaxation is further followed by a production run for 10^5 cycles. During the production run, the bead positions are saved after every 10^3 cycles. Approximately 144 independent runs are considered for each chain length and adsorption energy. For non-tethered chains, no production run is necessary; the single conformation obtained after relaxation is saved as an initial conformation. Hence, for non-tethered chains each MC run generates exactly one initial conformation.

During the first relaxation phase, a move is chosen randomly to be pivot, crankshaft, or displacement such that there are 50% pivot moves, 25% crankshaft moves, and 25% displacement moves per cycle on average. For non-tethered chains, no interactions with the wall are considered during this phase, whereas the wall effects are considered for tethered chains. After the first relaxation phase, non-tethered chains are brought in the immediate vicinity of the wall and chain-wall interactions are switched on. For both tethered and non-tethered chains, the run proceeds further using only crankshaft and displacement moves.

5.2.3 Non-equilibrium Brownian dynamics simulation

We use non-equilibrium Brownian dynamics to simulate polymer chains under shear flow. The initial chain conformation is determined by equilibrium sampling as described above, except that the chain is not tethered at one end. For shorter chains, absence of

a tether point often results in the chain drifting away from the wall during relaxation, though this is not an issue for longer chains. To circumvent this problem, we reject any move that leads to complete desorption of the chain from the wall during relaxation. This sampling scheme generates chains only in an adsorbed condition, and moreover, removes any chain-end bias due to tethering.

At time $t = 0$, a simple shear flow $\mathbf{u} = \dot{\gamma} z \hat{\mathbf{x}}$ is imposed parallel to the wall in the positive x-direction, where $\dot{\gamma}$ is the shear rate and $\hat{\mathbf{x}}$ is the unit vector along x-axis (see Figure 5.1). The bead positions are advanced in time by numerically solving the nondimensionalized stochastic differential equation

$$\mathbf{r}(t + \delta t) = \mathbf{r}(t) + \left[\mathbf{u}(t) - \mathbf{D}(t) \cdot \nabla U(t) + \frac{\partial}{\partial \mathbf{r}} \cdot \mathbf{D}(t)\right] \delta t + \mathbf{w}, \tag{5.4}$$

where $\mathbf{r}(t)$ is the vector of bead positions at time t, $\mathbf{r}(t + \delta t)$ is the vector of bead positions at time $t + \delta t$, $\mathbf{u}$ is the unperturbed solvent velocity at the bead positions, $\mathbf{D}$ is the diffusivity tensor, U is the total interaction potential, δt is the time step, and $\mathbf{w}$ represents the displacement due to Brownian motion. Beads that are bound to the surface are not allowed to move parallel to the wall; only motion along the wall-normal direction is allowed. This prevents the unphysical situation of the chain continuously translating along the wall and mimics the binding of the chain to distinct surface sites. Approximately 480 trajectories were generated for each shear rate, adsorption energy, and chain length. The time step for advancing the beads is adaptive with a maximum step size of 0.001τ. The duration of each simulation run is 1000τ. To reduce computational effort, trajectories of chains that have desorbed and moved far away from the wall are no longer followed. Based on preliminary simulations, we determined this cutoff distance to be $15a$ for the bead closest to the wall, i.e. the bead closest to the wall was more than fifteen bead radii away; chains that have ventured so far away from the wall were found

not to readsorb.

In Equation (5.4), the diffusivity tensor consists of 3×3 blocks denoted by the subscript ij,

$$\mathbf{D}_{ij} = \mathbf{\Omega}_{ij} + \delta_{ij}\mathbf{I}, \qquad i,j = 1,\ldots,N \tag{5.5}$$

where

$$\mathbf{\Omega}_{ij} = (1-\delta_{ij})\,\mathbf{\Omega}_{ij}^{RPY} + \mathbf{\Omega}_{ij}^{W}. \tag{5.6}$$

In the above equation, $\mathbf{\Omega}_{ij}^{RPY}$ is the Rotne-Prager-Yamakawa (RPY) tensor (Rotne and Prager, 1969; Yamakawa, 1970)

$$\mathbf{\Omega}_{ij}^{RPY} = \begin{cases} \frac{3a}{4r_{ij}}\left[\left(1+\frac{2a^2}{3r_{ij}^2}\right)\mathbf{I} + \left(1-\frac{2a^2}{r_{ij}^2}\right)\frac{\mathbf{r}_{ij}\mathbf{r}_{ij}}{r_{ij}^2}\right] & r_{ij} \geq 2a \\ \left(1-\frac{9r_{ij}}{32a}\right)\mathbf{I} + \left(\frac{3r_{ij}}{32a}\right)\frac{\mathbf{r}_{ij}\mathbf{r}_{ij}}{r_{ij}^2} & r_{ij} < 2a \end{cases} \tag{5.7}$$

and $\mathbf{\Omega}_{ij}^{W}$ is the wall mobility tensor. The latter can be written as

$$\mathbf{\Omega}_{ij}^{W} = \mathbf{\Omega}_{PF,ij}^{W} - \frac{2a^2}{3}\mathbf{\Omega}_{c,ij}^{W}, \tag{5.8}$$

where $\mathbf{\Omega}_{PF,ij}^{W}$ is the mobility tensor obtained by Blake (1971) for a point force near a solid wall in Stokes flow and $(2a^2/3)\,\mathbf{\Omega}_{c,ij}^{W}$ is a correction term due to finite bead size. The expressions for $\mathbf{\Omega}_{PF,ij}^{W}$ and $\mathbf{\Omega}_{c,ij}^{W}$ can be found in Appendix B of Hoda and Kumar (2007c). The divergence of the diffusivity tensor in Equation (5.4) is (Hoda and Kumar, 2007c)

$$\left[\frac{\partial}{\partial \mathbf{r}} \cdot \mathbf{D}\right]_i = \left(\frac{1.125a}{z_i^2} - \frac{1.5a^3}{z_i^4}\right)\hat{\boldsymbol{z}}. \tag{5.9}$$

The Brownian displacement $\mathbf{w}$ is sampled from a multivariate Gaussian distribution with zero mean and covariance of $2\delta t\mathbf{D}$. If $\mathbf{x}$ is a standard normal vector, $\mathbf{w} = \sqrt{2\delta t}\,\mathbf{B}\cdot\mathbf{x} = \sqrt{2\delta t}\mathbf{y}$, such that $\mathbf{B}\mathbf{B}^T = \mathbf{D}$. To determine $\mathbf{y}$ we use the Krylov-subspace-based method

due to Ando et al. (2012) Briefly, the method involves substituting $\mathbf{B}$ with the square-root matrix $\sqrt{\mathbf{D}}$, which satisfies $\mathbf{B}\mathbf{B}^T = \mathbf{D}$ as well due to the symmetry of $\mathbf{D}$. Further, we look for a vector $\tilde{\mathbf{y}}$ that approximates $\mathbf{y}$ with certain predefined accuracy from the Krylov subspace generated by $\mathbf{D}$ and $\mathbf{x}$. This approximation $\tilde{\mathbf{y}}$ is constructed iteratively by increasing the dimension m of the Krylov subspace. The iterations stop when the error between successive iterates drops below some predefined threshold. It turns out that m is much smaller than $3N$ (recall that $\mathbf{D}$ is a $3N \times 3N$ matrix), and hence only a few iterations are necessary per time step.

5.3 Results and discussion

Before presenting results for shear-induced desorption, we first discuss the conformations of an adsorbed chain in the absence of flow as a function of adsorption energy and molecular weight. As we will see later, the equilibrium structure is important because it determines how such structures will behave in presence of flow past them.

5.3.1 Equilibrium conformation of adsorbed chains

The equilibrium conformation of an isolated adsorbed chain is usually described in terms of three kinds of subchains – (i) *trains*, which have all their segments in contact with the surface, (ii) *tails*, which are non-adsorbed chain ends, and (iii) *loops*, which are sections of the chain between two trains (see Figure 1.2 for a schematic). For a chain consisting of N segments the train fraction (also known as the bound fraction), defined as m/N where m is the number of segments directly in contact with the surface, provides an important measure for characterizing the equilibrium chain structure. The average train, loop, and tail fractions depend on the segment-surface interaction energy as well as the number of segments in the chain. The equilibrium chain structure is determined by a

balance between the chain-surface attraction and the entropic repulsion.

Figure 5.2 shows the average train fraction $\langle m/N \rangle$ as a function of the adsorption energy ε_w for different chain lengths. For each value of chain length, $\langle m/N \rangle$ approaches unity on increasing ε_w. In other words, on increasing the adsorption energy the chain progressively spreads out until it lies completely flat against the surface. Moreover, with an increase in chain length, $\langle m/N \rangle$ approaches zero when ε_w is low, whereas at high ε_w it asymptotes to some positve value. As is well known (Eisenriegler, 1993; Descas et al., 2004), there exists a certain ε_w^c, called the critical point of adsorption such that as $N \to \infty$,

$$\left\langle \frac{m}{N} \right\rangle \to \begin{cases} 0, & \varepsilon_w < \varepsilon_w^c \\ \text{finite}, & \varepsilon_w > \varepsilon_w^c. \end{cases}$$

Beyond the critical point, an infinite chain undergoes a transition from an isotropic coil to a flattened pancake-like conformation. This transition has the characteristics of a second-order phase transition (Eisenriegler et al., 1982), where the average train fraction acts as the order parameter. Thus for an infinite chain, adsorption occurs only when $\varepsilon_w > \varepsilon_w^c$. For $\varepsilon_w > \varepsilon_w^c$, adsorption is considered to be weak if the adsorption energy is close to the critical point, i.e. $(\varepsilon_w - \varepsilon_w^c)/\varepsilon_w^c \ll 1$, and strong otherwise. Exactly at the critical point, the following scaling relation holds (Eisenriegler, 1993):

$$\left\langle \frac{m}{N} \right\rangle \sim N^{\phi - 1}, \tag{5.10}$$

where $\phi \approx 0.59$. Although the above scaling relation is universal, the value of ε_w^c is model dependent and can be calculated using the scaling relation itself. In Figure 5.3, $\langle m/N \rangle$ is plotted against N for different values of ε_w. The slope for each of the graphs is shown in the inset of Figure 5.3 as a function of ε_w. For a non-adsorbing wall, the slope is -1, whereas for a strongly adsorbing wall it approaches zero, becoming independent

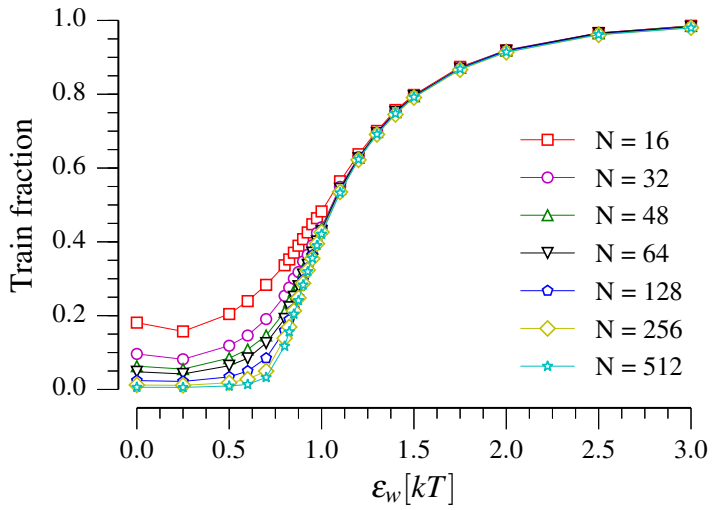

Figure 5.2. Average train fraction as a function of adsorption energy for different chain lengths.

of ε_w. Exactly at the critical point ε_w^c, the slope of $\langle m/N \rangle$ versus N should equal $\phi - 1$, with $\phi = 0.59$ in the long chain limit. This allows us to determine the critical point as the value of ε_w corresponding to a slope of -0.41. Using interpolation on the graph shown in the inset, we obtain $\varepsilon_w^c \approx 0.758$. Note that this is an approximate value, as the scaling result is valid only in the long chain limit.

Figure 5.4 shows the average length of tails as a function of adsorption energy for different chain lengths. For a non-adsorbing wall (recall that we are discussing tethered chains) the entire chain forms a tail in order to maximize its conformational entropy, with longer chains possessing longer tails. As the adsorption energy increases, tail lengths decrease since adsorption becomes more energetically favorable. Beyond the critical point of adsorption the chains start flattening against the surface, which results in a sudden plummeting of tail length. For higher values of ε_w the tails are vanishingly small, and practically independent of chain length and adsorption energy.

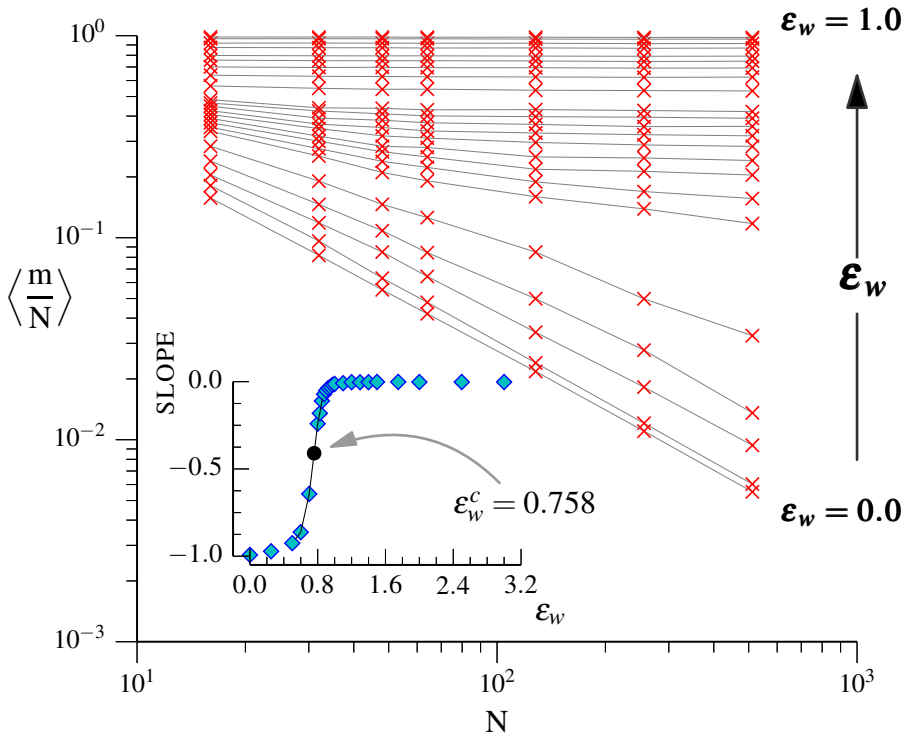

Figure 5.3. Average train fraction as a function of chain length for different adsorption energies. (*Inset*) Slope of average train fraction versus chain length as a function of adsorption energy, showing the critical point of adsorption corresponding to the slope of -0.41.

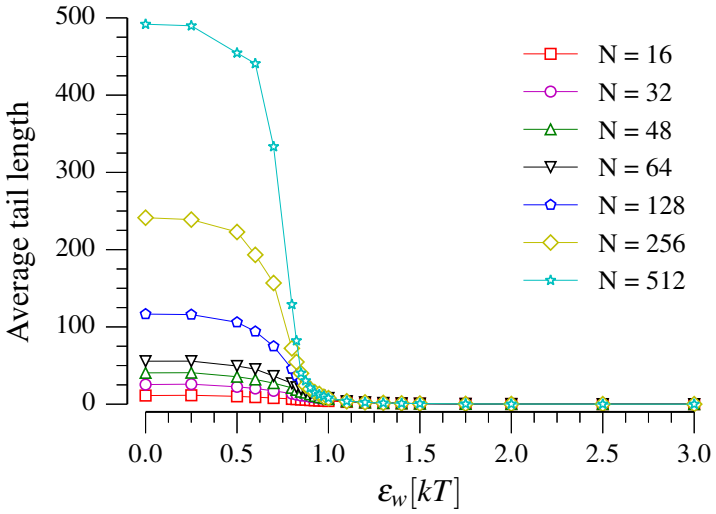

Figure 5.4. Average length of tails as a function of adsorption energy for different chain lengths.

Figure 5.5 shows the average length of loops as a function of adsorption energy for different chain lengths. The loops being connecting subchains between trains, their length is determined by the number of segments in the trains and the tails. At small ε_w, the chains form large tails with small loops and trains. As ε_w increases, the tails shorten much more rapidly than the trains can grow, causing a peak to appear in the average loop length. Note that close to the critical point, the train fraction decreases with an increase in chain length (see Figure 5.2), leading to formation of larger loops for longer chains. As in the case of tails, for higher values of ε_w the loop length diminishes to a small constant value independent of chain length and adsorption energy, as most of the chain lie in direct contact with the surface.

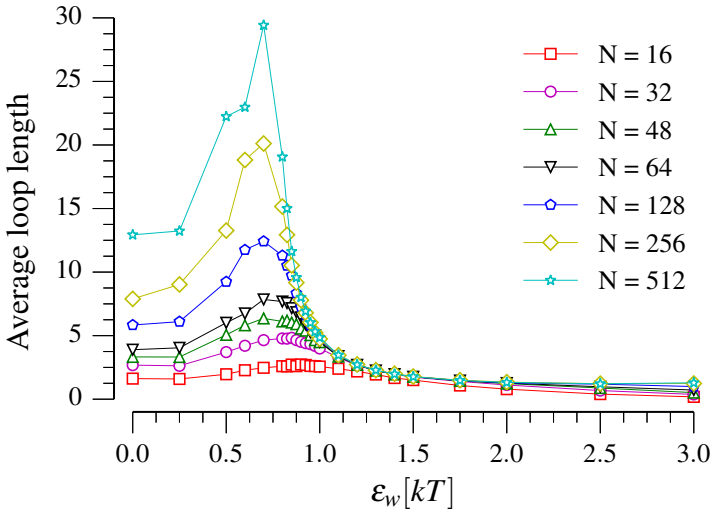

Figure 5.5. Average length of loops as a function of adsorption energy for different chain lengths.

5.3.2 Shear-induced desorption

In the presence of shear flow, an adsorbed chain is no longer in equilibrium. Hydrodynamic forces compete with surface attraction to generate repeated cycles of extension and retraction. The mechanism of desorption under high shear rates involves a complicated interplay among the imposed flow field, the chain-wall attraction, and Brownian fluctuations. Desorption means the chains detach from the surface and drift away from it. One way to quantify desorption is via the fraction of chains in the ensemble in the adsorbed state. We start with a number of adsorbed chains, hence initially the fraction adsorbed is unity. A decrease of this quantity as time progresses signifies desorption. Since we are primarily interested in understanding desorption, we track how the fraction adsorbed changes over time as a function of shear rate, adsorption energy, and the chain length.

Effect of shear rate

Figure 5.6 shows the time evolution of the fraction adsorbed for 128-bead chains at different shear rates. The adsorption energy ε_w is $0.8kT$, which is close to the critical point $\varepsilon_w^c \approx 0.758kT$. Note that at low shear rates ($\dot{\gamma} \leq 0.15/\tau$), the fraction adsorbed levels off to a non-zero plateau value. This plateau value is not a true steady state in the sense that it does not represent a balance between opposing fluxes. In contrast, the steady state discussed in Chapters 3 and 4 in the context of kinetic theory of a dumbell model represented a balance between the diffusive flux and the advective flux and was a true steady state. For simulations involving isolated chains, it is not possible to have two opposing fluxes; thus a single chain will eventually desorb (though the time required may be much longer than that possible to reach in a simulation). The time required to reach the true steady state was shown in Chapter 4 to be many orders of magnitude in terms of the longest relaxation time of the chain. But the time required to attain the pseudo-steady state is only 200τ, where τ is the bead diffusion time. The plateau value in the fraction adsorbed should be understood simply as the fraction of chains in the ensemble that are more tightly bound to the surface. Bearing this caveat in mind, let us agree to call to this non-zero pseudo-steady condition as steady-state for the rest of this paper.

The steady-state value decreases with increase in shear rate. At higher shear rates ($\dot{\gamma} = 0.30/\tau$ and $\dot{\gamma} = 0.50/\tau$) it vanishes and all the chains gradually desorb from the wall. Even for cases where complete desorption is achieved, desorption is faster at higher shear rates. The qualitative nature of the graphs is very similar to the observations reported by Lee and Fuller (1985a), as can be seen by comparing with Figure 2.2 (a). This behavior with respect to shear rate is a consequence of an increase in chain-wall HI with increase in shear rate, as supported by results from our previous work (see Sec. 3.4.2

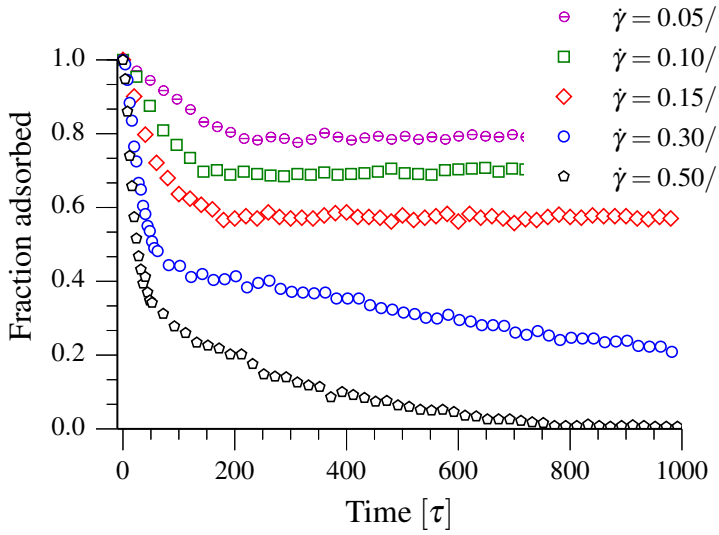

Figure 5.6. Fraction adsorbed as a function of time for 128-bead chains at different shear rates. The surface adsorption energy is $0.8kT$.

and Sec. 4.4) using a kinetic theory for dumbbells. In the absence of polymer-surface HI, the chains may detach, but will not migrate away.

Effect of adsorption energy

Figure 5.7 shows the fraction adsorbed as a function of time for a 128-bead chain for different adsorption energies. The shear rate is $0.15/\tau$. We find that at this shear rate, a steady-state value is reached for all adsorption energies. The inset in Figure 5.7 shows the steady-state fraction adsorbed plotted against the adsorption strength. We see that an increase in adsorption energy inhibits desorption. Indeed, for ε_w beyond $0.9kT$ there is barely any desorption at all. The results corresponding to high ε_w are reminiscent of the experiments of Soga and Granick (1998), who observed very little desorption (see Figure 2.3).

To understand the effect of adsorption energy, we need to look back at the equilibrium

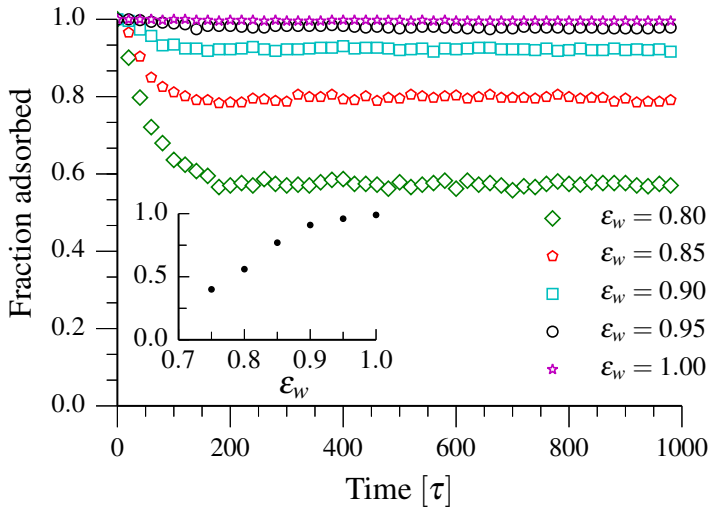

Figure 5.7. Fraction adsorbed as a function of time for 128-bead chains at different adsorption strengths. The adsorption energy ε_w is in units of kT. The shear rate for all cases is $0.15/\tau$. (*Inset*) The fraction adsorbed at steady state as a function of the adsorption strength.

conformations in Sec. 5.3.1. Close to the critical point of adsorption ($\approx 0.76kT$), loops and tails proliferate and the bound fraction is low. When exposed to flow, large velocity gradients develop across the chains, leading to desorption. But as the adsorption energy increases, the chains adopt a flatter conformation, the bound fraction increases, and the loops become smaller. This results in a smaller velocity gradient across the chains, and hydrodynamic effects are weak. Moreover, since the strongly adsorbed chains are closer to the surface, they not only get less stretching (due to the smaller velocity gradient) but their HI is more strongly screened. Consequently, desorption drops with increase in adsorption energy.

Effect of molecular weight

Figure 5.8 illustrates the effect of molecular weight on desorption through a series of plots at different adsorption energies. Each plot shows the time traces of fraction adsorbed at a shear rate of $0.5/\tau$ for different chain lengths. The first thing to note is that the shear rate is very high (see Figure 5.6 to get a sense of the shear rate involved), so significant desorption is expected. Indeed, all the graphs show a monotonic decrease in the fraction adsorbed, and no steady state appears within the time range shown. At low adsorption energies ($\varepsilon_w = 0.75kT$ and $0.8kT$), longer chains desorb more rapidly than shorter ones. This is quite evident by comparing the graphs for $N = 32$ – 256. The experiments of Lee and Fuller (1985a) clearly demonstrate such a trend (see Figure 2.2 (b)), although all of their observations are conducted at the same adsorption strength (as the same polymer and surface is used), presumably low. The reason for such a trend can be attributed to the larger loops and dangling tails accompanying longer chains, resulting in higher drag and HI-induced migration. Additional evidence in favor of this argument may be gleaned from the near overlap of the graphs for 16 and 32-bead chains when $\varepsilon_w = 0.75kT$. Apparently, these chains are too short to exhibit significant differences in hydrodynamic behavior that could lead to significantly different desorption curves. Even then, at $\varepsilon_w = 0.75$ desorption is slightly faster for $N = 32$ compared to $N = 16$, but this small variation quickly disappears on increasing the adsorption energy to $0.8kT$.

In contrast, at high adsorption energies ($\varepsilon_w = 0.95kT$ and $1.0kT$) shorter chains desorb faster than longer chains. Compare the plots corresponding to $\varepsilon_w = 0.75kT$ and $\varepsilon_w = 1.0kT$ to observe a clear reversal in the trend with respect to chain length. The reversal occurs through intermediate states, e.g. at $\varepsilon_w = 0.85kT$, when all the graphs appear to collapse before separating out in the opposite direction. At high adsorption energies, chain-wall attraction dominates; the chains lie flat on the surface and chain-wall

HI is minimal. But hydrodynamic drag still exists, and high shear rates aided by thermal fluctuations and excluded volume interaction may lead to detachment of sections of chains from the wall. These detached portions can then be subject to wall HI, slowly peeling the chain away. Desorption occurring this way is easier for shorter chains, as they have fewer sticking points with the wall. Note that this mechanism is very different from the one primarily driven by wall HI in the case of low adsorption energies. We speculate that had the experiments of Soga and Granick (1998) investigated the effect of molecular weight, behavior similar to that shown in Figure 5.8 for high adsorption energies would have been observed.

5.3.3 Desorption pathway

Based on the discussion above, we present a pictorial representation of the steps involved in desorption (see Figure 5.9). The solid and dashed arrows denote alternate paths, and the blue arrows represent steps that occur repeatedly (but not necessarily cyclic). Upon imposition of flow, an adsorbed polymer chain first undergoes deformation in the flow direction leading to flattening against the wall. If adsorption is weak, shear-induced deformation leads to elongated loops and tails that can successively detach and desorb due to strong polymer-wall HI. When the enlongated loops/tails align in the flow direction, the vorticity of the shear flow may result in their rotatation back toward the wall followed by readsorption. The chain is then again subject to partial detachment by the flow and the cycle continues until complete desorption takes place.

On the other hand, if the adsorption energy is strong, the chains are already flattened against the wall, and the shear-induced deformation is not particularly pronounced. In this case desorption may still occur, but the mechanism is different from the weak adsorption case. Thermal fluctuations initiate random protrusions in the velocity gradient direction that lead to the emergence of tails or loops that align in the flow direction. At

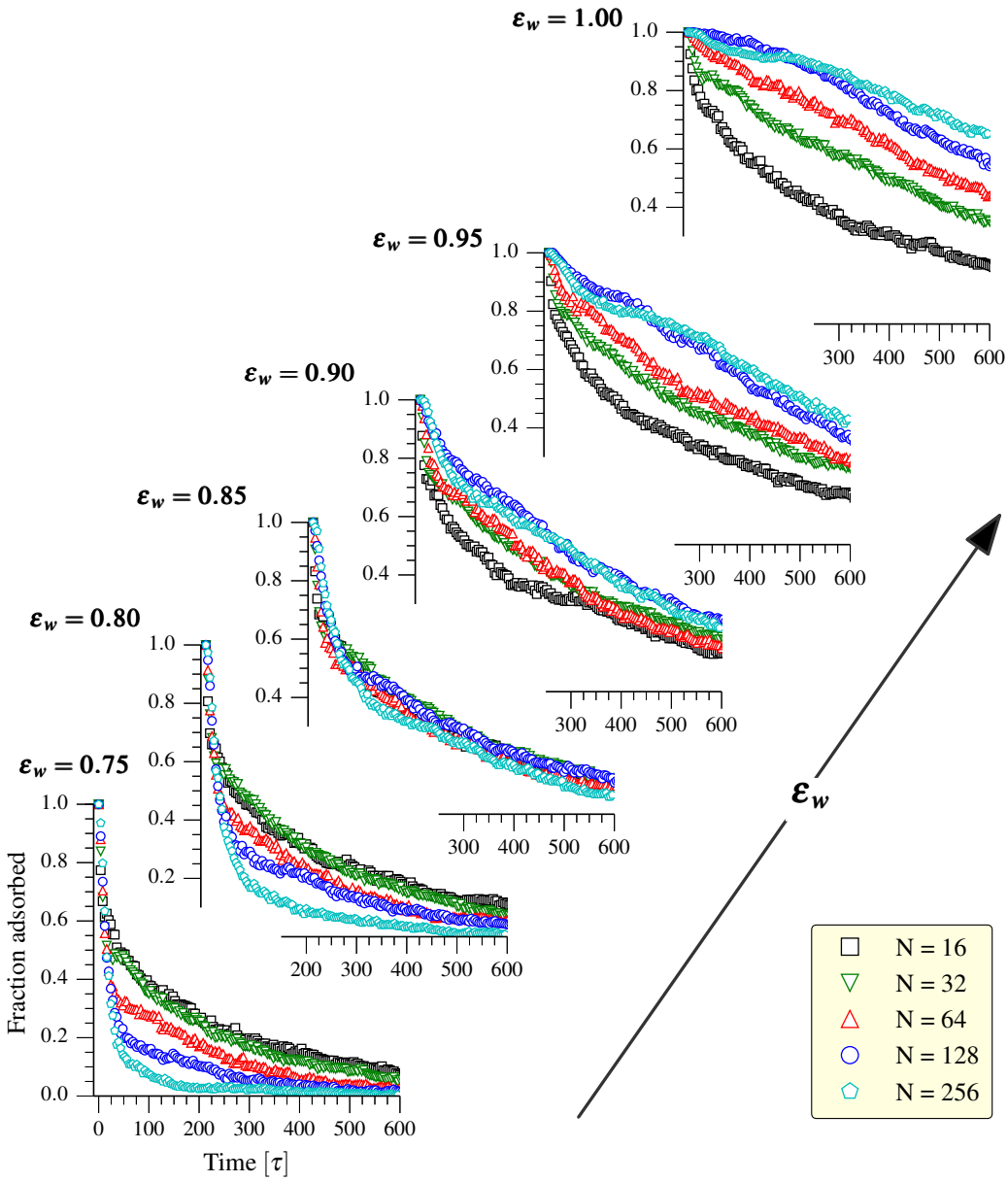

Figure 5.8. Fraction adsorbed versus time for chains of different lengths and at different adsorption energies. The shear rate is $0.5/\tau$ is all cases.

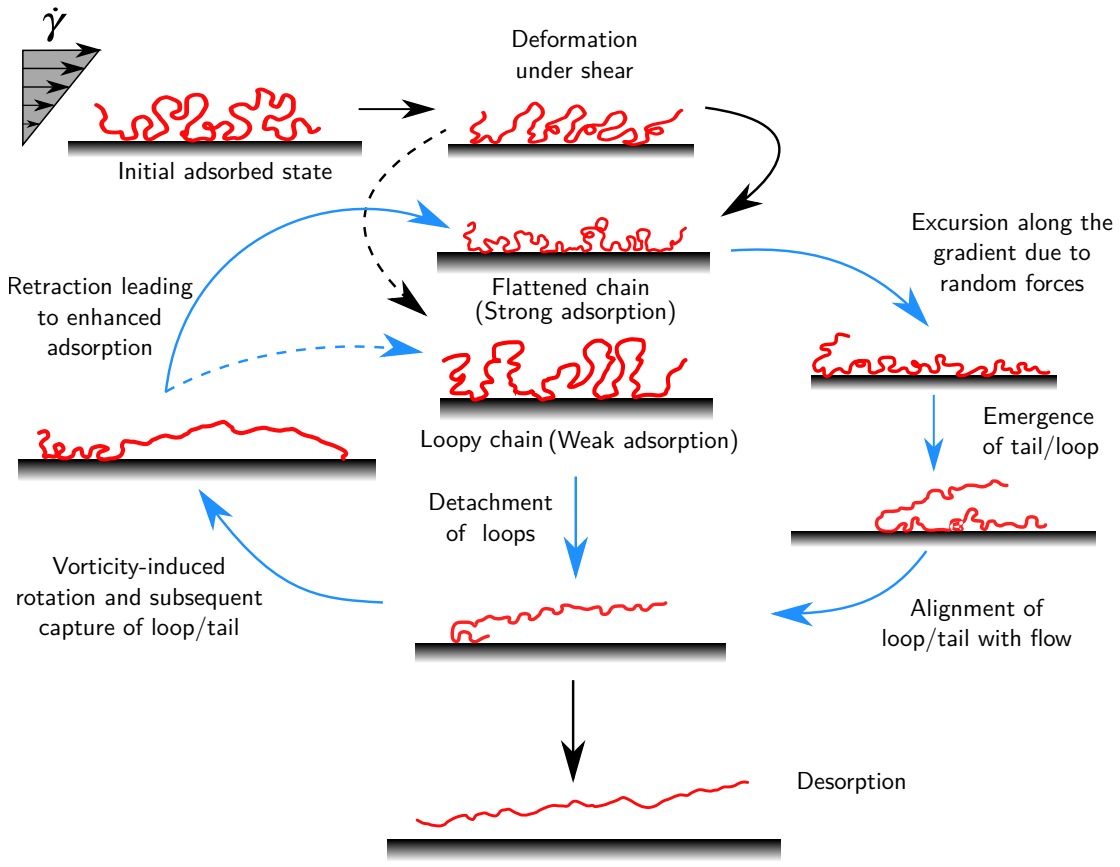

Figure 5.9. Schematic showing the pathway of desorption for strong and weakly adsorbed chains. Dotted lines denote alternate pathways (see text for details).

this point, if HI is sufficiently strong the chains may desorb. However, if shear-vorticity rotates the chain back to the wall it will readsorb and the thermally activated protrusion development process begins anew.

5.4 Conclusions

In this chapter, we have studied the effect of shear rate, adsorption energy, and molecular weight on desorption of isolated polymer chains under shear flow using Brownian dynamics simulations. Our simulations included intrachain as well as chain-wall HI. We found that

polymer desorption is governed by a delicate balance between chain repulsion due to wall HI and the attraction due to an adsorbing wall.

Irrespective of molecular weight and adsorption energy, an increase in shear rate leads to an increase in desorption. This is a consequence of stronger drag on the chain as well as stronger HI between the chain and the wall. However, the amount desorbed decreases with an increase in adsorption energy.

When adsorption is weak (close to the critical point of adsorption), at a shear rate high enough to observe complete desorption, longer chains desorb faster than shorter ones. This is a consequence of stronger HI in longer chains due to larger loops and tails compared to that in shorter chains. In contrast, in the case of strong adsorption longer chains have very small loops and tails, and as a result, the effect of HI is weaker and shorter chains desorb faster because they have fewer sticking points.

Our results indicate that the trends observed by Lee and Fuller (1985a) with respect to shear rate and molecular weight hold when adsorption is weak (adsorption energy close to the critical point of adsorption), while those observed by Soga and Granick (1998) hold for higher adsorption energies.

Chapter 6

Conclusions and future directions

This work was primarily motivated by several conflicting experimental observations regarding the influence of shear flow on the adsorption and desorption of polymers. Using kinetic theory and Brownian dynamics (BD) simulations we have attempted to unravel the underlying physics behind these observations, particularly focusing on the experiments of Lee and Fuller (1985a) and Soga and Granick (1998). Here we summarize our key findings and discuss several directions for future research.

We began by developing a kinetic theory for a simple bead-spring dumbbell model of a polymer chain near an attractive wall. For a dumbbell the amount adsorbed and the film thickness at steady-state can be calculated analytically. We showed that under shear flow hydrodynamic interaction (HI) with the wall generates a repulsive effect on the dumbbells that competes with wall attraction to govern the amount adsorbed and film thickness. Increase in shear rate increases the HI-induced repulsion, and hence the amount adsorbed decreases with an increase in shear rate. In the limit of strong attraction, we also derived a scaling law relating the critical shear rate required for desorption and the parameters of the adsorption potential.

Next we worked out the time evolution of the amount adsorbed based on the dumbbell

model. The transient problem leads to an advection-diffusion equation in terms of the dumbbell concentration, which we solved numerically to obtain the amount adsorbed as a function of time. The calculations were carried out for adsorption onto a bare wall as well as for desorption of a preadsorbed film. We found that for adsorption the amount adsorbed decreases with an increase in shear rate at constant molecular weight, whereas at constant shear rate the amount adsorbed also decreases with an increase in molecular weight. For desorption, the dependence on shear rate and molecular weight are reversed. We also note here that the time required to attain steady-state for either adsorption or desorption was found to be several orders of magnitude in terms of the dumbbell relaxation time. These results based on the dumbbell model are in qualitative agreement with the experimental results of Lee and Fuller (1985a).

Finally, we studied desorption under shear flow using Brownian dynamics (BD) simulations of bead-spring chains. We found that chain-wall HI causes longer chains to desorb faster than shorter ones when adsorption is weak, whereas for strong adsorption shorter chains desorb faster. This is a result of weakly adsorbed longer chains forming larger loops and tails that interact hydrodynamically generating greater lift on the chain as compared to shorter chains. On the other hand, when adsorption is strong the chains adopt a flattened conformation, making longer chains harder to desorb because of the greater surface interaction energy. Our simulation results explain the apparent contradiction in the experimental observations for desorption reported by Lee and Fuller (1985a) and Soga and Granick (1998).

Apart from the two experimental studies above, we had mentioned several other experiments on the adsorption of polymers in Sec. 2.1.4 that also lack a detailed understanding. Here we discuss the extent to which our results explain these experiments and point out the outstanding issues that need to be resolved in future work.

In the experiments by Chin and Hoagland (1991) on the adsorption of PS dissolved

in cyclohexane, the amount adsorbed was reported to decrease with an increase in shear rate. This clearly agrees with our prediction from kinetic theory (see Sec. 4.4), where the decrease in the amount adsorbed was shown to be a consequence of enhanced polymer-surface HI at higher shear rates inhibiting transport of the polymer molecules toward the surface.

However, when decalin was used as the solvent instead of cyclohexane, no effect of increasing the shear rate on the amount adsorbed was observed over the entire range studied from 0 – 1200 s^{-1}. This is surprising, since both cyclohexane and decalin are nearly θ-solvents for PS. Similar solvent quality indicates that the chain conformations in the bulk will be the same for both, but whether the presence of the solvent can affect the segement-surface interaction energy is not clear.

Similar to the adsorption experiments, increasing shear rate produced no effect on desorption of PS in the presence of decalin. The range of shear rates studied was 0 – 120 s^{-1}. The desorption experiments were not performed for cyclohexane, so a direct comparison of the effect of the solvent is not possible. It is likely that the shear rates involved are too low to exhibit significant shear-induced desorption (cf. shear rates larger than 2000 s^{-1} were required for desorption in the experiments of Lee and Fuller (1985a) with PS/cyclohexane). However, significant desorption (about 30% of the amount adsorbed from a stagnant solution) was found to occur at all shear rates, even in the absence of flow. Note that this desorbed amount did not show any dependence on the shear rate. The mechanism of this desorption (even in the absence of flow) is not understood. It is possible, as suggested by the authors, that desorption is due to the removal of very weakly bound chains at the periphery of the adsorbed layer. Unfortunately, such effects do not show up in our results as our simulations are performed for an ensemble of non-interacting chains. Simulations involving multiple chains will be able to shed more light on this issue (see Sec. 6.1.1).

Next we look at the experiments of Chang and Chung (1991) on the desoprtion of PEO and PVA. An important distinction between the experimental study and our simulations is that in the experiment the polymers were desorbed from the surface of latex spheres in the presence of an ambient shear flow whereas the surface considered in our simulations is a planar wall. Moreover the thickness of the adsorbed layer was reported in the experiments instead of the amount adsorbed. This presents a certain ambiguity as it is difficult to infer whether the film was being compressed or the chains were indeed desorbing due to shear flow. For PEO, the layer thickness showed an initial decrease with time before approaching a plateau value, but no effect was observed on increasing either shear rate or molecular weight. While the nature of polymer-surface HI for a suspension of spheres is not known apriori, the above observation indicates that it is possibly much weaker than a planar wall. In case of weak HI, neither shear rate nor molecular weight will have an impact on desorption. However, the reduction is film thickness with time still remains unexplained. More insight into this problem can be obtained if future simulation studies consider desorption from curved surfaces (see Sec. 6.1.2).

For PVA of molecular weight 1.5×10^4 g/mol, reduction in film thickness was observed only for the highest shear rate (1.6×10^4 s^{-1}). When using higher molecular weight samples (4.9×10^4 g/mol), no desorption was observed at all on increasing shear rate or molecular weight. The authors suggested that the presence of acetate groups in PVA may lead to stronger adsorption of PVA molecules compared to PEO, i.e., the adsorption energy for PVA is much stronger than that of PEO. From our simulations, we found that when the adsorption energy is strong shorter chains exhibit more desorption than longer chains (see Sec. 5.3.2), as observed for PVA in the experiments.

6.1 Future directions

There exist several directions in which the research presented above may be extended. We present three possible topics below that are particularly important from the technological point of view.

6.1.1 Beyond single chains

Our kinetic theory and BD simulations were developed at the isolated molecule level, i.e. all interchain interactions were neglected. This is a major simplifying approximation for adsorbed polymer layers. Even when the adsorbed layer is formed from a dilute solution, the diluteness appoximation breaks down near the interfacial region and semidilute solution behavior is expected. The only situation where interchain interactions can be discarded is when physically a single molecule exists in the system, e.g., manipulating DNA within a microfluidic/nanofluidic device. Clearly, a more accurate model for the adsorbed layer needs to take care of interactions between multiple chains, e.g., excluded volume interactions or entanglement effects.

Two kinds of scenarios are of interest here: (i) flow past brushes (see Figure 1.5) and (ii) adsorption/desorption of polymeric layers under flow. In both of these cases an important question is how the presence of multiple chains impact the chain-wall HI. Another issue worth considering is how the solvent quality changes adsorption/desorption behavior. Some work has been done in this area from an isolated-chain perspective (Radtke et al., 2014), but not for an adsorbed layer under flow. Specifically for brushes, it is known that the grafting density changes the brush structure as well as the desorption behavior (Anastassopoulos et al., 2006), which adds another possible line of investigation.

Theories for handling multiple chain interactions in presence of flow are virtually non-existent, and therefore one needs to resort to Brownian/Molecular dynamics simulations.

The simulation method discussed in Sec. 5.2.3 can be adapted in principle for multiple chains as well, but it will turn out to be computationally very inefficient. It appears that a more tractable method might be based on solving the Stokes equations over the entire domain, followed by evaluation of the random forces on each bead (Hernández-Ortiz et al., 2007) Another attractive method might be based on solving the randomly forced Stokes equations, as is done in fluctuating hydrodynamics problems (Chaudhri et al., 2014).

6.1.2 Curved surfaces

In our work, the surfaces we considered were flat and chemically structureless. Future research should focus on extending the present work to cases where the adsorbing surface is curved. An important problem involving curved surfaces is that of desorption of polymers grafted onto latex spheres (see Figure 1.6 and the associated discussion). It may also be worthwhile to look at adsorption onto rough surfaces or those containing chemical heterogeneities (Hoda and Kumar, 2007a; Hoda and Kumar, 2007b; Hoda and Kumar, 2008; Milchev, 2011). In the absence of flow, scaling theories (Pincus et al., 1984; Hershkovits et al., 2007) and mean-field theories (Skau and Blokhuis, 2002) have been proposed for adsorption onto curved surfaces, but it is non-trivial to extend them to account for the effects of flow. As far as computer simulations are concerned, the crucial element in these systems is of course to account for the chain-surface HI, which may have to be calculated numerically (for a flat surface the analytical expression for HI-tensor is known). If the surfaces are reasonably well-behaved, coupling BD to a boundary integral simulation (Kumar and Graham, 2012) for calculating the HI is a possible strategy.

6.1.3 Semiflexible and rigid polymers

Another direction for future research is investigation of the adsorption behavior of semiflexible and rigid rod-like polymers (e.g., DNA, actin, microtubules) in presence of flow. The hydrodynamic behavior of these kind of molecules is different from that of the flexible chains we considered in our work, because of the contribution due to the bending energy in governing the chain conformation. Rigid rod-like polymers do not exhibit entropic relaxation against the imposed flow, hence the HI-induced drift when subjected to flow is much weaker (Saintillan et al., 2006). Simulation studies in the absence of flow indicate that semiflexible chains show enhanced adsorption compared to flexible chains (Kramarenko et al., 1996; Hsu and Binder, 2013). But the effects of flow on adsorption/desorption of semiflexible polymers and their implications for emerging technologies like selective adsorption for separation of semiflexible polymers like DNA in microfluidic devices (Wu et al., 2013) remain an open question.

Bibliography

Anastassopoulos, D. L., N. Spiliopoulos, A. A. Vradis, C. Toprakcioglu, S. M. Baker, and A. Menelle, "Shear-induced desorption in polymer brushes", Macromolecules **39**, 8901 (2006).

Anastassopoulos, D. L., N. Spiliopoulos, A. A. Vradis, C. Toprakcioglu, A. Menelle, and F. Cousin, "Neutron reflectivity study of end-adsorbed bimodal polymer systems under static conditions and shear flow", Macromolecules **46**, 6972 (2013).

Ando, T., E. Chow, Y. Saad, and J. Skolnick, "Krylov subspace methods for computing hydrodynamic interactions in Brownian dynamics simulations", J. Chem. Phys. **137**, 064106 (2012).

Atkinson, J., C. J. Goh, and N. Phan-Thien, "Bead-spring models for an adsorbed polymer molecule in a shear flow", J. Chem. Phys. **80**, 6305 (1984).

Aubert, J. H., "Interfacial properties of dilute polymer solutions", J. Colloid Interface Sci. **96**, 135 (1983).

Aubert, J. H. and M. Tirrell, "Effective viscosity of dilute polymer solutions near confining boundaries", J. Chem. Phys. **77**, 553 (1982).

Bagassi, M., G. Chauveteau, J. Lecourtier, J. Englert, and M. Tirrell, "Behavior of adsorbed polymer layers in shear and elongational flows", Macromolecules **22**, 262 (1989).

Baker, S. M., G. S. Smith, D. L. Anastassopoulos, C. Toprakcioglu, A. A. Vradis, and D. G. Bucknall, "Structure of polymer brushes under shear flow in a good solvent", Macromolecules **33**, 1120 (2000).

Baltensperger, R. and M. R. Trummer, "Spectral differencing with a twist", SIAM J. Sci. Comput. **24**, 1465 (2002).

Baschnagel, J., H. Meyer, F. Varnik, S. Metzger, M. Aichele, M. Müller, and K. Binder, "Computer simulations of polymers close to solid interfaces: Some selected topics", Interface Sci. **11**, 159 (2003).

Besio, G. J., R. K. Prud'homme, and J. B. Benziger, "Effect of elongational flow on polymer adsorption", Macromolecules **21**, 1070 (1988).

Bird, R. B., P. J. Dotson, and N. L. Johnson, "Polymer solution rheology based on a finitely extensible bead-spring chain model", J. Non-Newtonian Fluid Mech. **7**, 213 (1980).

Bird, R. B., C. F. Curtiss, R. C. Armstrong, and O. Hassager, *Dynamics of polymeric liquids, Vol. 2: Kinetic theory*, 2nd ed. (Wiley-Interscience, NY).

Blake, J. R., "A note on the image system for a stokeslet in a no-slip boundary", Math. Proc. Cambridge **70**, 303 (1971).

Boyd, J. P., "The optimization of convergence for chebyshev polynomial methods in an unbounded domain", J. Comput. Phys. **45**, 43 (1982).

Boyd, J. P., "Orthogonal rational functions on a semi-infinite interval", J. Comput. Phys. **70**, 63 (1987).

Boyd, J. P., *Chebyshev and Fourier spectral methods*, 2nd ed. (Dover Publications, NY).

Brown, H. R., "Chain pullout and mobility effects in friction and lubrication", Science **263**, 1411 (1994).

Brown, P., G. Byrne, and A. Hindmarsh, "VODE: A variable-coefficient ODE solver", SIAM J. Sci. and Stat. Comput. **10**, 1038 (1989).

Canuto, C., M. Y. Hussaini, A. Quarteroni, and T. A. Zang, Jr, *Spectral methods: Fundamentals in single domains* (Springer-Verlag Berlin Heidelberg).

Chang, S. H. and I. J. Chung, "Effect of shear flow on polymer desorption and latex dispersion stability in the presence of adsorbed polymer", Macromolecules **24**, 567 (1991).

Chatterjee, T., A. I. Nakatani, and A. K. Van Dyk, "Shear-dependent interactions in hydrophobically modified ethylene oxide urethane (HEUR) based rheology modifier-latex suspensions: Part 1. Molecular microstructure", Macromolecules **47**, 1155 (2014).

Chaudhri, A., J. B. Bell, A. L. Garcia, and A. Donev, "Modeling multi-phase flow using fluctuating hydrodynamics", arXiv preprint arXiv:1407.6749 (2014).

Chin, S. and D. A. Hoagland, "Adsorption and desorption of polystyrene from dilute solutions in shear and elongational flow", Macromolecules **24**, 1876 (1991).

Chopra, M. and R. G. Larson, "Brownian dynamics simulations of isolated polymer molecules in shear flow near adsorbing and nonadsorbing surfaces", J. Rheol. **46**, 831 (2002).

Cohen Stuart, M. A. and A. de Keizer, "Oxide surface", in, Vol. 103, edited by J. A. Wingrave, Surfactant Science Series (Marcel Dekker, NY) Chap. Adsorption kinetics of polymeric molecules, pp. 157–200.

Cohen Stuart, M. A., W. T. S. Huck, J. Genzer, M. Müller, C. Ober, M. Stamm, G. B. Sukhorukov, I. Szleifer, V. V. Tsukruk, M. Urban, F. Winnik, S. Zauscher, I. Luzinov, and S. Minko, "Emerging applications of stimuli-responsive polymer materials", Nat. Mater. **9**, 101 (2010).

Cohen, Y., "Hydrodynamic thickness of adsorbed polymers in steady shear flow", Macromolecules **21**, 494 (1988).

Cohen, Y. and A. B. Metzner, "Adsorption effects in the flow of polymer solutions through capillaries", Macromolecules **15**, 1425 (1982).

Cowell, W. R., ed. (1984), *Sources and development of mathematical software* (Prentice-Hall Inc, NJ, NJ).

Cox, J. K., A. Eisenberg, and R. B. Lennox, "Patterned surfaces via self-assembly", Curr. Opin. Colloid Interface Sci. **4**, 52 (1999).

de Gennes, P.-G., "Polymers at an interface; A simplified view", Adv. Colloid Interface Sci. **27**, 189 (1987).

de Pablo, J. J., H. C. Öttinger, and Y. Rabin, "Hydrodynamic changes of the depletion layer of dilute polymer solutions near a wall", AIChE J. **38**, 273 (1992).

Decher, G, "Fuzzy nanoassemblies: Toward layered polymeric multicomposites", Science **277**, 1232 (1997).

Desai, T., P. Keblinski, and S. K. Kumar, "Computer simulations of the conformations of strongly adsorbed chains at the solid–liquid interface", Polymer **47**, 722 (2006).

Descas, R., J.-U. Sommer, and A. Blumen, "Static and dynamic properties of tethered chains at adsorbing surfaces: A Monte Carlo study", J. Chem. Phys. **120**, 8831 (2004).

Dijt, J. C., M. A. Cohen Stuart, and G. J. Fleer, "Kinetics of adsorption and desorption of polystyrene on silica from decalin", Macromolecules **27**, 3207 (1994).

Dutta, S., K. D. Dorfman, and S. Kumar, "Adsorption of single polymer molecules in shear flow near a planar wall", J. Chem. Phys. **138**, 034905, 034905 (2013).

Eisenriegler, E., K. Kremer, and K. Binder, "Adsorption of polymer chains at surfaces: Scaling and Monte Carlo analyses", J. Chem. Phys. **77**, 6296 (1982).

Eisenriegler, E., *Polymers near surfaces* (World Scientific, Singapore).

Fleer, G. J, M. A. Cohen Stuart, J. M. H. M. Scheutjens, T. Cosgrove, and B. Vincent, *Polymers at interfaces* (Chapman & Hall, London).

Garcia, L., B. Z. Chowdhry, and M. J. Snowden, "Encyclopedia of surface and colloid science", in, Vol. 7, edited by P. Somasundaran, 2nd ed. (CRC Press, Boca Raton) Chap. Stabilization of colloids by polymers, pp. 5775 –5787.

Gramain, P. and P. Myard, "Elongational deformation by shear flow of flexible polymers adsorbed in porous media", Macromolecules **14**, 180 (1981).

Granick, S., S. K. Kumar, E. J. Amis, M. Antonietti, A. C. Balazs, A. K. Chakraborty, G. S. Grest, C. Hawker, P. Janmey, E. J. Kramer, R. Nuzzo, T. P. Russell, and C. R. Safinya, "Macromolecules at surfaces: Research challenges and opportunities from tribology to biology", J. Polym. Sci., Part B: Polym. Phys. **41**, 2755 (2003).

Grest, G. S. and K. Kremer, "Molecular dynamics simulation for polymers in the presence of a heat bath", Phys. Rev. A **33**, 3628 (1986).

Grisafi, S. and C. J. Durning, "Adsorption of free-draining, Gaussian, bead-spring macromolecules at a plane interface", J. Colloid Interface Sci. **130**, 45 (1989).

Grisafi, S. and C. J. Durning, "Polymer adsorption at a planar interface", J. Colloid Interface Sci. **130**, 35 (1989).

Hernández-Ortiz, J. P., J. J. de Pablo, and M. D. Graham, "Fast computation of many-particle hydrodynamic and electrostatic interactions in a confined geometry", Phys. Rev. Lett. **98**, 140602 (2007).

Herrchen, M. and H. C. Öttinger, "A detailed comparison of various FENE dumbbell models", J. Non-Newtonian Fluid Mech. **68**, 17 (1997).

Hershkovits, E., A. Tannenbaum, and R. Tannenbaum, "Polymer adsorption on curved surfaces: a geometric approach", J. Phys. Chem. C **111**, 12369 (2007).

Hesthaven, J. S., S. Gottlieb, and D. Gottlieb, *Spectral methods for time-dependent problems* (Cambridge University Press, Cambridge, UK).

Hoda, N. and S. Kumar, "Brownian dynamics simulations of polyelectrolyte adsorption in shear flow: Effects of solvent quality and charge patterning", J. Chem. Phys. **128**, 164907 (2008).

Hoda, N. and S. Kumar, "Brownian dynamics simulations of polyelectrolyte adsorption onto charged patterned surfaces", Langmuir **23**, 1741 (2007).

Hoda, N. and S. Kumar, "Brownian dynamics simulations of polyelectrolyte adsorption onto topographically patterned surfaces", Langmuir **23**, 11747 (2007).

Hoda, N. and S. Kumar, "Brownian dynamics simulations of polyelectrolyte adsorption in shear flow with hydrodynamic interaction", J. Chem. Phys. **127**, 234902 (2007).

Hoda, N. and S. Kumar, "Kinetic theory of polyelectrolyte adsorption in shear flow", J. Rheol. **51**, 799 (2007).

Horinek, D., A. Serr, M. Geisler, T. Pirzer, U. Slotta, S. Q. Lud, J. A. Garrido, T. Scheibel, T. Hugel, and R. R. Netz, "Peptide adsorption on a hydrophobic surface results from an interplay of solvation, surface, and intrapeptide forces", Proc. Natl. Acad. Sci. U.S.A. **105**, 2842 (2008).

Hsu, H.-P. and K. Binder, "Effect of chain stiffness on the adsorption transition of polymers", Macromolecules **46**, 2496 (2013).

Kawaguchi, M. and A. Takahashi, "Polymer adsorption at solid-liquid interfaces", Adv. Colloid Interface Sci. **37**, 219 (1992).

Kopriva, D. A., *Implementing spectral methods for partial differential equations* (Springer Science + Business Media B.V., Berlin).

Kramarenko, E. Y., R. G. Winkler, P. G. Khalatur, A. R. Khokhlov, and P. Reineker, "Molecular dynamics simulation study of adsorption of polymer chains with variable degree of rigidity. 1. Static properties", J. Chem. Phys. **104**, 4806 (1996).

Kumar, A. and M. D. Graham, "Accelerated boundary integral method for multiphase flow in non-periodic geometries", J. Comput. Phys. **231**, 6682 (2012).

Lee, J.-J. and G. G. Fuller, "Ellipsometry studies of adsorbed polymer chains subjected to flow", Macromolecules **17**, 375 (1984).

Lee, J.-J. and G. G. Fuller, "Adsorption and desorption of flexible polymer chains in flowing systems", J. Colloid Interface Sci. **103**, 569 (1985).

Lee, J.-J. and G. G. Fuller, "The effect of segment/boundary hydrodynamic interactions on the dynamics of adsorbed polymer chains subjected to flow", J. Colloid Interface Sci. **107**, 308 (1985).

Ma, H. and M. D. Graham, "Theory of shear-induced migration in dilute polymer solutions near solid boundaries", Phys. Fluids **17**, 083103 (2005).

Mavrantzas, V. G., A. N. Beris, F. Leermakers, and G. J. Fleer, "Continuum formulation of the Scheutjens-Fleer lattice statistical theory for homopolymer adsorption from solution", J. Chem. Phys. **123**, 174901 (2005).

McGlinn, T. C., D. J. Kuzmenka, and S. Granick, "Influence of shear on polymer adsorption kinetics", Phys. Rev. Lett. **60**, 805 (1988).

Migler, K. B., H. Hervet, and L. Leger, "Slip transition of a polymer melt under shear stress", Phys. Rev. Lett. **70**, 287 (1993).

Milchev, A., "Single-polymer dynamics under constraints: scaling theory and computer experiment", J. Phys. Condens. Matter **23**, 103101 (2011).

Milchev, A. and K. Binder, "Static and dynamic properties of adsorbed chains at surfaces: monte carlo simulation of a bead-spring model", Macromolecules **29**, 343 (1996).

Netz, R. R. and D. Andelman, "Oxide surfaces", in, Vol. 103, edited by J. A. Wingrave, Surfactant Science (Marcel Dekker, NY) Chap. Adsorbed and Grafted Polymers at Equilibrium, pp. 115 –156.

O'Shaughnessy, B. and D. Vavylonis, "Non-equilibrium in adsorbed polymer layers", J. Phys. Condens. Matter **17**, R63 (2005).

Orszag, S. A., "Spectral methods for problems in complex geometries", J. Comput. Phys. **37**, 70 (1980).

Panwar, A. S. and S. Kumar, "Brownian dynamics simulations of polyelectrolyte adsorption in shear flow", J. Chem. Phys. **122**, 154902 (2005).

Peterlin, A., "Hydrodynamics of macromolecules in a velocity field with longitudinal gradient", J. Polym. Sci., Part B: Polym. Phys. **4**, 287 (1966).

Peyret, R., *Spectral methods for incompressible viscous flow* (Springer-Verlag, Berlin).

Pfeiffer, H. P., L. E. Kidder, M. A. Scheel, and S. A. Teukolsky, "A multidomain spectral method for solving elliptic equations", Comput. Phys. Commun. **152**, 253 (2003).

Phillips, D. C., R. L. York, O. Mermut, K. R. McCrea, R. S. Ward, and G. A. Somorjai, "Side chain, chain length, and sequence effects on amphiphilic peptide adsorption at hydrophobic and hydrophilic surfaces studied by sum-frequency generation vibrational spectroscopy and quartz crystal microbalance", J. Phys. Chem. C **111**, 255 (2007).

Piessens, R., E. de Doncker-Kapenga, C. W. Überhuber, and D. Kahaner, *Quadpack: A subroutine package for automatic integration* (Springer-Verlag, Berlin).

Pincus, P. A., C. J. Sandroff, and T. A. Witten, "Polymer adsorption on colloidal particles", J. Phys. France **45**, 725 (1984).

Press, W. H., S. A. Teukolsky, W. T. Vetterling, and B. P. Flannery, *Numerical recipes in Fortran 77* (Cambridge University Press, Cambridge, UK).

Radtke, M., M Radtke, and R. Netz, "Shear-induced dynamics of polymeric globules at adsorbing homogeneous and inhomogeneous surfaces", Eur. Phys. J. E **37**, 20 (2014).

Robb, C. S., "Applications of physically adsorbed polymer coatings in capillary electrophoresis", J. Liq. Chromatogr. Relat. Technol. **30**, 729 (2007).

Roth, C., B. Neal, and A. Lenhoff, "van der Waals interactions involving proteins", Biophys. J. **70**, 977 (1996).

Rotne, J. and S. Prager, "Variational treatment of hydrodynamic interaction in polymers", J. Chem. Phys. **50**, 4831 (1969).

Rubinstein, M. and R. H. Colby, *Polymer physics* (Oxford University Press, Oxford, UK).

Russel, W. B., D. A. Saville, and W. R. Schowalter, *Colloidal dispersions* (Cambridge University Press, Cambridge, UK).

Saintillan, D., E. S. G. Shaqfeh, and E. Darve, "Effect of flexibility on the shear-induced migration of short-chain polymers in parabolic channel flow", J. Fluid Mech. **557**, 297 (2006).

Sato, T. and R. Ruch, *Stabilization of colloidal dispersions by polymer adsorption* (Marcel Dekker).

Scheutjens, J. M. H. M. and G. J. Fleer, "Statistical theory of the adsorption of interacting chain molecules. 1. Partition function, segment density distribution, and adsorption isotherms", J. Phys. Chem. **83**, 1619 (1979).

Scheutjens, J. M. H. M. and G. J. Fleer, "Statistical theory of the adsorption of interacting chain molecules. 2. Train, loop, and tail size distribution", J. Phys. Chem. **84**, 178 (1980).

Schneider, S. W., S. Nuschele, A. Wixforth, C. Gorzelanny, A. Alexander-Katz, R. R. Netz, and M. F. Schneider, "Shear-induced unfolding triggers adhesion of von Willebrand factor fibers", Proc. Natl. Acad. Sci. U.S.A. **104**, 7899 (2007).

Schulz, D. N. and J. E. Glass, eds. (1991), *Polymers as rheology modifiers*, ACS Symposium Series 462 (American Chemical Society, Washington D. C.).

Sendner, C. and R. R. Netz, "Shear-induced repulsion of a semiflexible polymer from a wall", Europhys. Lett. **81**, 54006 (2008).

Serr, A., C. Sendner, F. Müller, T. R. Einert, and R. R. Netz, "Single-polymer adsorption in shear: Flattening vs. hydrodynamic lift and surface potential corrugation effects", Europhys. Lett. **92**, 38002 (2010).

Siderius, D. W. and L. D. Gelb, "Extension of the Steele 10-4-3 potential for adsorption calculations in cylindrical, spherical, and other pore geometries", J. Chem. Phys. **135**, 084703, 084703 (2011).

Sing, C. E., "Blood clotting inspired polymer physics", Thesis (Massachusetts Institute of Technology).

Skau, K. and E. Blokhuis, "Mean-field theory for polymer adsorption on curved surfaces", Eur. Phys. J. E **7**, 13 (2002).

Soga, I and S Granick, "Flow-induced deformation and desorption of adsorbed polymers", English, Langmuir **14**, 4266 (1998).

Steele, W. A., "The physical interaction of gases with crystalline solids: i. gas-solid energies and properties of isolated adsorbed atoms", Surf. Sci. **36**, 317 (1973).

Stromberg, R. R., D. J. Tutas, and E. Passaglia, "Conformation of polystyrene adsorbed at the θ-temperature", J. Phys. Chem. **69**, 3955 (1965).

van Oss, C. J., R. J. Good, and M. Chaudhury, "The role of van der Waals forces and hydrogen bonds in "hydrophobic interactions" between biopolymers and low energy surfaces", J. Colloid Interface Sci. **111**, 378 (1986).

Weideman, J. A. and S. C. Reddy, "A MATLAB differentiation matrix suite", ACM Trans. Math. Softw. **26**, 465 (2000).

Wolfe, K. A., M. C. Breadmore, J. P. Ferrance, M. E. Power, J. F. Conroy, P. M. Norris, and J. P. Landers, "Toward a microchip-based solid-phase extraction method for isolation of nucleic acids", Electrophoresis **23**, 727 (2002).

Woo, N. J., E. S. G. Shaqfeh, and B. Khomami, "Effect of confinement on dynamics and rheology of dilute dna solutions. i. entropic spring force under confinement and a numerical algorithm", J. Rheol. **48**, 281 (2004).

Wu, J., R. Kodzius, W. Cao, and W. Wen, "Extraction, amplification and detection of dna in microfluidic chip-based assays", Microchim. Acta, 1 (2013).

Yamakawa, H., "Transport properties of polymer chains in dilute solution: Hydrodynamic interaction", J. Chem. Phys. **53**, 436 (1970).